1987

Single- And Two-Phase Reacting Flow Predictions---Modeling of Non-Equilibrium Effects, Turbulent Particle Dispersion and Nitrogen-Oxide Formation in Pulverized Coal Combustion.

Dong Soon Jang
Louisiana State University and Agricultural & Mechanical College

Order Number 8811410

Single- and two-phase reacting flow predictions—modeling of nonequilibrium effects, turbulent particle dispersion and nitrogen oxide formation in pulverized coal combustion

Jang, Dong Soon, Ph.D.

The Louisiana State University and Agricultural and Mechanical Col., 1987

U·M·I
300 N. Zeeb Rd.
Ann Arbor, MI 48106

PLEASE NOTE:

In all cases this material has been filmed in the best possible way from the available copy. Problems encountered with this document have been identified here with a check mark __✓__.

1. Glossy photographs or pages _____
2. Colored illustrations, paper or print _____
3. Photographs with dark background _____
4. Illustrations are poor copy _____
5. Pages with black marks, not original copy _____
6. Print shows through as there is text on both sides of page _____
7. Indistinct, broken or small print on several pages __✓__
8. Print exceeds margin requirements _____
9. Tightly bound copy with print lost in spine _____
10. Computer printout pages with indistinct print _____
11. Page(s) _____ lacking when material received, and not available from school or author.
12. Page(s) _____ seem to be missing in numbering only as text follows.
13. Two pages numbered _____. Text follows.
14. Curling and wrinkled pages _____
15. Dissertation contains pages with print at a slant, filmed as received _____
16. Other _____

_____

_____

U·M·I

SINGLE- AND TWO-PHASE REACTING FLOW PREDICTIONS-MODELING OF NONEQUILIBRIUM EFFECTS, TURBULENT PARTICLE DISPERSION AND NITROGEN OXIDE FORMATION IN PULVERIZED COAL COMBUSTION

A Dissertation

Submitted to the Graduate Faculty of the
Louisiana State University and
Agricultural and Mechanical College
in partial fulfillment of the
requirements for the degree of
Doctor of Philosophy

in

The Department of Mechanical Engineering

by
DONG SOON JANG

B.S.N.E. Seoul National University, 1975
M.S.M.E. Louisiana State University, 1984

December, 1987

ACKNOWLEDGEMENTS

The author extends his sincere thanks for the direction, advice and encouragement provided by his major professor, Dr. S. Acharya. It was a great honor for the author to have had such an opportunity to study computational method under him. In addition, Dr. T. W. Lester and Dr. G. D. Catalano provided many valuable suggestions and contacts. Dr. R. W. Courter and Dr. R. G. Hussey have provided constant encouragement as author's committee members. Discussions with Mr. David West and Mr. Larry Herbert (Dow Chemical Co., Plaquemine, LA) were also very helpful.

The author extends his sincere gratitude to Dr. Sungwoo Suh for his encouragement and guidance during his stay in Baton Rouge. Special thanks also go to many of the author's friends at Louisiana State University. Having had the privilege of knowing such people made the entire venture worthwhile.

The author acknowledges the financial support of the Department of Mechanical Engineering, Dow Chemical Co., and Professor Harry Braud (Department of Agricultural Engineering).

Finally, the author sincerely thanks his parents, parents-in-law, his wife and daughter for their love and patience.

TABLE OF CONTENTS

TABLE OF CONTENTS (Continued)

LIST OF TABLES

LIST OF FIGURES

ABSTRACT

The objective of this dissertation study is to evaluate and improve the modeling of individual processes associated with single- and two-phase turbulent reaction processes. In particular, attention is focused on the pulverized coal combustion process, and a reliable comprehensive computer code for pulverized coal combustion systems is developed to assist in design developments.

Primary emphasis in this work has been on the modeling of non-equilibrium turbulent reactions, turbulent particle dispersion, and pollutant species formation. In addition, contributions have been made towards improving the numerical algorithm for pressure-velocity linked system in swirling flows.

Two turbulent reaction models are developed for resolving non-equilibrium effects. The first model is a modified perturbation model for the calculation of non-equilibrium effects in intensive turbulent combustion. This method appears to be well suited for application to single- and two-phase flame stability studies. The second model is a moment closure method for the simulation of a moderately fast or slow reactions. This method is applied to the modeling of fuel bound nitrogen oxide formation in pulverized coal combustion systems.

A systematic performance evaluation of existing turbulent particle dispersion models such as the empirical gradient models and the stochastic method has been made. An improvement is made the stochastic method by incorporating the effects of the particle

fluctuation velocities at the inlet stream. With this modification significant improvement in particle dispersion predictions are obtained compared to the predictions of the gradient models and the stochastic method without this modification.

The comprehensive computer code developed in this study is validated by comparisons of the predictions with a series of experimental data in an IFRF furnace. Some deficiencies are noted in the prediction of minor species like carbon monoxide and in the prediction of flame lift-off. These topics are important future tasks to be undertaken.

CHAPTER 1

INTRODUCTION

1.1 BACKGROUND

This dissertation deals with the modeling of single- and two-phase reacting flows with particular emphasis on phenomenological model improvements. The physical situation of particular interest in this dissertation is that of pulverized coal combustion in a furnace geometry, and most of the test problems presented in later chapters are centered around this situation.

Pulverized coal combustion in an industrial furnace is typically characterized by a three-dimensional, two-phase, turbulent, reacting and radiatively participating flow field. To obtain realistic predictions, each of the aforedescribed processes must be correctly modeled and then combined together into a comprehensive computer code. Model improvements of individual processes will result in more accurate predictions of the overall pulverized coal combustion process. In this dissertation, attention is focused on model improvements for three specific processes that are encountered in single and two phase combustion. The first is the modeling of non-equilibrium effects such as local flame quenching or extinction in single phase, fast reacting flows. The second model improvement is centered around the modeling of the dispersion of the second phase (coal particles in this study) by the turbulence in the gas flow. The implications of this improved modeling of turbulent particle dispersion on comprehensive pulverized coal combus-

tion predictions is carefully examined by detailed comparisons with measurements. Finally, the modeling of minor species is examined, and again, attention is focused in pulverized coal combustion where NO_x is the minor species of primary importance. A model developed for NO_x formation is presented.

Comprehensive models of pulverized coal combustion have been presented by a number of investigators (Lockwood et al., 1980; Smith et al., 1981; Boysan et al., 1986; Truelove, 1986; Boyd and Kent, 1986). In the discussion that follows, an overview of the basic methodology intrinsic to all these predictive procedures and, to a certain extent, to the procedure in this dissertation is given.

In this study, a two-dimensional, cylinderical axisymmetric geometry is considered, as shown in Fig. 1. Coal particles enter the furnace through the central primary stream together with the carrier gas, and oxidizer enters through the outer secondary stream or annulus. The numerical scheme is based on an Eulerian calculation for the gaseous phase and a Lagrangian one for the particle phase. The coupling between particle and gas phase is resolved through particle source terms of mass, momentum and energy in the corresponding governing equations of the gas phase (Crowe et al., 1977).

The gaseous governing equation are non-linear, second-order partial differential equations. The finite difference method is based on the control volume formulation. In order to resolve the pressure-velocity coupling in the momentum equation, a number of algorithms have been proposed such as SIMPLE (Patankar and Spald-

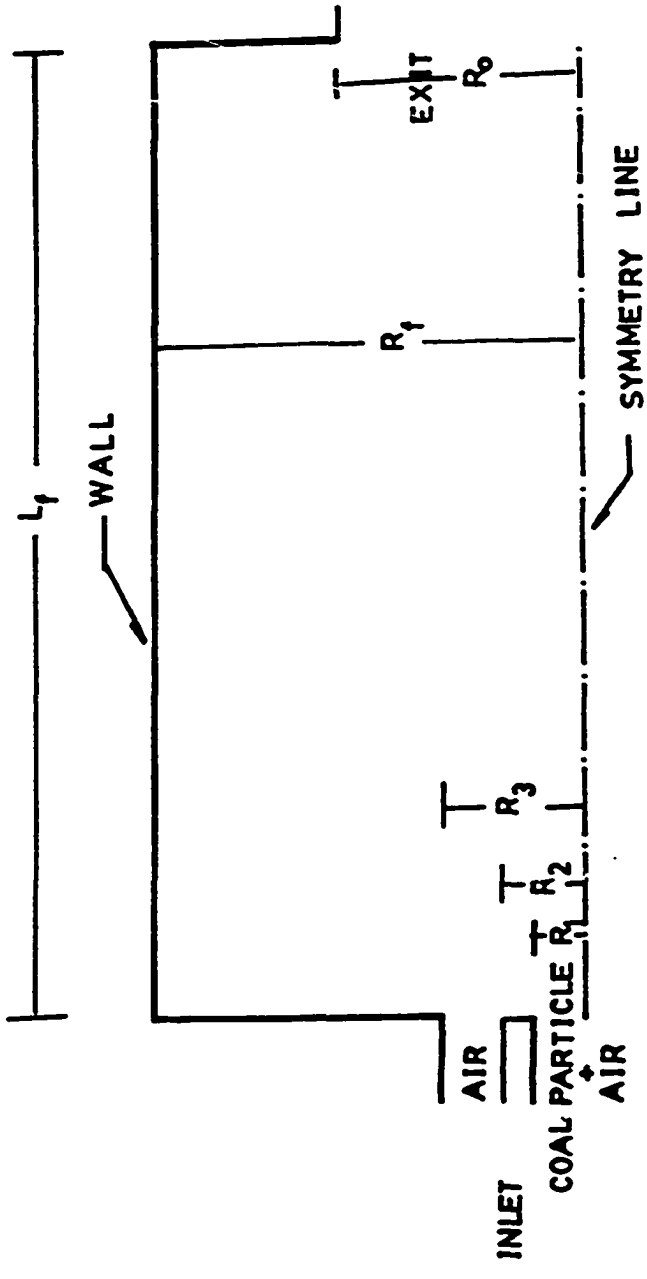

Fig. 1.1 Typical furnace geometry

ing, 1972), SIMPLER (Patankar, 1980), SIMPLEC (Van Doormaal and Raithby, 1984), and PISO (Issa, 1986). Since the computational efficiency depends upon the proper resolution of the pressure-velocity coupled system, the choice of a robust and numerically convergent algorithm is critical in obtaining good solutions.

Turbulence modeling of gaseous fluid mechanics evades a firm theoretical basis. When the statistical moment method is used the closure problem arises, i.e., there are more unknowns than available equations. Even though Batchelor (1953) has pointed out the potential of higher order correlation approximation methods, it is highly impractical to include a large number of higher order correlation terms in the actual calculation. In addition, the recent notion of large scale structure (Laufer, 1975; Roshko, 1976) suggests that the turbulent motion is comprised of quasi-deterministic, unsteady, large scale eddy motions and small scale random fluctuations. However, the overwhelming majority of phenomenological turbulence models do not explicitly incorporate the concept of coherent large scale or organized eddy motion (Reynolds, 1976). The application of large scale eddy motion together with the fine scale random fluctuations has been reported, but not well established (Knight and Murray, 1981). Thus the widely used two equation (k-ε) turbulence model (Launder and Spalding, 1972) is commonly adopted. In this model, the Boussinessq gradient hypothesis is used for the second-order correlation term and a Prandtl-Kolmogorov relationship is used to correlate the eddy viscosity to the turbulent kinetic energy (k) and its dissipation rate (ε). However, the isotropic exchange coefficient assumption of the k-ε turbulence

model has been seriously questioned (Lilley, 1974) for swirling flow.

Although more complex Reynolds stress models have been developed (Launder et al. 1975; Rubesin, 1977) to overcome these difficulties, none of these models have shown significant improvements over the k-ε model. Recently, rather systematic investigations have been performed of the original and/or modified k-ε model under swirling flow conditions (Srinivasan and Mongia, 1981; Ramos, 1984). Significant improvements in the predictions were achieved by specifying accurate inlet conditions and by increasing the numerical accuracy of the algorithm.

The fuel for gaseous combustion in the pulverized coal-fired process comes mainly from the devolatilized coal-off gas, and the reaction of this coal-off gas may be assumed to occur basically in a non-premixed fashion. Irrespective of the degree of premixedness, gaseous turbulent combustion is a remarkably complex subject whose detailed characteristics are not well known, even without the presence of a second phase viz., coal particles. A series of reviews (Libby and Williams, 1980; Jones and Whitelaw, 1982, 1984) suggest that there is much work to be accomplished before our understanding of this subject is adequate.

The basic problem of the gaseous turbulent combustion lies in the proper modeling of the turbulent correlation term which arises in the non-linear chemical reaction source term. The direct statistical moment closure method, as in the turbulence modeling of the Reynolds stresses, again gives rise to the closure problem. The higher correlation terms cannot be neglected due to the signif-

icant fluctuations of temperature, density and species concentration. Most combustion models circumvent the difficulty by ignoring the chemical kinetic aspects of the problem and model the reaction using turbulent mixing as the rate limiting step. In other words, chemical equilibrium is presumed.

Typical examples of turbulence-only models are the eddy break up model for a premixed flame (Spalding, 1971; Magnussen and Hjertager, 1976) and flame sheet approximation using a conserved scalar (Bilger, 1976) for a non-premixed flame. Magnussen and Hjertager (1976) suggested that their proposed model was applicable to both premixed and non-premixed flames. Although these models have been shown to be successful tools in predicting overall profiles of main species, serious drawbacks exist, since the methods do not incorporate local flame quenching or extinction effects, and minor species are not well predicted, where chemical kinetics play an important role.

Local flame extinction usually occurs when the turbulent mixing rate overwhelms the rate of chemical reaction, that is, for very small Damkohler numbers. Local flame extinction may be evidenced by flame lift-off and blow-off which occurs when the exit velocity of burner exceeds a certain critical velocity. Flame quenching phenomena is of practical importance in connection with flame stabilization, and limits of stable operation must be known in developing rational designs of burners used in, for example, non-premixed flame combustors for power production or in flaring applications for the petroleum industry.

In modeling flame quenching, a scalar dissipation rate is usually defined by using the analogy of spectral transfer of turbulent kinetic energy. However, the modeling of scalar dissipation rate is not well justified, and usually resort is made to empiricism. A number of applications have been reported where the concept of scalar dissipation rate had been used for the prediction of non-equilibrium effects or flame lift-off heights (Bilger, 1979, 1980; Liew et al. 1984; Peters and Williams, 1983). In general, this area is not well established and is in a state of development.

Particle motion in a flow is usually described by the steady-state aerodynamic drag force. Generally buoyant forces, virtual mass effects, Basset forces, and rotational effects are neglected. The neglect of these terms is a common practice in the study of pulverized coal combustion, and may be justified by the large ratio of particle density to gas density. Considering the crossing trajectory effect (Shih and Lumley, 1986) in the migration of particle from one eddy to another, the Basset forces (the deviation of the shear stress during the transient period from the steady value) may become significant in highly turbulent flows.

Even in the simplified approach, where the aerodynamic drag is the only force accounted for, the non-linear feature of the drag causes serious difficulties in the calculation of particle trajectory in turbulent flows. The modeling of the correlation term between the drag coefficient fluctuation and the difference of particle and gas velocity fluctuation has been addressed using a gradient assumption (Lockwood, 1980; Smith et al., 1981) with the ad hoc specification of empirical constants. An alternative ap-

proach, which has been proposed by Gosman and Ioannides (1980) employs a stochastic method, which circumvents the correlation modeling by solving the instantaneous equation of motion, and by the random sampling of turbulent properties based on the k-ε turbulence model. Shuen et al. (1983a) have shown that this approach works well in relatively simple parabolic or jet type flows. However, rather limited investigation has been made of the performance of the stochastic method in elliptic flows. Stochastic inlet conditions and the number of stochastic iterations have not been well studied (Truelove, 1986; Boyd and Kent, 1986).

Devolatilization laws that are commonly used are the constant evaporation rate model (Baum and Street, 1971), the two competing reaction scheme (Kobayaski, 1977), and the multi-parallel reaction model (Anthony et al., 1975). Char reaction rate is controlled by oxygen mass diffusion rate and chemical reaction rate. The harmonic mean of these rates is usually used to describe the overall reaction rate. Several experimental data are available for char reaction rate (Baum and Street, 1971; Field et al., 1969; Lester et al., 1981).

Due to highly emitting and absorbing nature of pulverized coal flames, radiation is a significant mode of heat transfer in pulverized coal combustion system. A common approach to model radiation is to use the four flux method which includes anisotropic and multiple scattering effects (Varma, 1979; Gosman and Lockwood, 1974).

As mentioned earlier, chemical kinetics plays an important role in minor pollutant species formation. Nitrogen oxide is one

of the most important pollutant species that is formed in pulverized coal combustion system. Coal contains approximately 1-2% nitrogen by weight depending on the coal type. Fuel NO can be formed from the homogeneous oxidation of nitrogen constituents released during the devolatilization process, or from heterogeneous oxidation of nitrogen compounds remaining in the char following devolatilization. Fuel NO formed in the gas phase from oxidation of devolatilized nitrogen species is considered to account for 60-80% of the total NO formed (Pershing and Wendt, 1977; Pohl and Sarofim, 1977). The modeling of fuel-bound NO formation has been reported by Hill (1983), where the nitrogen oxide formation rates are assumed to be only a function of local stoichiometry as in the thermal NO modeling of Fennimore and Fraenkel (1981). However, a number of ad hoc assumptions have been made, and in general, NO_x modeling in pulverized coal combustion systems warrants more attention.

1.2 OBJECTIVE

The goal of this study is to evaluate some of the existing models used in the simulation of pulverized coal combustion systems and thereby develop more appropriate models for input into a reliable comprehensive computer code. Considering the wide range of topics associated with pulverized coal combustion processes, emphasis is placed on four specific aspects. These are (1) improving numerical solution methods, (2) improved modeling of gaseous turbulent combustion by incorporating nonequilibrium effects, (3) im-

proved modeling of turbulent particle dispersion, and (4) modeling of nitrogen oxide formation in pulverized coal combustion systems.

Specific objectives in each task are:

(1) Numerical solution method: Since the comprehensive computer simulation is time consuming and the flow field calculation depends on the proper pressure - velocity coupling scheme in the momentum equations, it is critical to evaluate the relative performances of existing solution methods of pressure velocity-linked systems, and develop more efficient algorithms. The proper resolution of coupling through source terms is also an important issue, and needs to be addressed.

(2) Gaseous turbulent combustion: The fast chemistry assumption has been generally used in treating turbulent reactions but this approach does not account for nonequilibrium effects such as local flame quenching, which is typical in all practical flames. Thus development of an appropriate model of nonequilibrium turbulent combustion is important.

(3) Turbulent particle dispersion: The accurate prediction of particle trajectory in a two phase reacting system such as pulverized coal combustion is critical to the satisfactory performance of the comprehensive model. The objective in this task is to evaluate the existing models of turbulent particle dispersion and to develop improved models.

(4) Nitrogen oxide formation: Since the fuel bound nitrogen oxide is one of the major pollutant species formed in pulverized coal-fired processes, the appropriate modeling of nitrogen oxice formation is important.

1.3 ORGANIZATION OF THE DISSERTATION

The dissertation research described herein is divided into eight chapters. The first chapter is meant to be an introduction to provide an overview of pulverized coal combustion modeling and is aimed at tying together what otherwise might seem to be vaguely related pieces of work. Chapter 2 briefly described the basic gas-, particle- and two-phase models, as well as the solution procedure, which is used for the comprehensive modeling study in this dissertation. Chapter 3 provides an evaluation of the relative performances of existing numerical algorithms for pressure-velocity linked systems, and an improved algorithm for high swirling flow calculation. The modeling of nonequilibrium turbulent reaction is discussed in Chapter 4, and a model for nonequilibrium effects such as flame extinction is developed for intensive, gaseous, non-premixed, turbulent combustion. The performance of this model is tested by comparison in the fast chemistry prediction. Chapter 5 presents the evaluation of existing models of turbulent particle dispersion such as the empirically gradient models and the stochastic model. An improved stochastic model for turbulent particle dispersion is presented. The overall evaluation of com-

prehensive computer code is presented in Chapter 6. Chapter 7 describes the development and application of a model to predict nitrogen oxide formation in pulverized coal combustion systems. Summary of present work and future recommendations are made in Chapter 8.

CHAPTER 2

SINGLE- AND TWO-PHASE MODELS FOR PULVERIZED COAL COMBUSTION

The purpose of this chapter is to briefly describe the important gas-, particle- and two-phase models which are in the comprehensive modeling of pulverized coal-fired processes. Gas phase turbulence and reaction models are provided in section 2.1 followed by a description of the solution procedure and model evaluations for isothermal, turbulent flows. The important particle phase equations, gas-particle coupling scheme, and two-phase radiation models are presented in the section 2.2, together with the particle and two phase solution techniques.

2.1 GAS PHASE MODELS

The gas phase is considered to be a turbulent reacting continuum field that can be described by the general governing equations in an Eulerian framework. The governing Navier-Stokes equation are reduced in this study with the following simplifications: (1) cylindrical coordinates, (2) 2-dimensional axi-symmetric geometry, (3) no body forces, (4) steady state, (5) Newtonian fluid, (6) no dilatation.

Turbulence is modeled by decomposing the variables into a time-mean component and a fluctuating component. The two-equation

(k-ε) model is used for closure (Launder and Spalding, 1972). Turbulence introduces great complexity into gas phase reaction modeling. One of the approaches commonly adopted is to assume fast equilibrium chemistry, so that the reaction is limited by the rate of turbulent mixing. Typical examples of fast chemistry models are the conserved scalar method (Bilger, 1976; Elgobashi and Pun, 1974) for nonpremixed flames, and the eddy breakup model (Spalding, 1971; Magnussen and Hjertager, 1976) for premixed flames. Magnussen and Hjertager (1976) have suggested that their model can be applicable to both premixed and nonpremixed combustion.

The conserved scalar method presumes that an equilibrium, irreversible, one step chemical reaction is valid instantaneously, so that fuel and oxidizer always combine in a stoichiometric ratio to form a single product whenever they both coexist simultaneously at the same point. Assuming further, that the diffusion coefficients for the mass fraction of fuel, oxidizer and enthalpy are equal and that the adiabatic wall conditions are valid, the instantaneous values of fuel and oxidizer mass fractions and enthalpy can be related to a conserved scalar like a mixture fraction.

The basic idea of the eddy breakup model is that the rate of reaction is controlled by the rate of turbulent dissipation (i.e. eddy breakup). The adoption of k-ε turbulence model for the modeling of eddy breakup is a common practice. As mentioned in Chapter 1, both models have been widely used and shown to be successful tools in predicting overall profiles of main species in intensive turbulent combustion like a natural gas-air flame.

2.1.1 Two Equation (k-ε) Turbulence Model

The Navier-Stokes equation is applicable to laminar flows as well as to turbulent motion, but it cannot be directly involved in the case of turbulent flows. This is because the length and time scales of turbulent motion are very small, for example, eddies which are responsible for the decay of turbulence in a gaseous flow are typically about 0.1mm (Spalding and Launder, 1972), while the flow domain of practical combustor may extend up to 10 meters. The capacity and speed of the present day computers is not sufficient to resolve such small length and time scales.

The usual technique for resolving this difficulty is to take the time-average and to assume small density variations. However, in reacting flows, the neglect of density fluctuation is not well justified due to the steep variation of the density in the flame zone. In order to avoid this difficulty, Favre averaging (Favre, 1969) is commonly used as a viable alternative, where quantities are weighted by the instantaneous density. When incompressible flow is assumed, the only unknown term is the Reynolds stress. The most common practice is to use the Bousinessq hypothesis, that is, the Reynolds stress can be replaced by the product of the mean velocity gradient and a quantity termed eddy or turbulent viscosity. The task, therefore, is to express the turbulent viscosity in terms of known or calculated quantitites. The popular approach is the use of the two-equation (k-ε) model (Launder and Spalding, 1972), where a Prandtl-Kolmogorov relationship is used to correlate the eddy viscosity μ_t to the turbulent kinetic energy and its

dissipation rate.

$$\mu_t = C_\mu \rho k^2/\varepsilon \qquad (2.1.1)$$

Thus this model is closed by solving transport equations for k and ε.

The governing equations that represent the turbulent fluid mechanics is expressed in cylindrical coordinates as

$$\frac{\partial}{\partial x}(\rho u\phi) + \frac{1}{r}\frac{\partial}{\partial r}(r\rho v\phi) = \frac{\partial}{\partial x}(\Gamma_\phi \frac{\partial \phi}{\partial x}) + \frac{1}{r}\frac{\partial}{\partial r}(r\Gamma_\phi \frac{\partial \phi}{\partial r}) + S_\phi \qquad (2.1.2)$$

where ϕ denotes general time mean dependent variables such as velocity components and other variables of the turbulence model. Γ_ϕ and S_ϕ stand for the corresponding turbulent diffusion coefficient and source term, respectively. Expressions for Γ_ϕ and S_ϕ are presented in Table 2.1.1 together with empirical constants for the k-ε turbulence model (Khalil et al., 1975), where σ denotes turbulent Prandtl/Schmidt number.

2.1.2 Turbulent Combustion - Fast Chemistry Model

Conserved Scalar Method

As mentioned earlier, the main features of conserved scalar method (Bilger, 1976) are the assumption of a single step, fast chemistry reaction and the assumption of mean effective mass exchange coefficients for all species. The consequence of these two assumptions is that a passive scalar can be defined as follows:

Table 2.1.1 Expressions for Γ_ϕ and S_ϕ for k-ε turbulence model

ϕ	Γ_ϕ	S_ϕ
u	μ_t	$\frac{\partial}{\partial x}(\mu_t \frac{\partial u}{\partial x}) + \frac{1}{r}\frac{\partial}{\partial r}(\mu_t\, r \frac{\partial v}{\partial x}) - \frac{\partial p}{\partial x}$
v	μ_t	$\frac{\partial}{\partial x}(\mu_t \frac{\partial u}{\partial r}) + \frac{1}{r}\frac{\partial}{\partial r}(\mu_t\, r \frac{\partial v}{\partial r}) - 2\mu_t \frac{v}{r^2} + \frac{\rho w^2}{r}$
w	μ_t	$-(\frac{\mu_t}{r^2} + \frac{\rho v}{r} + \frac{1}{r}\frac{\partial \mu_t}{\partial r})\, w$
k	$\frac{\mu_t}{\sigma_k}$	$G_{kl} - \rho\varepsilon$
ε	$\frac{\mu_t}{\sigma_\varepsilon}$	$\frac{\varepsilon}{k}(C_1 G_{kl} - C_2 \rho\varepsilon)$

$$G_{kl} = \mu_t[2\{(\frac{\partial u}{\partial x})^2 + (\frac{\partial v}{\partial r})^2 + (\frac{v}{r})^2\} + (\frac{\partial w}{\partial x})^2 + (r\frac{\partial}{\partial r}(\frac{w}{r}))^2 + (\frac{\partial u}{\partial r} + \frac{\partial v}{\partial x})^2]$$

$C_1 = 1.44$
$C_2 = 1.92$
$C_\mu = 0.09$
$\sigma_\varepsilon = 1.22$
$\sigma_k = 0.9$

$$\Phi = m_{fu} - \frac{m_{ox}}{s} \tag{2.1.3}$$

where m is the mass fraction and s is the stoichiometric oxygen requirement per unit mass of fuel. The governing equations for the passive scalar variable is characterized by the lack of any source or sink term. One of the most popular passive scalar employed in turbulent combustion is the mixture fraction defined

$$\tilde{f} = \frac{\Phi - \Phi_{ox}}{\Phi_{fu} - \Phi_{ox}} \tag{2.1.4}$$

where subscripts fu and ox stand for fuel and oxidizer streams, respectively and tilde ~ denotes instantaneous value. Using the mixture fraction f, the instantaneous values of species mass fractions and enthalpy are related as shown in Fig. 2.1.1.

In order to calculate the time-mean values of mass fractions, temperature and density, consideration should be given to the turbulent fluctuations, which are often large compared to their mean values (Kent and Bilger, 1973). In other words, the variance of the mixture fraction termed g and the instantaneous variation of f with time should be appropriately modeled. Expressions Γ_ϕ and S_ϕ are presented in Table 2.1.2 for the variables f and g. To model the temporal variations of f the probability density function (pdf) of f is chosen and different pdf's have been proposed by various authors. Most typical examples of these are a clipped Gaussian pdf (Elgobashi and Pun, 1974) and a beta pdf (Richardson et al., 1953). In the present study, the Gaussian pdf is adopted, which is shown

Table 2.1.2 Expressions for Γ_ϕ and S_ϕ for turbulent combustion models

	ϕ	Γ_ϕ	S_ϕ
Conserved Scalar Method	f	$\frac{\mu_t}{\sigma_f}$	0
	g	$\frac{\mu_t}{\sigma_g}$	$C_{g1}G_{g1} - C_{g2}\rho\frac{\varepsilon}{k}g$
Eddy Breakup Model	m_{fu}	$\frac{\mu_t}{\sigma_{fu}}$	$\dot{\omega}_{m_{fu}}$
	h	$\frac{\mu_t}{\sigma_h}$	$\dot{\omega}_{m_{fu}}H_{fu}$

$$G_{g1} = \mu_t[(\frac{\partial f}{\partial x})^2 + (\frac{\partial f}{\partial r})^2]$$

$C_{g1} = 2.8 \qquad C_{g2} = 2.0$

$\sigma_f = \sigma_g = \sigma_{m_{fu}} = \sigma_h = 0.9$

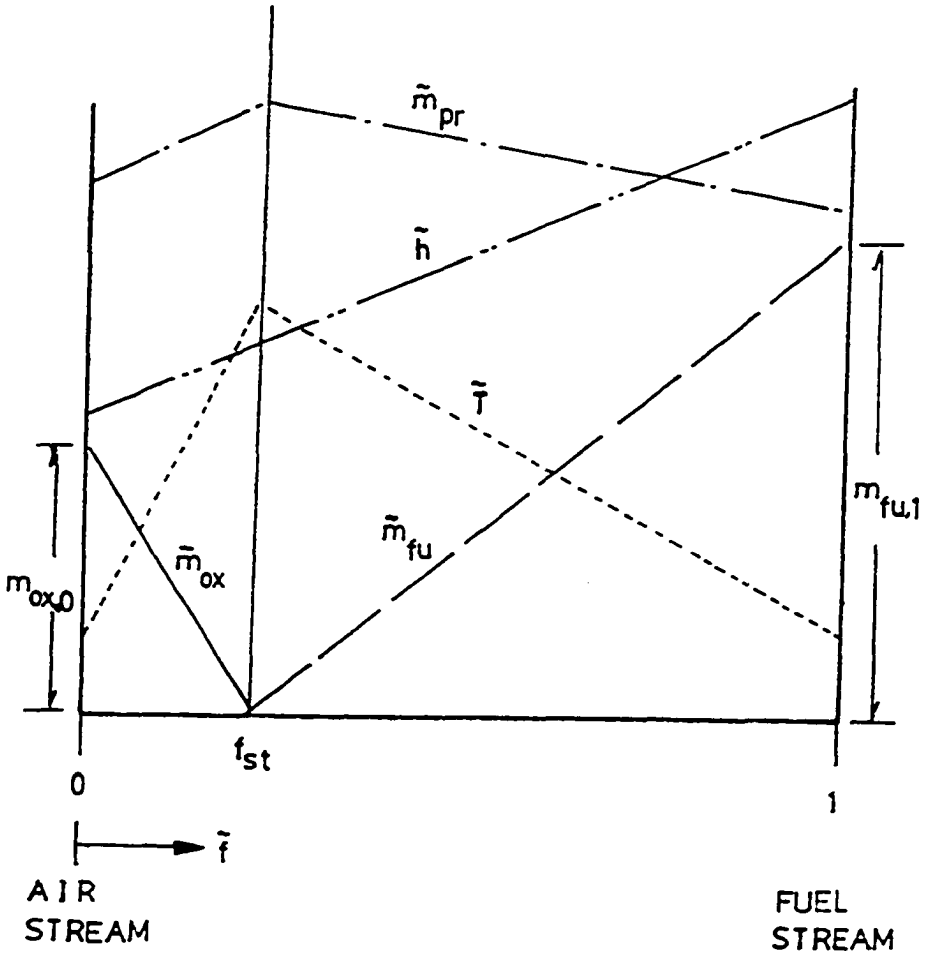

Fig. 2.1.1 Relations between instantaneous quantities: mass fractions, enthalpy, temperature and mixture fraction

in Fig. 2.1.2. Because of clipping, the pdf, $p(\tilde{f})$ is represented by

$$p(\tilde{f}) = \exp\,[-(\tilde{f}-F)^2/2\sigma^2][U(\tilde{f}-0) - U(\tilde{f}-1)]/$$

$$\sigma(2\pi)^{\frac{1}{2}} + 2A_0\delta(\tilde{f}-0) + 2A_1\delta(\tilde{f}-1) \qquad (2.1.5)$$

In Eq (2.5), $U(\zeta)$ is a unit step function defined by $U(\zeta)=0$, $\zeta<0$; $U(\zeta)=1$, $\zeta>0$; and $\delta(\zeta)$ denotes the Dirac Delta function, A_0 and A_1 are given by

$$A_0 = \int_{-\infty}^{0} \exp\,[-(\tilde{f}-F)^2/2\sigma^2]\,d\tilde{f}/[\sigma(2\pi)^{\frac{1}{2}}] \qquad (2.1.6)$$

$$A_1 = \int_{1}^{\infty} \exp\,[-(\tilde{f}-F)^2/2\sigma^2]\,d\tilde{f}/[\sigma(2\pi)^{\frac{1}{2}}] \qquad (2.1.7)$$

F and σ are respectively the mean and the standard deviation for the normal Gaussian distribution function. Note that A_0 and A_1 represent the intermittency in a nonpremixed flame.

The time mean value, f, and the variance g, of $p(\tilde{f})$ are given by the first and second moment about $\tilde{f}=0$. The corresponding expressions are

$$f = A_1 + \int_{0}^{1} \tilde{f} \exp\,[(\tilde{f}-F)^2/2\sigma^2]\,d\tilde{f}/[\sigma(2\pi)^{\frac{1}{2}}] \qquad (2.1.8)$$

$$g = A_1 - f^2 + \int_{0}^{1} \tilde{f}^2 \exp\,[-(\tilde{f}-F)^2/2\sigma^2]\,d\tilde{f}/[\sigma(2\pi)^{\frac{1}{2}}] \qquad (2.1.9)$$

Thus, when we know the solution of f and g, at any local point, values of F and σ, $p(\tilde{f})$ can be obtained from Eq. 2.1.5. Further all other mean variables like species mass fractions and enthalpy can be calculated since they are instantaneously related to $\tilde{f}$. The

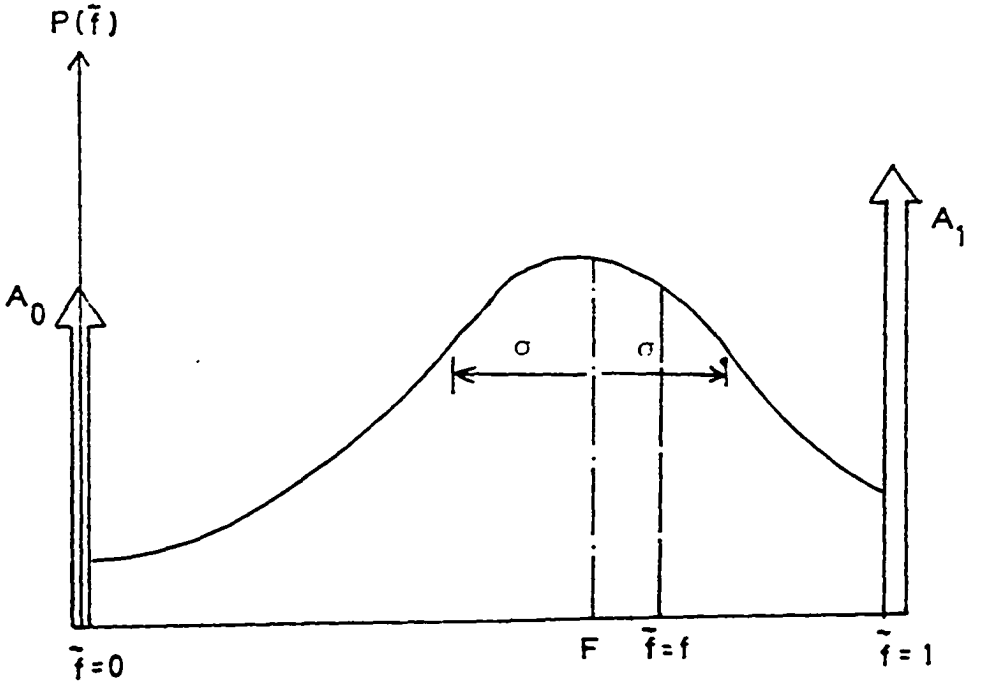

Fig. 2.1.2 The clipped Gaussian pdf, $p(\tilde{f})$

values of F and σ can be efficiently obtained from a table set up of σ and F against the corresponding values of f and g.

The mean value, ϕ of a instantaneous quantity can be evaluated from:

$$\phi = \int_0^1 \tilde{\phi}(f)\tilde{p}(f)df \qquad (2.1.10)$$

Eddy breakup model

The basic idea in an eddy breakup model lies in the calculation of the turbulent mixing time using a proper turbulence model. Many different variants of the eddy breakup model for combustion have been proposed, but all require a turbulence time scale in the formulation. This time scale represents the time required for the turbulence to stretch an eddy by vortex stretching mechanisms to a sufficiently small transverse length scale, in which fuel and oxidizer in a non-premixed system or fuel-oxidizer mixture and combustion products in a premixed system can be rapidly mixed and burned. A typical expression developed by Spalding (1971) for premixed flame is

$$\dot{\omega}_{fu} \sim \overline{m'^2_{fu}}\,\frac{\varepsilon}{k} \qquad (2.1.11)$$

where $\overline{m'^2_{fu}}$ is the root-mean-square concentration fluctuation, and ε and k are turbulent kinetic energy and dissipation rate.

The idea behind using ε/k in Eq. (2.1.11) is that the rate of reaction is controlled by the rate of turbulent dissipation or eddy breakup. However, this expression also requires the calculation of turbulent fluctuations of species mass fraction. In order to

overcome this difficulty, Magnussen and Hjertager (1976) proposed a modified eddy breakup model, in which the species fluctuation quantity in Eq. (2.1.11) is replaced by the mean concentration of the intermittent quantity by assuming a relationship between the fluctuations and the mean concentrations. Using the idea of Magnussen and Hjertager, the source term of fuel mass fraction is expressed as:

$$\dot{\omega}_{fu} = \text{minimum of } \left| \bar{\rho} A \bar{m}_{fu} \varepsilon/k,\ \bar{\rho} A (\bar{m}_{ox}/s),\ \bar{\rho} A' (\bar{m}_{pr}/(1+s)\varepsilon/k \right| \quad (2.1.12)$$

The eddy breakup combustion model requires the solution of the species and enthalpy balance equations with volumetric reaction source terms as shown in Eq. (2.1.12). The corresponding Γ_ϕ and S_ϕ expressions together with empirical constants have already been presented in Table 2.1.2.

2.1.3 Thermodynamic properties

The density of a mixture of air, gases, and the combustion products is expressed by the ideal gas equations. The specific heat is calculated from the expressions of Van Wylen and Sonntag (1978). Other gaseous properties such as viscosity and thermal conductivity are obtained from the tabulated data in NASA Technical Report (Svehla, 1962). The definition used is for the stagnation enthalpy of the mixture:

$$h = m_{fu} H_{fu} + \Sigma m_i C_{pi} T \quad (2.1.13)$$

where the gas phase kinetic energy is neglected and the heat of reaction of fuel, H_{fu}, can be determined from the fuel properties. In the present study, single-step, irreversible reactions are

assumed and the values of H_{fu} for the fuel components are taken from Glassman (1977).

2.1.4 Solution Procedure

The finite difference form of the elliptic conservation equations will be solved by an iterative technique. The difficulty in the solution process is because of the unknown pressure gradient term in the axial and radial velocity equations. This problem is solved by a procedure called SIMPLER (Semi-Implicit Method for Pressure Linked Equations Revised). This method has been accorded a book length description by Patankar (1980). Therefore, only a brief description will be provided here.

SIMPLER is a finite difference calculation procedure, where the domain of interest is first discretized into control volumes and then the grid points are placed at the center of the control volumes. A boundary grid point is also placed midway along the control volume face which coincides with the boundary of the computational domain (Fig. 2.1.3). The x and y components of velocity, i.e., u and v, are stored at the staggered points shown by arrows in Fig. 2.1.4a. All other variables are stored at the main grid points.

The finite difference equations for each ϕ are obtained by intergrating Eq. (2.1.2) over the appropriate control volume. The convection and diffusion terms become surface integrals of the convection and diffusion fluxes resulting in the following equation:

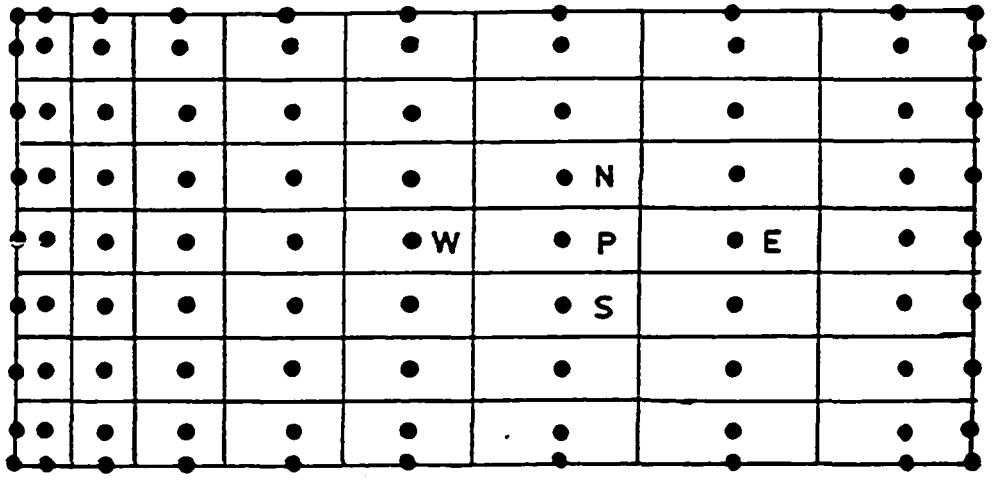

Figure 2.1.3: Schematic of the grid layout

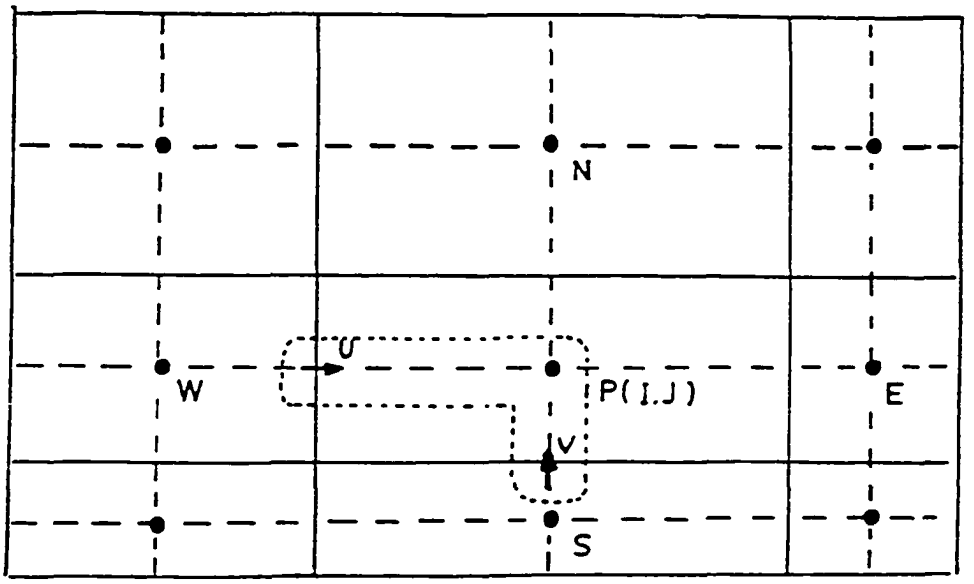

(a)

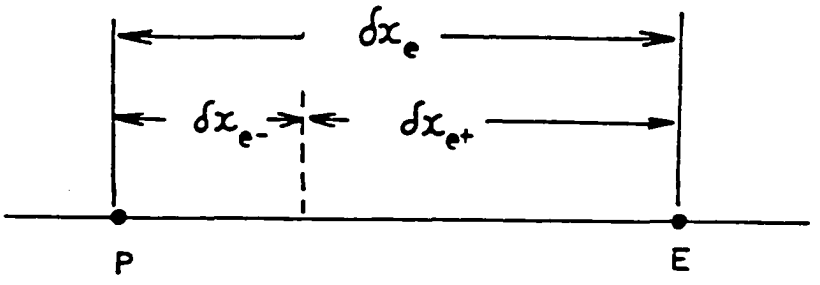

(b)

Fig. 2.1.4 (a) Schematic of staggered grid layout
(b) Nomenclature used in the grid

Table 2.1.3 The form of the components of the linearized source

$$\int_V S_\phi \, dV = S_p \, \phi_p \, \Delta V + S_c \, \Delta V$$

ϕ	S_p	S_c
u	0	$\frac{\partial}{\partial x}(\mu_t \frac{\partial u}{\partial x}) + \frac{1}{r}\frac{\partial}{\partial r}(\mu_t \, r \frac{\partial v}{\partial x}) - \frac{\partial p}{\partial x}$
v	$-2\frac{\mu_t}{r^2}$	$\frac{\partial}{\partial x}(\mu_t \frac{\partial u}{\partial r}) + \frac{1}{r}\frac{\partial}{\partial r}(\mu_t \, r \frac{\partial v}{\partial r}) - \frac{\partial p}{\partial r}$
w	$-\frac{\mu_t}{2}$	$-(\frac{\rho v}{r} + \frac{1}{r}\frac{\partial \mu_t}{\partial r})\, w$
k	$-\frac{\rho\varepsilon}{k}$	G_{kl}
ε	$-\frac{C_2\rho\varepsilon}{k}$	$\frac{C_1 C_\mu \, \rho \, k \, G_{kl}}{\mu_t}$

$$[\rho u\phi - \Gamma_\phi \frac{\partial \phi}{\partial x}]_e A_e - [\rho u\phi - \Gamma_\phi \frac{\partial \phi}{\partial r}]_w A_w$$

$$+ [\rho v\phi - \Gamma_\phi \frac{\partial \phi}{\partial r}]_n A_n$$

$$- [\rho v\phi - \Gamma_\phi \frac{\partial \phi}{\partial r}]_s A_s = [S_p\phi_p + S_c]\Delta V \qquad (2.1.14)$$

where S_p^ϕ and S_c^ϕ are tabulated in Table 2.1.3 and subscripts n, s, e, and w refer to north, south, east, and west control volume faces. The convective and diffusive fluxes across the control volume faces are expressed in terms of grid point ϕ values by using a power law scheme (Patankar, 1980), which provides a more accurate solution than other proposed schemes such as central difference, upwind, and hydrid schemes. Using the power law scheme, the total flux (J) across the "e" control volume face can be written as

$$J_e = F_e \phi_p + \{D_e A(|P_e|) + [- F_e, 0]\} (\phi_p - \phi_E) \quad , \qquad (2.1.15)$$

where

$$A(|P_e|) = [0, (1 - 0.1|P_e|)^5] \qquad (2.1.16)$$

and the symbol [a, b] is used to denote the greater of a and b. The Peclet number P_e which is the ratio of the convection flux and the diffusion conductance is given by

$$P_e = \frac{F_e}{D_e} \quad , \qquad (2.1.17)$$

where F_e is the flow rate $(\rho u)_e A_e$ and D_e is the diffusion conductance $(\frac{\Gamma_\phi A_e}{\Delta x})$. The approximate expression for the coefficient of diffusion at control volume face is given by the harmonic mean which is

$$\frac{\Gamma_e}{(\delta x)} = \left[\frac{(\delta x)e^-}{\Gamma_P} + \frac{(\delta x)e^+}{\Gamma_E}\right]^{-1} \quad , \tag{2.1.18}$$

where the distance (δx)e, (δx)e-, and (δx)e+ associated with the interface e are shown in Figure 2.1.4b.

The final discretization equation can be written as

$$a_P\phi_P = a_E\phi_E + a_W\phi_W + a_N\phi_N + a_S\phi_S + b \tag{2.1.19}$$

$$a_E = D_e\, A(\, P_e\,) + [-Fe,\ 0] \tag{2.1.20}$$

$$a_W = D_W\, A(\, P_w\,) + [F_\omega,\ 0] \tag{2.1.21}$$

$$a_N = D_n\, A(\, P_n\,) + [-F_n,\ 0] \tag{2.1.22}$$

$$a_S = D_s\, A(\, P_s\,) + [F_s,\ 0] \tag{2.1.23}$$

$$b = S_c\, \Delta V \tag{2.1.24}$$

$$a_p = a_E + a_W + a_N + a_S - S_p\, \Delta V \tag{2.1.25}$$

The system of algebraic equations, represented by Eq. (2.1.19) is solved iteratively by using a line-by-line TDMA (TriDiagonal-Matrix Algorithm). For physically realistic solutions, all coefficients (a_p and neighbor coefficients a_{nb}) must always be positive and S_p should be made negative whenever possible. Table 2.1.3 shows the expressions for the source terms S_c and S_p for the variable ϕ terms.

The correct velocity and pressure fields are obtained when the solution to the momentum equation will result in a velocity field that satisfies the continuity equation. The discretized momentum and continuity equations are given by

$$a_e\, u_e = \Sigma\, a_{nb}\, u_{nb} + b + (p_p - p_E)A_e \tag{2.1.26}$$

$$[(\rho u)_e - (\rho u)_w]\Delta y\Delta z + [(\rho v)_n - (\rho v)_s]\Delta z\Delta x = 0 \tag{2.1.27}$$

The SIMPLER algorithm consists of solving pressure equation to obtain pressure field and solving pressure-correction equation to

correct the velocities. Before describing the SIMPLER algorithm, the pressure correction and pressure equations will be derived.

Pressure Correction Equation

The momentum equation (2.1.26) can be solved only when the pressure field is given. Unless the correct pressure field is employed, the resulting velocity field will not satisfy the continuity equation. Such an imperfect velocity field based on a guessed pressure field p* will be denoted by u*. This "starred" velocity field will result from the solution of the following equation.

$$a_e u_e^* = \Sigma a_{nb}\, u_{nb}^* + b + (p_p^* - p_E^*)A_e \qquad (2.1.28)$$

Our aim is to find a way of improving the guessed pressure p* such that the resulting starred velocity field will progressively get closer to satisfying the continuity Eq. (2.1.27). Let us propose that the correct pressure p is obtained from

$$p = p^* + p' \qquad (2.1.29)$$

where p′ will be called the pressure correction. The corresponding velocity correction u′ can be introduced in a similar manner:

$$u = u^* + u' \qquad (2.1.30)$$

If equation (2.1.28) is subtracted from equation (2.1.26), we get

$$a_e u_e' = \Sigma a_{nb}\, u_{nb}' + (p_p' - p_E')A_e \qquad (2.1.31)$$

By dropping the term $\Sigma a_{nb}\, u_{nb}'$, the velocity correction formula can be written as

$$u_e = u_e^* + d_e\,(p_p' - p_E') \qquad (2.1.32)$$

where

$$d_e = \frac{A_e}{a_e} \qquad (2.1.33)$$

The correction formula for the y-velocity component can be obtained similarly:

$$v_n = v_n^* + d_n (p_p' - p_N') \tag{2.1.34}$$

By substituting u_e and v_n given by velocity correction formula into Eq. (2.1.27), the following pressure correction equation is obtained:

$$a_p p_p' = \Sigma a_{nb} p_{nb}' + b \tag{2.1.35}$$

where

$$b = [(\rho u^*)_w - (\rho u^*)_e]\Delta y\Delta z + [(\rho v^*)_s - (\rho v^*)_n]\Delta z\Delta x \tag{2.1.36}$$

It can be seen from equation (2.1.28) that the term b in the pressure correction equation is essentially (the negative) of the left-hand side of the continuity equation (2.1.27) evaluated in terms of the starred velocities. If b is zero, it means that the starred velocities satisfy the continuity equation. The term b thus represents a 'mass source', which the pressure correction must annihilate for correct velocities.

Pressure Equation

An equation for obtaining the pressure field can be derived as follows: The momentum equation (2.1.26) is written as

$$u_e = \hat{u}_e + d_e (p_P - p_E) \tag{2.1.37}$$

where the pseudo velocity $\hat{u}_e$, which is composed of the neighbor velocities, is defined as

$$\hat{u}_e = \frac{\Sigma a_{nb} u_{nb} + b}{a_e} \tag{2.1.38}$$

Similarly,

$$v_n = \hat{v}_n + d_e (p_P - p_N) \tag{2.1.39}$$

In a manner similar to the derivation of pressure-correction equation, can be written by substituting the expressions for u_e and v_n given above into the continuity equation

$$a_p p_p = \Sigma a_{nb} p_{nb} + b \tag{2.1.40}$$

where

$$b = [(\rho\hat{u})_w - (\rho\hat{u})_s] \Delta y\Delta z + [(\rho\hat{v})_s - (\rho\hat{v})_n] \Delta z\Delta y \tag{2.1.41}$$

The major difference between the pressure-correction equation (2.1.35) and the pressure equation (2.1.40) is that no approximations have been introduced in the derivation of the pressure equation. Thus, if a correct velocity field were used to calculate the pseudo velocities, the pressure equation would at once give the correct pressure.

The SIMPLER algorithm consists of the following steps (Patankar, 1980):

1. Start with a guessed velocity field.
2. Calculate the coefficients for the momentum equations and hence calculate $\hat{u}$, $\hat{v}$ from equation (2.1.38) by substituting the values of the neighbor velocities u_{nb}.
3. Calculate the coefficients for the pressure equation (2.1.40), and solve it to obtain the pressure field.
4. Treating the pressure field as p*, solve the momentum equations to obtain u*, v*.
5. Calculate the mass source b [equation (2.1.36)] and solve and p′ equation.
6. Correct the velocity field by use of equations (2.1.32) and (2.1.34).
7. Solve the discretization equation for other ϕ's.

8. Return to step 2 and repeat until convengence.

The system of algebraic equations, represented by Eq. (2.1.19), is solved iteratively by using a line-by-line TDMA mentioned earlier. The designation TDMA refers to the fact that when the coefficient matrix for these equations is written, all the non-zero coefficients align themselves along the three diagonals of the matrix. In the line-by-line TDMA one considers the values at grid points along a vertical gridline to be unknown (values at P, N and S in Fig. 2.1.3), but substitutes the most recent values at E and W in the algebraic equation which then reduces to a tridiagonal system of equations. The TDMA is then used to solve for ϕ in this vertical direction. In this manner one can traverse along all the lines in the vertical direction sequentially from left to right and right to left of the computational domain. Similarly, the line-by-line TDMA is applied to the horizontal gridlines from bottom to top and top to bottom.

At each iteration it is necessary to employ some degree of underrelaxation when solving the system of algebraic equations.

$$\phi = \lambda \phi_{new} + (1 - \lambda) \phi_{old} \qquad (2.1.42)$$

Unacceptably slow convergence or divergence of the solution is obtained if the factors are too low or too high, respectively. Large pressure corrections arise which produce large u- and v-velocity corrections. If these corrections are too large per iteration, the nonlinearity of the finite difference equations causes divergence.

Velocity and pressure corrections per iteration become smaller as the solution proceeds towards convergence. Thus underrelaxation

factors (expecially for u- and v- velocities) are assigned small initial values and then increased, for faster convergence, as the iteration proceeds. Typical values for swirling flows are 0.2 - 0.4 for the velocity components and 0.4 - 0.7 for the scalar variables. For the nonswirling cases, values up to 0.9 are successfully used for all dependent variables.

Increased accuracy of the initial estimate of dependent variables clearly reduce the amount of computational work required.

Since the user generally desires to utilize such a computer code to solve a series of problems, he generally has converged solutions from previous computer runs of a similar problem. By storing these dependent variables on a disk, a much better initial estimate becomes available for problems of similar or the same configuration.

Final convergence is decided by checking the sum of mass source (b) in the p´ equation and the change of dependent variables during each iteration. Typically, the solution is considered to be converged if the mass source is less than 10^{-6} and no appreciable changes of dependent variables are noticed from one iteration to the next.

Boundary Conditions

The elliptic form of conservation equations represented by equation (a) necessitates the specification of boundary condition for each variable. The computational domain is a symmetrical half section of a furnace (Fig. 1.1). Neumann conditions ($\frac{\partial \phi}{\partial r} = 0$) along the axis of symmetry are imposed for all ϕ except for the radial

velocity. Conditions along the inlet and outlet streams and the walls are given below.

Inlet streams: The inlet axial velocity (u_{IN}) is given and parallel injection is assumed, i.e., $v_{IN} = 0$. The inlet tangential velocity (w_{IN}) is calculated using the expression of swirl number defined (Khalil et al., 1975) as

$$S = \frac{\int \rho\, w\, u\, r^2\, dr}{\int \rho\, u^2\, dr\, R_c} \tag{2.1.43}$$

where R_c is a characteristic radius for the swirl number calculation. Turbulence intensity (I) defined by equation (2.1.44) is specified for k and is used to calculate the inlet value of k

$$I = \frac{(2/3k)^{\frac{1}{2}}}{(u^2)^{\frac{1}{2}}} \tag{2.1.44}$$

Alternatively, the percentage of turbulence kinetic energy (poake) is employed instead of the turbulence intensity.

$$k = \text{poake}\ \frac{u^2}{2} \tag{2.1.45}$$

The dissipation rate (ε) is determined from the following correlation (Smith, 1979):

$$\varepsilon = \frac{C_\mu^{3/4}\ k^{3/2}}{0.25\ D_e} \tag{2.1.46}$$

where D_e corresponds to the characteristic length for the corresponding inlet stream, that is, the radius of fuel nozzle (R_1) and the width of annulus for air stream.

Outlet stream: The axial velocity component is adjusted to satisfy the overall continuity with the inlet gas mass flow rates. It is assumed that all the other variables satisfy Neumann condi-

tion ($\frac{\partial \phi}{\partial x} = 0$).

Wall: A wall function treatment is necessary in near wall region, since the expression of μ_t given by equation (2.1.1) is accurate only for the fully turbulent flow region (and not in the near-wall region) and also to avoid the detailed calculation (requiring a large number of grid points). For the velocity components parallel to a wall, the diffusion fluxes are calculated by defining a effective diffusion coefficient (μ_{eff}) from the empirical law of the wall as

$$\mu_{eff} = \mu \qquad \text{if} \quad y^+ < 11.5$$
$$= \frac{\mu y}{2.5\, \ell n(9y^+)} \qquad \text{if} \quad y^+ \geq 11.5 \qquad (2.1.47)$$

where

$$y^+ = \rho k^{\frac{1}{2}} C_\mu^{\frac{1}{4}} \frac{y_1}{\mu} \qquad (2.1.48)$$

and y_1 is a normal distance from a wall to the corresponding first internal grid point. For the velocity components normal to a wall, Neumann boundary conditions are employed. For the turbulent kinetic energy, generation of turbulent kinetic energy (G_{kl} in Table 2.1.1 is modified by using tangential shear stress wall function (Lilley, 1981):

For north wall,

$$G_{kl} = 2\mu_t[(\frac{\partial u}{\partial x})^2 + (\frac{\partial v}{\partial r})^2 + (\frac{v}{r})^2] + (\tau_{rx}^2 + \tau_{r\theta}^2)/\mu_{eff}$$
$$+ \mu_t(\frac{\partial w}{\partial x})^2 \qquad (2.1.49)$$

where $$\tau_{rx} = \mu_{eff} \frac{\partial u}{\partial r} \qquad (2.1.50)$$

$$\tau_{r\theta} = \mu_{eff} \left(\frac{\partial w}{\partial r} - \frac{w}{r}\right) \tag{2.1.51}$$

For side wall,

$$G_{kl} = 2\mu_t\left[\left(\frac{\partial u}{\partial x}\right)^2 + \left(\frac{\partial v}{\partial r}\right)^2 + \left(\frac{v}{r}\right)^2\right] + \left(\tau_{xr}^2 + \tau_{x\theta}^2\right)/\mu_{eff}$$

$$+ \mu_t\left(\frac{\partial w}{\partial r} - \frac{w}{r}\right)^2 \tag{2.1.52}$$

where $$\tau_{xr} = \mu_{eff} \frac{\partial v}{\partial x} \tag{2.1.53}$$

$$\tau_{x\theta} = \mu_{eff} \frac{\partial w}{\partial x} \tag{2.1.54}$$

The near wall value of ε, from a local equilibrium assumption, is obtained as

$$\varepsilon = \frac{C_\mu^{3/4}\, k^{3/2}}{0.4\, y_l} \tag{2.1.55}$$

Table 2.1.4 summarizes the boundary conditions used in the present study. The symbol N in the table stands for Neumann condition. Footnote (a) to (d) imply the following:

(a) Inlet values are directly specified as Dirchlet conditions.

Table 2.1.4 Boundary conditions for dependent variables.

Algebraic Variables	Inlet	Outlet	North Wall	Side wall	Symmetry axis
u	(a)	(b)	(c)	N	N
v	0	N	N	(c)	0
w	(a)	N	(c)	(c)	N
k	(a)	N	(c)	(c)	N
ε	(a)	N	(d)	(d)	N

(b) The axial velocities at the outlet are adjusted from their immediate upstream values to satisfy overall continuity.

(c) The tangential shear stress wall functions are employed to calculate the diffusion fluxes.

(d) The near wall values of ε are fixed from a local equilibrium assumption.

2.1.4 Turbulence Model Evaluation

Numerical predictions of fluid flow, based on this model, have been reported and comparisons have been made with experimental data under isothermal or reacting flow conditions (Hutchinson et al., 1976; Khalil et al., 1975; Srinivasan and Mongia, 1980; Ramos, 1984). In general, the reported agreement is good.

In this study, a number of predictions have been made and compared with experimental data to verify the accuracy of the turbulence model implementation. Data chosen for these comparisons are the isothermal experimental data of Baker et al. (1974) and Owen (1975). Detailed flow conditions are shown in Table 2.1.5. Fig. 2.1.5 and 2.1.6 show the predicted axial velocity and turbulent kinetic energy distribution and the comparison with the experimental data of Baker et al. (1974). In Fig. 2.1.7, comparison is made against the experimental data of Owen (1975) together with the predictions of Fletcher (1983). In general, agreements are satisfactory.

Table 2.1.5 Flow conditions and combustor dimension

		Baker et al. (1974)	Owen (1975)
Primary Stream	Species		Air
	Velocity (m/s)		2.44
	Turbulent Intensity (%)	Plugged	10
	Radius (m)		0.0318
	Temperature (k)		298
Secondary Stream	Species	Air	Air
	Velocity (m/s)	4.18	29.3
	Turbulent Intensity (%)	14	10
	Temperature (k)	298	298
	Radius (m)	0.055	0.0445
Combustor	Radius (m)	0.15	0.064
	Length (m)	0.90	0.61

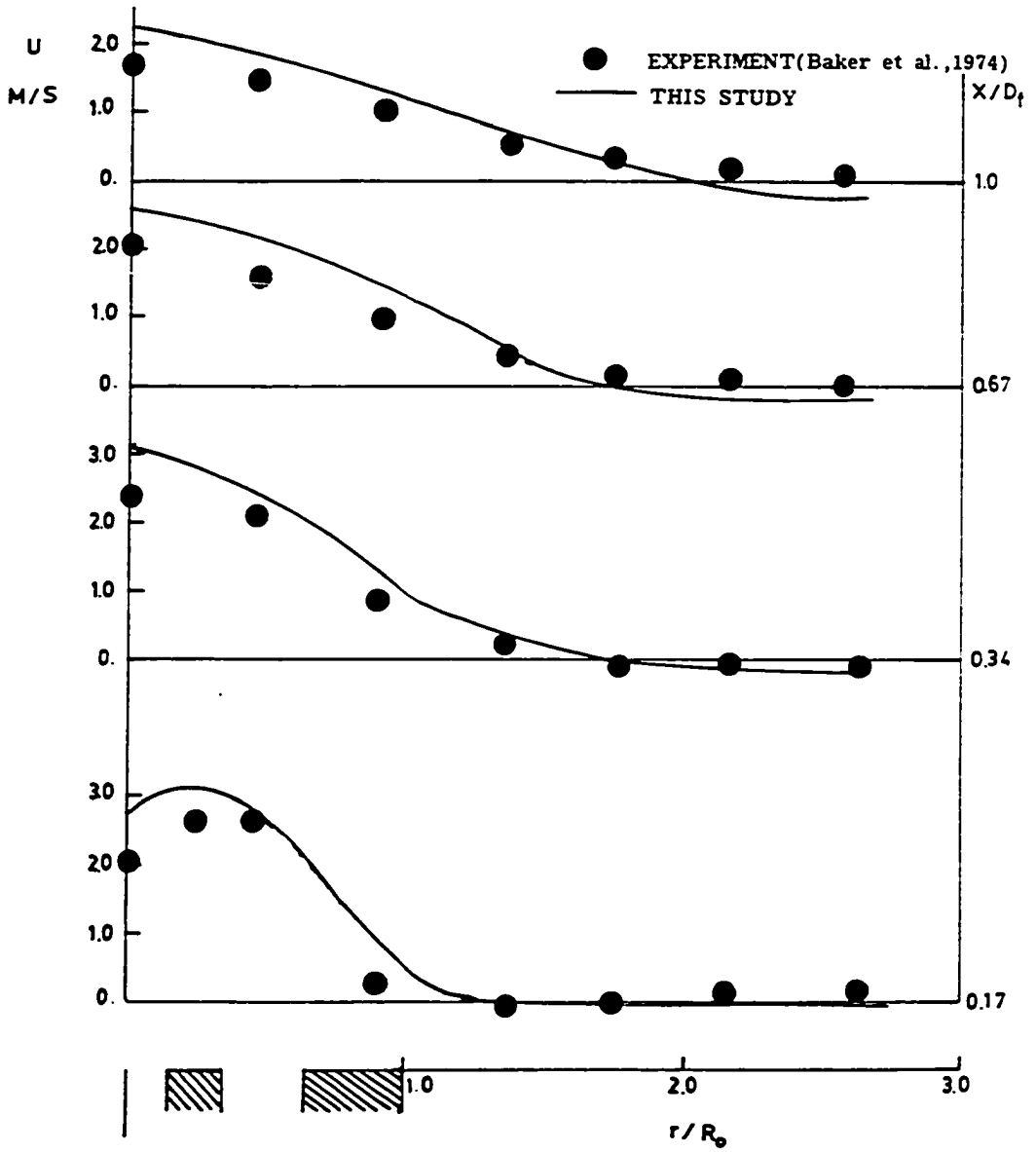

Fig. 2.1.5 Mean axial velocity profile in isothermal, axisymmetric flow

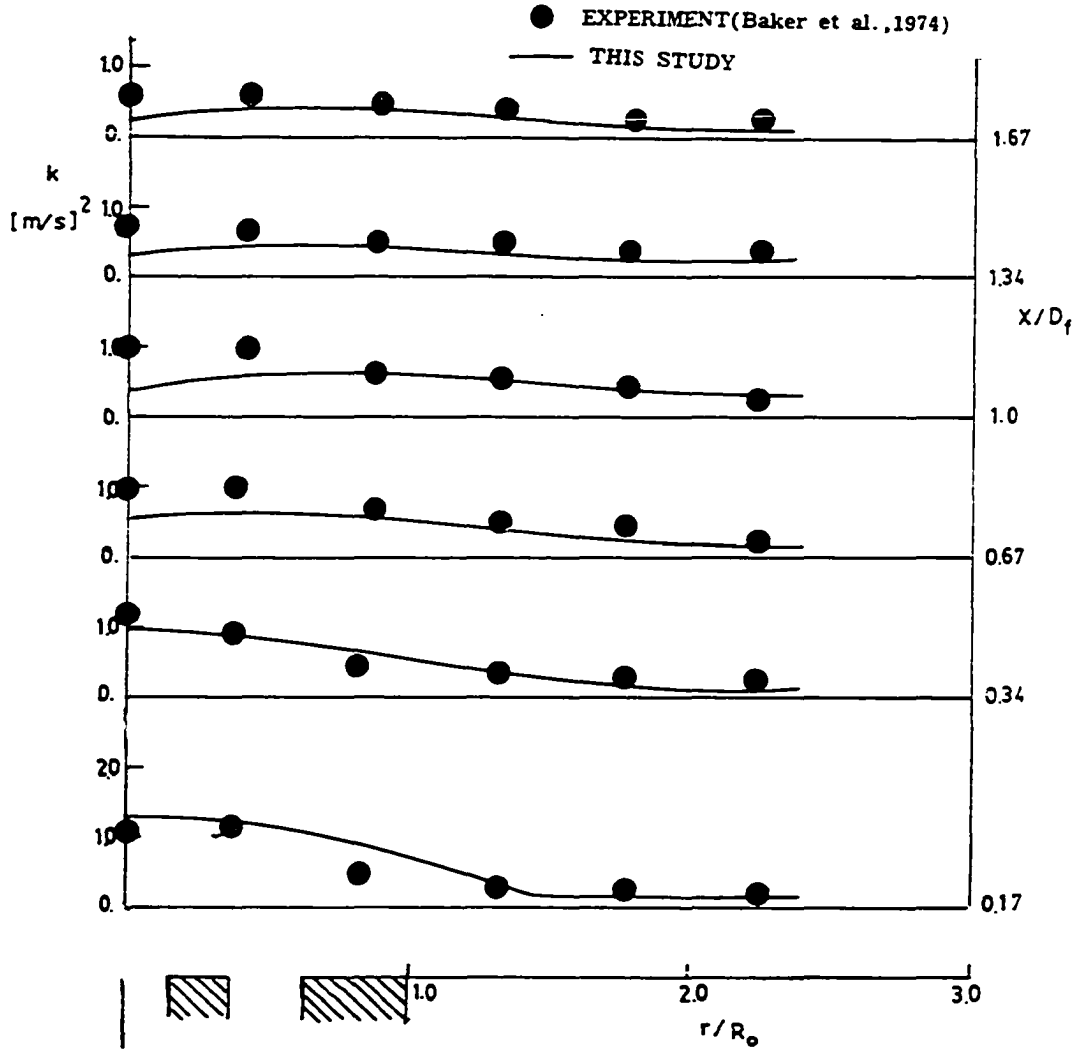

Fig. 2.1.6 Turbulent kinetic energy profile in isothermal, axisymmetric flow

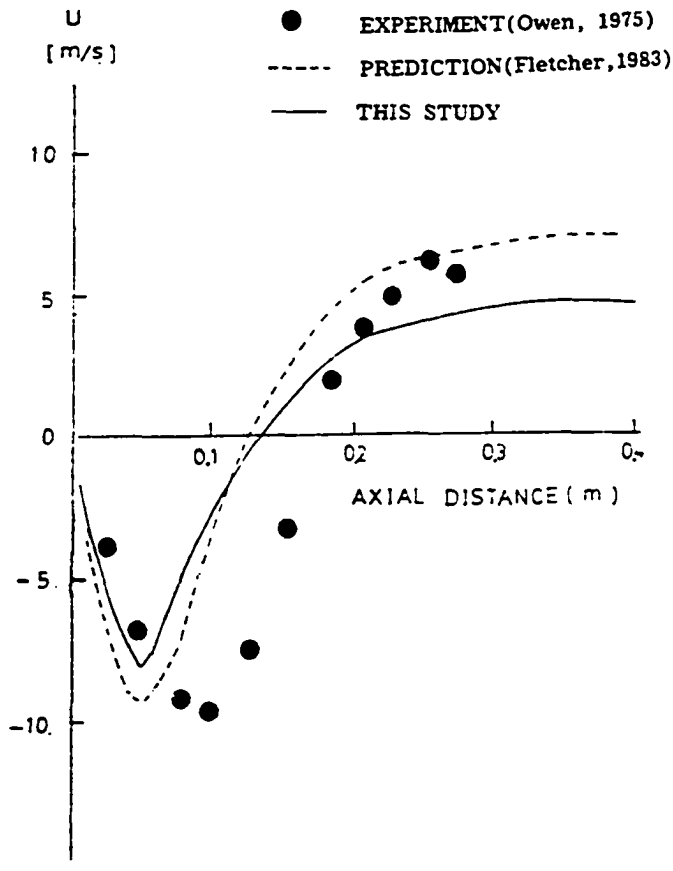

Fig. 2.1.7 Mean axial velocity profile along the centerline in isothermal, axisymmetric flow

2.2 PARTICLE AND TWO PHASE MODELS

Pulverized coal flames typically have a void fraction near unity and the individual particles are quite dispersed. Therefore, a Lagrangian treatment of the particles is performed, representing the particle field as a series of trajectories in terms of particle size group and initial radial locations at the burner exit.

The coal reaction rates are assumed to be slow compared to the turbulence time scale. This allows the particle properties to be calculated from the mean gas properties. The particle motion is governed by the effects of both the turbulent fluctuations and also the mean velocity. Since a detailed discussion of turbulent particle dispersion is given in Chapter 5, only a brief description is provided in this chapter.

The volatilized coal-off gas is assumed to consist of methane, oxygen and nitrogen. Since detailed chemical kinetics is not being considered for the volatile reactions, the accurate elemental composition description is sufficient for the determination of gas phase flame temperature. Particles are defined to consist of coal, char and ash. Char reaction rate is assumed to be governed by oxygen mass diffusion rate and chemical reaction rate. The harmonic mean of these rates is usually used to describe the overall reaction rate (Smoot, 1981).

2.2.1 Particle Phase Equations

Equation of Motion

The equations of particle motion can be expressed as

$$\frac{du_p}{dt} = \alpha\ (u_g - u_p) \qquad (2.2.1)$$

$$\frac{dv_p}{dt} = \alpha\ (v_g - v_p) \qquad (2.2.2)$$

where u and v are the axial and radial velocities, and subscripts p and g refer to the particle and gas phases, respectively. The term α is defined as

$$\alpha = 18\ \mu_g\ C_D\ Re_p/(24\ \rho_p\ d_p^2) \quad , \qquad (2.2.3)$$

where Re_p is the particle Reynolds number given by

$$Re_p = \rho_g\ |\vec{u}_g - \vec{u}_p|\ d_p/\mu_g \quad , \qquad (2.2.4)$$

and C_D is the drag coefficient which is specified according to the expression given by Wallis (1969).

The velocities in equation (2.2.1) - (2.2.4) are instantaneous quantities and the time-averaged forms of the equations may be expressed as

$$\frac{d\bar{u}_p}{dt} = \bar{\alpha}\ (\bar{u}_g - \bar{u}_p) + \overline{\alpha'(u_g' - u_p')} \qquad (2.2.5)$$

$$\frac{d\bar{v}_p}{dt} = \bar{\alpha}\ (\bar{v}_g - \bar{v}_p) + \overline{\alpha'(v_g' - v_p')} \qquad (2.2.6)$$

The second term, on the right side of equations (2.2.5) - (2.2.6) represents the dispersion of the particles due to turbulence in the gas phase, and it is this term that characterizes the turbulent

particle dispersion. Two empirical gradient models (Lockwood et al., 1980; Smith et al., 1981) and a stochastic method (Gosman and Ioannides, 1981) have been reported in the literature. Detailed description of these models and improvements considered in this dissertation are given in Chapter 5.

Particle Energy and Continuity Equations

The particle energy equation must be solved to obtain the particle temperature. The heat of reaction of the coal is assigned to particle phase. The particle energy equation in the Lagrangian form is:

$$m_p C_p \frac{dT_p}{dt} = \pi d_p Nu k_g (T_g - T_p) - H(\frac{dm_p}{dt}) + L(\frac{dm_p}{dt}) + Q_r \qquad (2.2.7)$$

The terms on the right side of the above equation represent heat transfer to or from the particle through convection, char reaction, volatilization and radiation. Nu and k_g denote Nusselt number and gaseous thermal conductivity, and H and L stand for enthalpy of char reaction and latent heat of devolatilization respectively.

Char reaction is suppressed until volatilization is complete and is modeled here, as suggested by Baum and Street (1971), by

$$\frac{dm_p}{dt} = - k_T \pi d_p^2 p \bar{F}_{ox} \qquad (2.2.8)$$

where k_T is the overall rate coefficient, p is the pressure, and F_{ox} is the oxygen volume fraction. The calculation of volatile

release from the particle is again based on the recommendation of Baum and Street (1971),

$$\frac{dx_v}{dt} = \min (Q_p/L, B) \qquad \text{for } T_p > 600 \text{ K}$$

$$\frac{dx_v}{dt} = o \qquad \text{for } T_p > 600 \text{ K} \tag{2.2.9}$$

Where x_v is the fraction of volatile mass released, Q_p is the particle heating rate and B is a maximum devolatilization rate equal to 30 s^{-1}.

2.2.2 Particle Phase Solution Procedure

The solution to the Lagrangian particle equations is obtained by forward integration process. Since the particle equations for a dependent variable ψ can be linearized and expressed as

$$\frac{d\psi}{dt} = A - B\psi, \tag{2.2.10}$$

an explicit forward integration leads to

$$\psi_{n+1} = \psi_n e^{-B\delta t} + A/B (1-e^{-B\delta t}) \tag{2.2.11}$$

where n and n+1 denote the beginning and end of the time increment δt.

The modified Euler's method of integration is employed for the Lagrangian particle continuity and energy equations, while the Euler's method is used for equations of particle motion.

2.2.3 Particle-Gas Coupling

The Eulerian gas phase equations are coupled to the Lagrangian

particle phase equations through particle source terms for mass (S_p^m), momentum (S_p^u and S_p^v) and enthalpy (S_p^h). In order to facilitate the calculation of the particle-gas coupling source terms, the main gas phase control volume is divided into four parts (I, II, III and IV) as shown in Fig. 2.2.1. From any point in one of the four parts, thirteen possible trajectories are assumed. The distance traveled by particle during each time increment δt is limited to the next adjacent subdivision. This restriction is made to maintain the accuracy of the calculation of source terms. By doing this, the particle source term contributions can be calculated efficiently. For example, if particle moves from point- to point- along the trajectory 3 (Fig. 2.2.1), the corresponding source term contributions to the u-momentum and v-momentum equations for the two gas phase control volumes (staggered control volume for the velocities and non-staggered for the mass) crossed by trajectory 3 written as

$$\begin{aligned}
\Delta U_{m,i} &= \Delta U_{m,o}\ \Delta x_1/\Delta x_o \\
\Delta U_{m,i+1} &= \Delta U_{m,o}\ (\Delta x_2 + \Delta x_3)/\Delta x_o \\
\Delta V_{m,j} &= \Delta V_{m,o}\ (\Delta x_1 + \Delta x_2)/\Delta x_o \\
\Delta V_{m,j+1} &= \Delta V_{m,o}\ \Delta x_3/\Delta x_o \\
\Delta m_{m,i} &= \Delta m_{m,o}\ \Delta x_o/\Delta x_o
\end{aligned} \qquad (2.2.12)$$

where $\Delta U_{m,o}$, $\Delta V_{m,o}$ and $\Delta m_{m,o}$ denote the total change in the u-momentum, the v-momentum and the mass along trajectory 3. The Δx_o stands for the total distance traveled during the time increment δt.

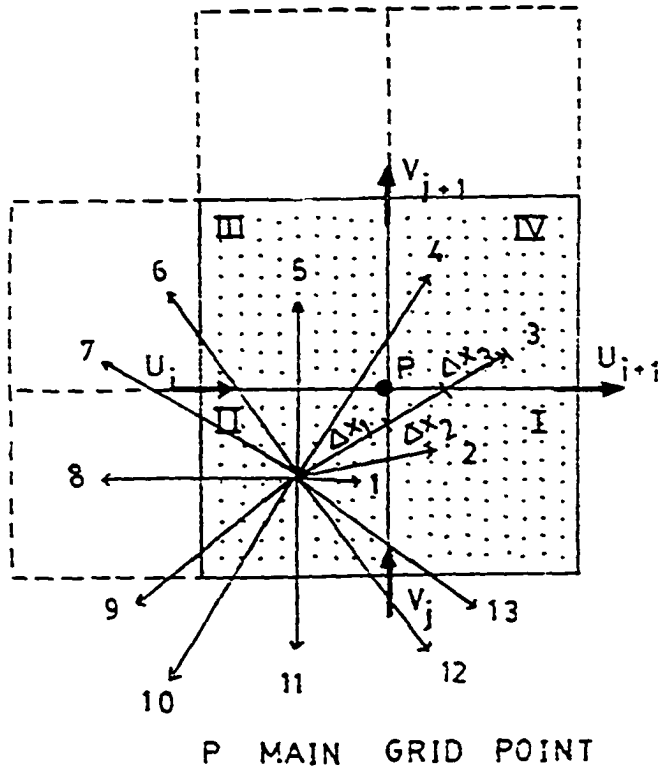

Fig. 2.2.1 Subdivisions of main control volume and possible trajectories

The particle field is modeled as a set of discrete trajectories, where each trajectory represents a number of particles of uniform particle size and particle starting location in the primary jet. It is,therefore, assumed the particle number flow rate along a trajectory is constant. Thus the total particle source term contribution for each particle trajectory during any time increment δt can be obtained from a knowledge of the initial particle mass flow rate.

2.2.4 Four Flux Radiation Model Background

Radiative heat transfer in furnaces is classified into gaseous, non-luminous emission and luminous coal particle emission. In gaseous emission, only the major emitting species such as CO_2 and H_2O are considered and emissivity data for these species are obtained from available data (Sarofim and Hottel, 1978). Radiation to or from a particle is considered to be only from char and ash and the contribution from soot is neglected. The information necessary for particle radiation includes particle size distribution, concentration, temperature and refractive indices. Radiation flux models are described in detail elsewhere (Gosman and Lockwood, 1974; Varma, 1979; Chu and Churchill, 1955), and only a brief description of the four flux model employed in this study is given below.

Governing Equation

In describing the flux radiation model, the anisotropic scattering term is approximated by assuming that all radiation is scattered into one of six mutually orthogonal directions - forward, backward, and to the four sides. The scattered component in each direction can be evaluated by defining anisotropic scattering components such as f, b and s together with the appropriate phase function (Varma, 1979). The terms f, b and s denote forward, backward and sidewise scattering components, respectively.

Considering energy balances in each of the six directions, six first order flux equations can be obtained. Further these first order equations can be combined into second order equations by the following approach of Gosman and Lockwood (1974). The net radiation flux (q) is defined in terms of a positive (I^+) and a negative (I^-) flux

$$\vec{q} = I^+ - I^- \tag{2.2.13}$$

and the flux sum is defined by:

$$\vec{F} = \vec{I}^+ + \vec{I}^- \tag{2.2.14}$$

By manipulating the six first order flux equations together with the axisymmetric condition, the following second-order working equations are obtained:

$$-\frac{d}{dx}\left(\Gamma_F \frac{dF_x}{dx}\right) = (C_1 + C_2) F_x + 2C_3F_r + 2C_4I_b \tag{2.2.15}$$

$$-\frac{1}{r}\frac{d}{dr}\left(\Gamma_F \frac{d}{dr} r F_r\right) = (C_1 + C_2) F_r + 2C_3F_x + 2C_4I_b \tag{2.2.16}$$

and $$F_\theta = 2C_5(F_x + F_r) + 2C_6I_b \tag{2.2.17}$$

where $$\Gamma_F = 1/K_t(1 - \omega_o(f-b)) \tag{2.2.18}$$

and the albedo for scatter, w_o, is expressed as

$$w_o = \frac{K_s}{K_a + K_s} = \frac{K_s}{K_t} \qquad (2.2.19)$$

The terms C_1, C_2, C_3 and C_4 are variables expressed by albedo and scattering components (Varma, 1979) and I_b denotes blackbody radiation.

Coefficients

In order to use the above model, the absorption and scattering coefficients should be evaluated. The absorption coefficient for the medium is given by the sum of the gas and particle absorption coefficients,

$$K_a = K_{ag} + K_{ap} \qquad (2.2.20)$$

The gas and particle absorption coefficients K_{ag} and K_{ap} are expressed as

$$K_{ag} = 1/\ell[\ell n(1 - \varepsilon_g)] \qquad (2.2.21)$$

$$K_{ap} = \sum_j \frac{\pi}{4} Q_a n_j d_j^2 \qquad (2.2.22)$$

Where ℓ, Q_a, n_j and d_j represent the value of the mean beam length, absorption efficiency, particle number density and the particle diameter in a representative particle trajectory j. The gaseous emissivity ε_g is obtained from the available information of CO_2 and H_2O emissivities at different temperatures (Hottel, 1954).

A similar expression can be derived for the scattering coefficient and is given as

$$K_s = \sum_j (\frac{\pi}{4}) Q_s n_j d_j^2 \qquad (2.2.23)$$

The Q_a and Q_s values are available in the literature (Smoot and Smith, 1986).

Solution Procedure

The governing equations for the radiation field does not fit the general form of the gas phase equations, since, not only is the velocity field not associated with the equations shown in Eqs. (2.2.15) - (2.2.16), but also the equations contain derivatives in only the coordinate direction and the application of the line by line TDMA in alternating directions is unnecessary. Once the governing equations for the radiation fluxes are solved, partitioning of the total volumetric heat transfer rate between the gas and particle phases is accomplished by using the respective absorption coefficients. For the gas phase enthalpy equation, the radiative source term can be written as

$$q_{rg} = K_{ag} (F_x + F_r \times F_\theta - I_b) \qquad (2.2.24)$$

Boundary Condition

A. Wall boundary condition: The following assumptions are made to define the boundary conditions at the walls.

1. The boundary is opaque to radiation, that is all thermal flux coming from the surface will be due to either emission or reflection.
2. The boundary is gray, that is, the emissivity of the wall is independent of the wavelength.
3. The boundary surface is diffuse to emission or reflection in all direction.

Since the boundary surfaces are opaque to radiation, the flux balance equation may be written as

$$I_n^- = (1 - \alpha_\omega)\, I_n^+ + \alpha_\omega \sigma T_\omega^4 \qquad (2.2.25)$$

Where α_ω and σ denote absorption coefficient and Stefan-Boltzmann constant respectively. The subscript n stands for the coordinate which is normal to the wall. Utilizing the flux equations (2.2.13) - (2.2.14), the following expression, which contains only the flux sum F_n, can be obtained,

$$\left.\frac{dF_n}{dn}\right|_{wall} = -\frac{\alpha_\omega}{2-\alpha} F_n + \frac{2\alpha_\omega \sigma T_\omega^4}{2-\alpha_\omega} \qquad (2.2.26)$$

Since Eq. (2.2.26) is a flux source term, consideration should be given in converting the flux source term into a volumetric source term.

B. Outgoing boundary condition without reflection:

The outgoing boundary condition without reflection can be set up in a similar fashion with the wall boundary condition. The final expression is written as:

$$\left.\frac{dF}{dn}\right|_{exit} = -\frac{1}{\Gamma} F_n + \left.\frac{2\alpha}{\Gamma} \sigma T^4\right|_{exit} \qquad (2.2.27)$$

Where Γ represents the sum of absorption and scattering coefficients, which is assumed to be unity in this study.

2.2.5 Two Phase Solution Procedure

The overall flow chart to solve the two-phase model is shown at Fig. 2.2.2. The procedure is outlined below:

1. The Eulerian gas field is solved with guessed particle source terms, i.e., S_p^m, S_p^u, S_p^v and S_p^h.
2. The radiation field is solved using the four flux method.

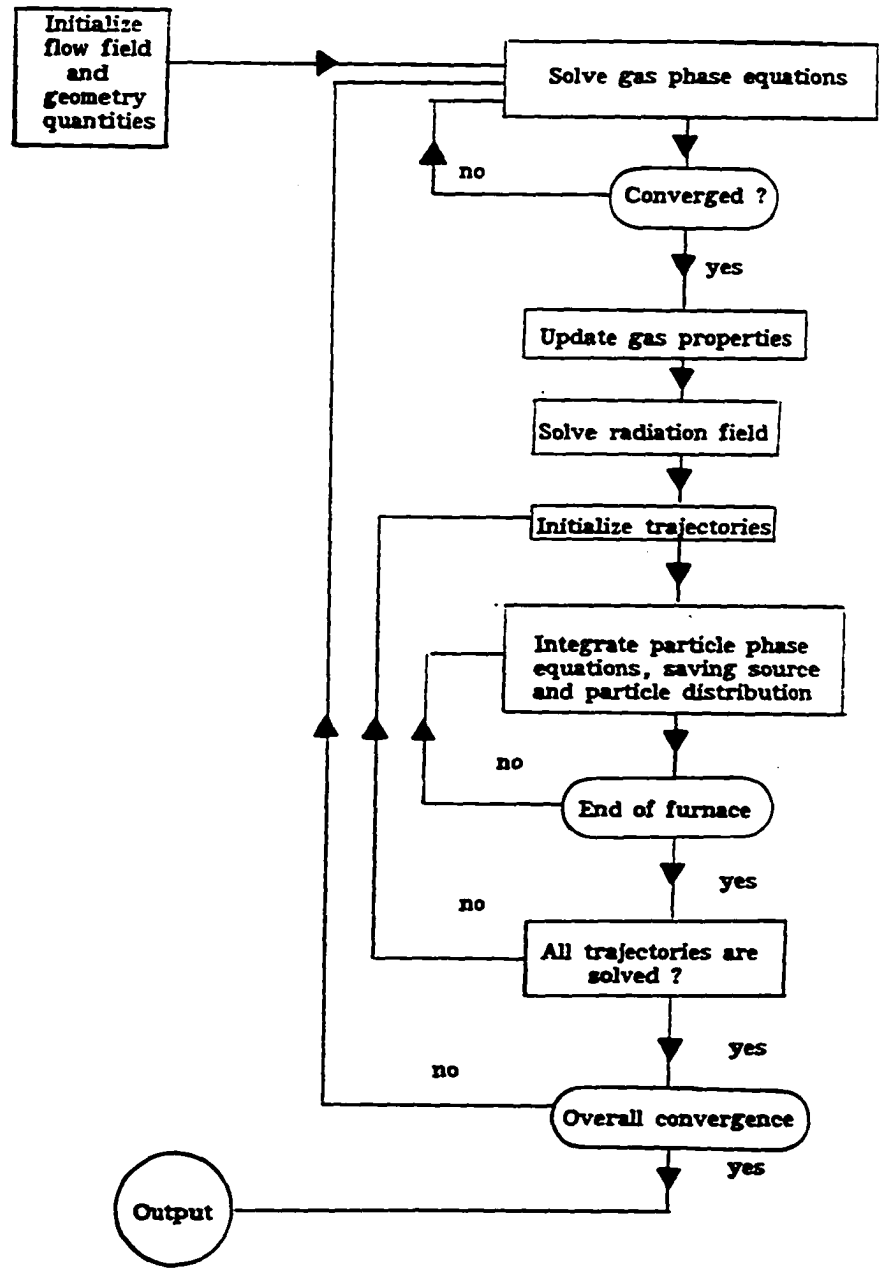

Fig. 2.2.2 Overall flow chart of two phase model calculation

3. The Lagrangian particle field is solved with a representative number of trajectories and the particle source term field is calculated.
4. The gas field is solved with the updated particle source term field.
5. Steps 1-4 are repeated and iteration continued until overall convergence is achieved.

2.3 CONCLUDING REMARKS ON SINGLE AND TWO PHASE MODELS

In this chapter, a brief description of the gas-, particle- and two phase models are given. The solution algorithms used for the comprehensive modeling of pulverized coal combustion, are also described.

CHAPTER 3

NUMERICAL ALGORITHM DEVELOPMENT

This chapter deals with the solution methods of second-order, elliptic, non-linear partial differential equations, using finite difference methods. When velocity components are the dependent variables, special attention has to be paid to the calculation for pressure which is implicitly specified by the continuity equation. In other words, there is no direct equation for obtaining pressure. When the correct pressure field is substituted into the momentum equations, the resulting velocity field will satisfy the continuity equation. This is the basic idea of the SIMPLE (semi-implicit method for the pressure linked equations)(Patankar and Spalding, 1972), algorithm which has been extensively used in resolving the pressure-velocity coupling in incompressible flow problems. The SIMPLE algorithm does a fairly good job of correcting velocities via a series of continuity satisfying velocity fields, but does a rather poor job of correcting the pressure due to the approximation associated with the pressure correction equation.

Examples of typical algorithms that improve on the SIMPLE method are SIMPLER (SIMPLE Revised) (Patankar, 1980) and SIMPLEC (SIMPLE Consistent) (Van Doormaal and Raithby, 1984). In SIMPLER a pressure equation is separately solved for, while in SIMPLEC a more accurate approximation for pressure correction equation is used. Recently Issa (1982) has proposed the PISO (pressure-implicit with splitting operators) algorithm, which is a noniterative time march-

ing procedure and has been shown to be superior to the SIMPLE method.

As a consequence of the need for more efficient solution methods, the evaluation of relative performance of various solution methods has been performed (Latimer and Pollard, 1985). In section 3.1 of this chapter a rather systematic evaluation of the performance of the time marching and/or iterative formulation of the SIMPLER, SIMPLEC and PISO algorithms has been presented for various incompressible steady flow problems. For high swirling flows, numerical convergence is still a problem even for stable iterative formulations as SIMPLER. In order to resolve this problem, a novel decomposition of the centrifugal force term (or the swirl term) appearing in the source term of the radial momentum equation is proposed in this chapter and is described in Section 3.2.

3.1 PRESSURE-VELOCITY COUPLING: COMPARISON OF THE PISO, SIMPLER AND SIMPLEC ALGORITHMS

Since its conception in 1972, the SIMPLE (Semi-Implicit Method for the Pressure Linked Equations) algorithm of Patankar and Spalding (1972) has been extensively used in resolving the pressure-velocity coupling in incompressible flow problems. Over the years, a number of modifications to the SIMPLE algorithm have been proposed (Raithby and Schneider, 1979; Patankar, 1980; Van Doormaal and Raithby, 1984) and have been shown to have better convergence properties. The SIMPLER (SIMPLE-Revised) algorithm of Patankar (1985) and SIMPLEC (SIMPLE-Consistent) algorithm of Van Doormaal

and Raithby (1984) are examples of such modifications and appear to exhibit better behavior than SIMPLE and its other variants. More recently, Issa and co-workers have proposed the PISO (Pressure-Implicit with Splitting of Operators) algorithm (Issa, 1982; Issa et al., 1986) which is a non-iterative time-marching procedure and has been shown in (Issa and Gosman, 1986) to be superior to the SIMPLE method. However, no direct comparison between the PISO algorithm and the SIMPLER and SIMPLEC methods has been made. This, therefore, is the objective of the work presented in this section.

It should be mentioned that the primary interest in this dissertation is on steady state results. Results with the PISO algorithm have been calculated, as proposed in (Issa, 1982), by solving the time dependent equations. Steady state solutions with the SIMPLER algorithm have generally been obtained by starting out with the steady state equations and then solving them by an iterative procedure requiring under-relaxation of the finite difference equations. This approach has been adopted here in obtaining the steady state results with the SIMPLER and SIMPLEC algorithms. In addition, to compare the iterative (with under-relaxation) and time marching procedures for calculating steady state solutions, representative steady state results with the time marching formulations of the SIMPLER and SIMPLEC methods have been obtained. Differences between the two approaches are noted and pointed out.

3.1.1 Solution Algorithms

Since the SIMPLE and SIMPLER algorithms are variants of the SIMPLE method, the SIMPLE algorithm will be described first, followed by the description of the SIMPLEC, SIMPLER and PISO algorithms. In describing these algorithms, it is presumed that the reader is familiar with the basic ideas and notations in the well known SIMPLE method of Patankar and Spalding (1972, 1980).

The differential equation expressing the conservation of momentum in two-dimensions can be written as

$$\frac{\partial}{\partial t}(\rho\phi) + \nabla \cdot (\rho\vec{u}\phi) = -\nabla p + \nabla \cdot (\Gamma\nabla\phi) + S_c + S_p \phi \quad , \quad (3.1.1)$$

where ϕ represents either u or v, Γ is the diffusion coefficient and $S_c + S_p \phi$ is the linearized source term. In the Patankar-Spalding method (1972, 1980), the domain is subdivided into a number of control volumes, each associated with a grid point. The scalar variables and pressure are stored at the grid points while the velocities are stored at the staggered locations as shown in Fig. 3.1.1. The finite difference equations are obtained by integrating the momentum equations over each staggered control volume and expressing the variations of ϕ in each coordinate direction by suitable profile approximations. The results in the discretization equations for u_e and v_n.

$$(a_e + \rho\Delta V/\Delta t)u_e = \Sigma\, a_{nb}\, u_{nb} + A_e(p_p - p_E) + S_c\, \Delta V + \frac{\rho\Delta V}{\Delta t}\, u_e^o, \quad (3.1.2)$$

$$(a_n + \rho\Delta V/\Delta t)v_n = \Sigma\, a_{nb}\, v_{nb} + A_n(p_p - p_N) + S_c\, \Delta V + \frac{\rho\Delta V}{\Delta t}\, v_e^o, \quad (3.1.3)$$

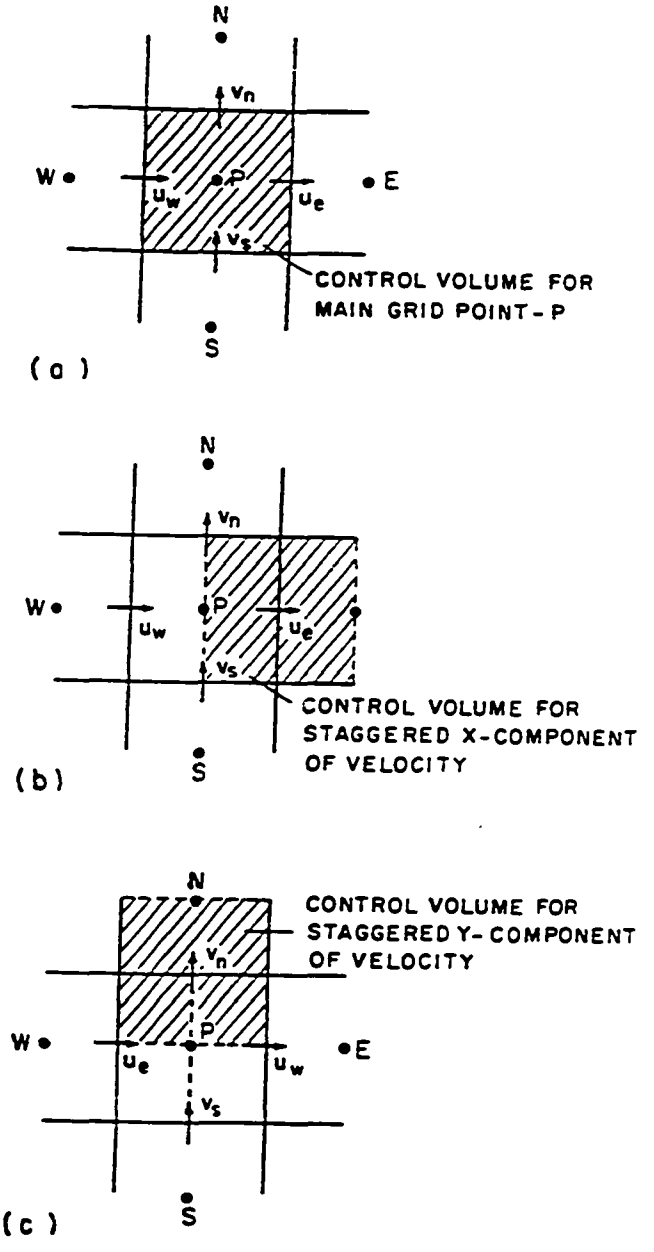

Fig. 3.1.1 Schematic of main and staggered control volumes.

where the summation on the right side of equations (3.1.2) and (3.1.3) is done along the four neighbors (indicated by subscripts nb) and the superscript o denotes the previous time step values. The expressions for the coefficients a_e, a_n and a_{nb} depend on the choice of the profile approximations in each coordinate direction.

Equations (3.1.2) and (3.1.3) represent the finite difference analog of the unsteady momentum equations and the steady state results can be obtained by marching in time. Since, only steady state solutions are of interest, it is not necessary to obtain converged results of the system of algebraic equations, at each time step. Therefore, in this section, at each time step, the coefficients are calculated only once, based on the previous time step solution, and a partially converged result of the system of equations is obtained. At successive time steps, the results approach the steady state values. This approach, eliminates the need for storing the dependent variable values at the present and previous time steps and is termed the Time-Marching procedure in this section.

An alternative approach, and one that is commonly employed, is to start with the steady state form of equations (3.1.2) and (3.1.3) and to solve these equations in an iterative framework using under-relaxation. The under-relaxed discretization equations have the following form

$$a_e \left(1 + \frac{1-\lambda}{\lambda}\right) u_e = \Sigma\, a_{nb}\, u_{nb} + A_e(p_P - p_E) + S_c\, \Delta V + \frac{1-\lambda}{\lambda}\, a_e\, u_e^{*} \quad , \tag{3.1.4}$$

$$a_n\left(1 + \frac{1-\lambda}{\lambda}\right) v_n = \Sigma\, a_{nb}\, v_{nb} + A_n(p_P - p_N) + S_c\, \Delta V + \frac{1-\lambda}{\lambda}\, a_n\, v_n^* \quad , \tag{3.1.5}$$

where λ is the under-relaxation factor and u_e^*, v_n^* indicate results from the previous iteration. Successive solution of equations (3.1.4) and (3.1.5), with the coefficients updated at each iteration, results in the steady state solutions. This approach is called the Iterative procedure.

In comparing the time-marching formulation (equations (3.1.2) and (3.1.3)) with the iterative one (equations (3.1.4) and (3.1.5)), it can be seen that the unsteady term in equation (3.1.1) and the under-relaxation practice have similar effects on the finite difference equations. In fact, equations (3.1.4) and (3.1.5) will take the same form as equations (3.1.2) and (3.1.3), if λ were expressed by the equation.

$$\frac{1-\lambda}{\lambda}\, a_e = \frac{\rho \Delta V}{\Delta t}$$

or $$\lambda = a_e/(a_e + \rho\Delta V/\Delta t). \tag{3.1.6}$$

It should be noted that λ in equation 3.1.6 depends on a_e, which in turn, depends on the velocities. Therefore, λ in the time marching formulation varies spatially and evolves with the solution. In contrast, in the iterative formulation, λ is a constant. As mentioned earlier, the two formulations will be compared with each other. In the discussion that follows, the discretized momentum equations (equations (3.1.2), (3.1.3) or (3.1.4), (3.1.5)) are first re-expressed (for convenience) as

$$\tilde{a}_e u_e = \Sigma a_{nb} u_{nb} + A_e(p_P - p_E) + b_e \quad , \tag{3.1.7}$$

$$\tilde{a}_n v_n = \Sigma a_{nb} v_{nb} + A_n(p_P - p_N) + b_e \quad . \tag{3.1.8}$$

SIMPLE Algorithm: For a guessed pressure field p*, the velocities u* and v* satisfy

$$\tilde{a}_e u_e^* = \Sigma a_{nb} u_{nb}^* + A_e(p_P^* - p_E^*) + b_e \quad , \tag{3.1.9}$$

$$\tilde{a}_n v_n^* = \Sigma a_{nb} v_{nb}^* + A_n(p_P^* - p_N^*) + b_e \quad . \tag{3.1.10}$$

If equations (3.1.9) and (3.1.10) are subtracted from (3.1.7) and (3.1.8), the fully implicit velocity correction (u′, v′) equations are obtained as

$$\tilde{a}_e u_e' = \Sigma a_{nb} u_{nb}' + A_e(p_P' - p_E') \quad , \tag{3.1.11}$$

$$\tilde{a}_n v_n' = \Sigma a_{nb} v_{nb}' + A_n(p_P' - p_N') \quad , \tag{3.1.12}$$

where $u' = u - u^*$, $v' = v - v^*$ and $p' = p - p^*$. (3.1.13)

In the SIMPLE algorithm, the velocity correction equations are obtained by dropping the $\Sigma a_{nb} u_{nb}'$ and $\Sigma a_{nb} v_{nb}'$ terms on the right side of the equations (3.1.11) and (3.1.12) resulting in

$$u_e = u_e^* + d_e(p_P' - p_E') \quad \text{and} \quad v_n = v_n^* + d_n(p_P' - p_N'), \tag{3.1.14}$$

where $$d_e = \frac{A_e}{\tilde{a}_e} \quad \text{and} \quad d_n = \frac{A_n}{\tilde{a}_n} \quad . \tag{3.1.15}$$

To obtain the pressure correction equation, equation (14) is substituted into the discretized continuity equation for the control volume around the main grid point, i.e.,

$$(\rho_p - \rho_p^o)\Delta V/\Delta t + \rho_e u_e A_e - \rho_w u_w A_w + \rho_n v_n A_n - \rho_s v_s A_s = 0. \tag{3.1.16}$$

The resulting pressure correction equation has the following form (see Fig. 1 for notation).

$$a_P p'_P = a_E p'_E + a_W p'_W + a_N p'_N + a_S p'_S + b, \tag{3.1.17}$$

where

$$a_E = \rho_e A_e d_e, \quad a_W = \rho_w A_w d_w, \quad a_N = \rho_n A_n d_n,$$
$$a_S = \rho_s A_s d_s \ , \tag{3.1.18}$$

$$a_P = a_E + a_W + a_N + a_S \ , \tag{3.1.19}$$

$$b = (\rho_P^0 - \rho_P)\Delta V/\Delta t + [\rho_w u_w^* A_w - \rho_e u_e^* A_e + \rho_s v_s^* A_s - \rho_n v_n^* A_n] \tag{3.1.20}$$

and u* denotes the previous iteration value.

Before describing the SIMPLE algorithm, it should be pointed out that the penta-diagonal system of equations represented by equations such as (3.1.9), (3.1.10) and (3.1.17) are solved by line by line Thomas Algorithm in which repeated sweeps of the Thomas algorithm are performed in each coordinate direction until the correct solution to the system of equations is obtained. As pointed earlier, since at any step, the coefficients are tentative (being non-linear), a very accurate solution to the system of equations is unnecessary and, in the interest of computations economy, is undesirable. Therefore, in most of the cases reported here, only a few (1 or 2) sweeps of the Thomas algorithm are performed in each coordinate direction before updating the coefficients for the next step. In this regard, the present approach may differ from others in which, at each time step or iteration, the Thomas algorithm sweeps are repeated until a pre-specified residual criterion is satisfied.

The SIMPLE algorithm consists of the following steps:

1. Guess the pressure field p^*.
2. Solve the momentum equations (equations (3.1.9) and (3.1.10) to obtain u^* and v^*.
3. Solve p' equation (equation (3.1.17)) and update pressure by $p=p^*+\lambda_p p'$ where λ_p is an under-relaxation factor.
4. Update velocity u and v by the velocity correction equation (3.1.14).
5. Repeat steps 2 to 4 until convergence (each step is a time step in the Time Marching formulation and an iteration in the Iterative formulation).

SIMPLEC Algorithm: The SIMPLEC algorithm follows the same general steps as the SIMPLE algorithm with the primary difference being in the formulation of the velocity correction equation. In this approach, $u'_e \Sigma a_{nb}$ is subtracted from both sides of equations (3.1.11) and the term $\Sigma a_{nb}(u'_{nb} - u'_e)$ on the right side of the equation is neglected. A similar operation is performed on the v' equation. The resulting velocity correction equations have the same form as equation (3.1.14) but, with d_e and d_n redefined as

$$d_e = \frac{A_e}{\tilde{a}_e - \Sigma a_{nb}} \quad , \quad d_n = \frac{A_n}{\tilde{a}_n - \Sigma a_{nb}} \quad . \qquad (3.1.21)$$

The pressure correction equation is exactly the same as described earlier (equation (3.1.17)) with the d's in equation (3.1.18) computed from equations such as equation (3.1.21) rather than equation (3.1.15).

The basic algorithm of the SIMPLEC method is identical to the steps in the SIMPLE method but, with λ_p in the pressure equation set equal to 1.

SIMPLER Algorithm: In developing the SIMPLER procedure, it was recognized that the pressure correction equation in the SIMPLE algorithm, in view of the approximation that $\Sigma\, a_{nb}\, u'_{nb} = \Sigma\, a_{nb}\, v'_{nb} \cong 0$, was responsible for the slow convergence of the pressure field. Thus a more suitable equation for updating the pressure field was derived. This was done by first defining a pseudo-velocity $\hat{u}_e$ and $\hat{v}_n$ as

$$\hat{u}_e = \frac{\Sigma\, a_{nb}\, u_{nb} + b_e}{\tilde{a}_e} \quad \text{and} \quad \hat{u}_e = \frac{\Sigma\, a_{nb}\, v_{nb} + b_n}{\tilde{a}_n} \qquad (3.1.22)$$

Thus, equations (3.1.7) and (3.1.8) are re-expressed as

$$u_e = \hat{u}_e + d_e\,(p_P - p_E) \text{ and } v_n = \hat{v}_n + d_n\,(p_P - p_N)\,, \qquad (3.1.23)$$

where d_e and d_n are defined by equation (15). Substituting equation (3.1.23) into equation (3.1.16) leads to the pressure equation:

$$a_P p_P = a_E p_E + a_W p_W + a_N p_N + a_S p_S + b\,, \qquad (3.1.24)$$

where a_E, a_W, a_N and a_S are given by equation (3.1.18), a_P by equation (3.1.19) and b by equation (3.1.20) with u* and v* replaced by $\hat{u}$ and $\hat{v}$. Equation (3.1.24) is a better approximation than the corresponding p′ equation (equation (3.1.17)) in the SIMPLE method.

The SIMPLER algorithm can be described by the following sequence of operations:

1. Using the currently available velocity field calculate $\hat{u}$, $\hat{v}$ from equation (3.1.22).
2. Calculate coefficients of the pressure equation (3.1.24) and solve for the updated pressure field.
3. Using this pressure field, solve the momentum equation to calculate u* and v*.
4. Solve the p′ equation (equation (3.1.17)).
5. Correct the velocity field by the velocity correction equation (3.1.14).
6. Repeat steps 1-5 until steady state or converged solutions are obtained.

PISO Algorithm: The PISO algorithm, as proposed by Issa (1982), is a time-marching procedure, in which during each time step, there is a predictor step and one or more corrector steps. Issa et al. (1986) recommends that the equations be first recast in an incremental form in order to minimize the computing effort and reduce storage requirements. For convenience in notation, converged solution at the previous time step is denoted by a superscript n while the solutions at the present time step are denoted by a superscript * at the predictor level, ** at the first corrector level and *** at the second corrector level.

Equation (3.1.7) can be expressed implicitly as

$$\tilde{a}_e \, u_e^* = \Sigma \, a_{nb} \, u_{nb}^* + A_e(p_P^n - p_E^n) + b_e^n \qquad (3.1.25)$$

and then, updated by

$$\tilde{a}_e\, u_e^{**} = \Sigma\, a_{nb}\, u_{nb}^{*} + A_e(p_P^{*} - p_E^{*}) + b_e^{n} \qquad (3.1.26)$$

Subtracting (3.1.25) from (3.1.26) gives the increment equation

$$u_e^{**} = \hat{u}_e + d_e(p_P^{*} - p_E^{*}) \quad , \qquad (3.1.27)$$

where $$\hat{u}_e = u_e^{*} - d_e(p_P^{n} - p_E^{n}) \qquad (3.2.18)$$

and d_e is given by equation (3.1.15). Similar equations can be derived for u_w^{**}, v_n^{**} and v_s^{**}. Equation (3.1.25) is the velocity predictor equation while equation (3.1.17) represents the first corrector step for velocity. Substitution of equation (3.1.27) into the continuity equation (3.1.16) leads to the pressure equation which is exactly of the same form as equation (3.1.24) with the $\hat{u}$ and $\hat{v}$ in the coefficients given by equations like (3.1.28) instead of equation (3.1.22). This equation is the predictor equation for pressure.

The next set of corrector equations can be derived by expressing equation (3.1.7) as

$$\tilde{a}_e\, u_e^{***} = \Sigma\, a_{nb}\, u_{nb}^{**} + A_e(p_P^{**} - p_E^{**}) + b_e^{n} \qquad (3.1.29)$$

and subtracting equation (3.1.26) from the above equation. This results in a second corrector equation for velocity

$$u_e^{***} = \hat{u}_e + d_e(p_P^{**} - p_E^{**}) \quad , \qquad (3.1.30)$$

where $$\hat{u}_e = u_e^{**} + \{\Sigma\, a_{nb}(u_{nb}^{**} - u_{nb}^{*})\}/\tilde{a}_e - d_e(p_P^{*} - p_E^{*}). \qquad (3.1.31)$$

Similar equations can be derived for u_w^{***}, v_n^{***} and v_S^{***}.

To derive the pressure corrector equation, equations of the form (3.1.30) are substituted into the discretized continuity equation, and again a system of equations represented by equation (3.1.24) is obtained. This equation represents the pressure corrector equation.

The PISO algorithm can be described by the following steps:

1. Using the previous time step solution (u^n, v^n, p^n), calculate the coefficients of the momentum equations (such as equation (3.1.25)) and solve this system of implicit equations. This represents the predictor step for velocity.
2. Using this predicted velocity, calculate coefficients of pressure equation (3.1.24) and solve for the pressure field. This is the predictor step for the pressure.
3. Correct (first corrector step for velocity) the velocity field using explicit type equations such as equation (3.1.27).
4. Using the corrected velocities, calculate the coefficients of the pressure equation in the corrector step and solve the implicit system of equations to obtain an updated pressure field.
5. Using the corrected pressure field, re-evaluate the velocity field (second corrector step) using explicit type equations such as equation (3.1.30).
6. March to the next time step.

In solving turbulent flow problems using the two-equation turbulence model (Launder and Spalding, 1972), the equations for the kinetic energy of the turbulence (k) and its dissipation rate (ε) are strongly coupled with each other and with the momentum equations. Thus to preserve the convergence properties of the PISO algorithm, a predictor-corrector operation in each time step is proposed by Issa et al. (1986). This splitting operation is essentially similar to that described earlier for the momentum equations

with an implicit predictor step and an explicit type corrector step. For other scalar variables, which are linked to the momentum equation through the density or the source term, a two-stage PISO scheme has been employed, in which only a predictor step following the first corrector step of the momentum equation is used to determine the value of the scalar variable at each time step.

3.1.2 Results and Discussion

Results are presented for both the time marching and iterative formulations with the intent of comparing the relative performance of the two approaches. Four test problems are studied. Test problem 1 deals with the sudden expansion of laminar flow in a plane geometry. In test problem 2, isothermal turbulent flow in an axisymmetric geometry with expansion at the inlet and contraction at the exit is examined. Test problem 3 considers reacting, swirling flow in an axisymmetric furnace configuration. The last test problem deals with laminar free convection in an externally heated square enclosure with perfectly conducting horizontal end walls. Two grid sizes are used in obtaining the results; a coarse 7 x 10 or 7 x 12 grid and a finer 20 x 20 grid. Calculations on a very fine grid (80 x 80) have not been made in view of the associated computational expense, and therefore, results in this section may not necessarily be valid for very fine grids. In discussing the results, the relative performances of the various algorithms and the comparison between the time-marching and iterative formulations will be examined. Results are obtained over a suitable range of

relaxation factors λ in the iterative formulation and over a range of dimensionless time steps $\frac{\Delta t\ U}{\Delta x}$ or $\frac{\Delta t\ V}{\Delta r}$ in the time-marching formulation. All results are driven to the same level of convergence.

TEST PROBLEM 1: Sudden Expansion of Flow in a Plane Channel.

A schematic of the test problem configuration is shown in Fig. 3.1.2. The equations of momentum and continuity are solved in the cartesian coordinate system with symmetry conditions imposed along the vertical centerline and zero-gradient conditions at the outflow boundary.

In comparing the PISO results with the iterative SIMPLER and formulation (Fig. 3.1.3), the computing effort with the PISO algorithm is clearly lower for both a coarse (7x12) grid and a finer (20x20) grid with a greater saving of computational effort at the finer grid size. PISO is also superior to the iterative SIMPLEC formulation on the 20 x 20 grid while two algorithms exhibit comparable behavior on the coarse 7 x 12 grid with SIMPLEC requiring slightly lower computing times. The SIMPLEC results, for both grid sizes, generally exhibit lower computing time requirements than the SIMPLER solutions. When the iterative and time-marching SIMPLER and SIMPLEC formulations are compared, the SIMPLEC time-marching algorithm exhibits the best behavior. Converged results with the SIMPLER time-marching method are obtained only for small time steps. It should be mentioned that in making the aforementioned comparisons, the general trends of the plotted lines are compared rather than comparing the cpu seconds for a particulr value along

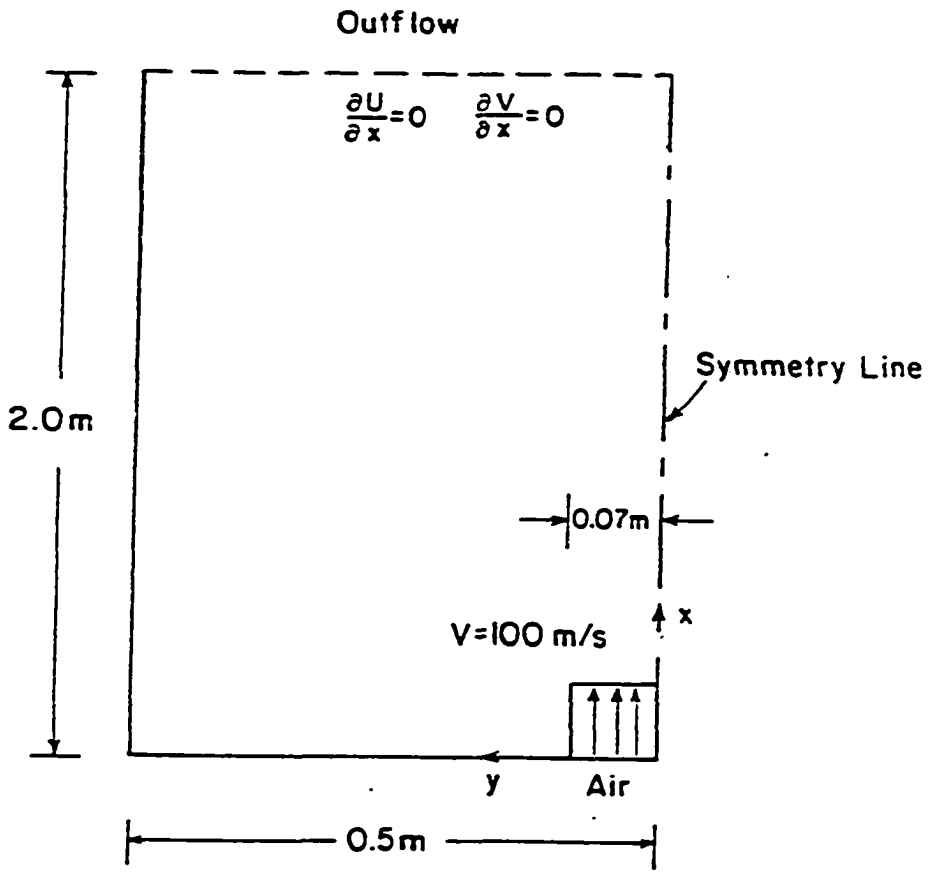

Fig. 3.1.2 Sudden expansion flow in a plane channel

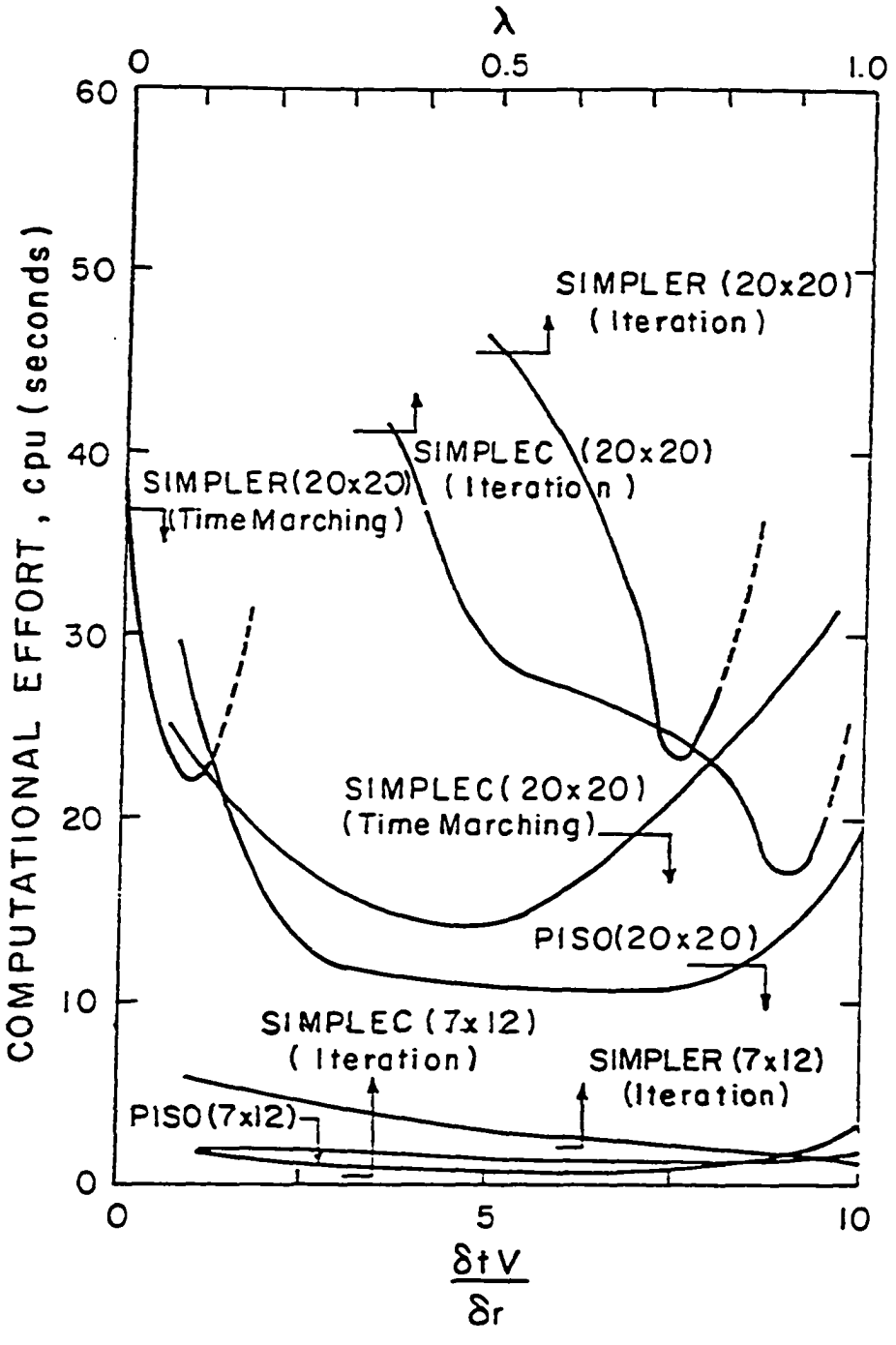

Fig. 3.1.3 Comparison of computational effort for the sudden expansion flow

the abscissa (λ or dimensionless time). It should also be noted that in evaluating the performance of the various algorithms, both the computational effort required and the range of λ or Δt over which the algorithm exhibits low computational requirement, are considered. In this regard, methods which exhibit a sharp dip in cpu seconds followed by a quick increase are not robust and stable methods.

To explain some of the observed behavior it should be noted that in the SIMPLER approach, the velocities are updated (equation (3.1.14)) based on pressure corrections obtained by neglecting $\Sigma\ a_{nb}\ u'_{nb}$ and $\Sigma\ a_{nb}\ v'_{nb}$ terms in the u' and v' equations. Since these terms could be significant, the SIMPELC algorithm improves on the velocity correction formula by neglecting $\Sigma\ a_{nb}\ (u'_{nb} - u'_{e})$ and $\Sigma\ a_{nb}\ (v'_{nb} - v'_{n})$ instead. However, unlike the SIMPLER algorithm no separate equation for pressure is solved, and therefore, neglect of the velocity correction terms in the u' and v' equations is reflected in the pressure equation ($p=p^*+p'$). Thus, it may be surmised that in the SIMPLEC method the velocity corrections are closer to the true value while the pressure corrections are less accurate as compared to the corresponding values in the SIMPLER algorithm. Keeping this in mind and noting that in the SIMPLER method, an additional system of equation represented by equation (3.1.24) needs to be solved, the distinct superiority of one method over another in all possible cases, is unlikely.

PISO, on the other hand, appears to combine the advantages of the SIMPLER and SIMPLEC algorithms. The pressure predictor equa-

tion in PISO is similar to that in the SIMPLER method (equation (3.1.23)) while in the velocity correction equations (equations (3.1.27) and (3.1.30)) are better approximations than those in the SIMPLER and SIMPLEC methods, since, no terms are neglected (as in the SIMPLER and even SIMPLEC approximation). Therefore, the solution is likely to converge faster, even if, PISO due to a larger sequence of operations per step, requires more computational effort in each time step.

TEST PROBLEM 2: Turbulent Flow in an Axi-Symmetric Geometry

The second test problem again deals with sudden expansion of flow but, for turbulent flow conditions in the axi-symmetric geometry shown in Fig. 3.1.4. A two-equation model for the turbulence is used (Launder and Spalding, 1972), in which differential equations for two additional scalar variables, the kinetic energy of turbulence k and its dissipation rate ε are solved. As mentioned earlier, the splitting operations recommended by Issa et al. (1986) for the k and ε equations are adopted here. To account for the near-wall viscous effects, the conventional wall-function method (Launder and Spalding, 1972) is used in this work.

Figure 3.1.5 presents the computing effort requirements of the various algorithms and reveals essentially similar trends as observed in test problem 1. The PISO and the SIMPLEC time marching algorithms exhibit the best behavior in terms of the computing effort required while the SIMPLER time marching formulation again exhibits reasonable behavior only for small time steps and over a small Δt range.

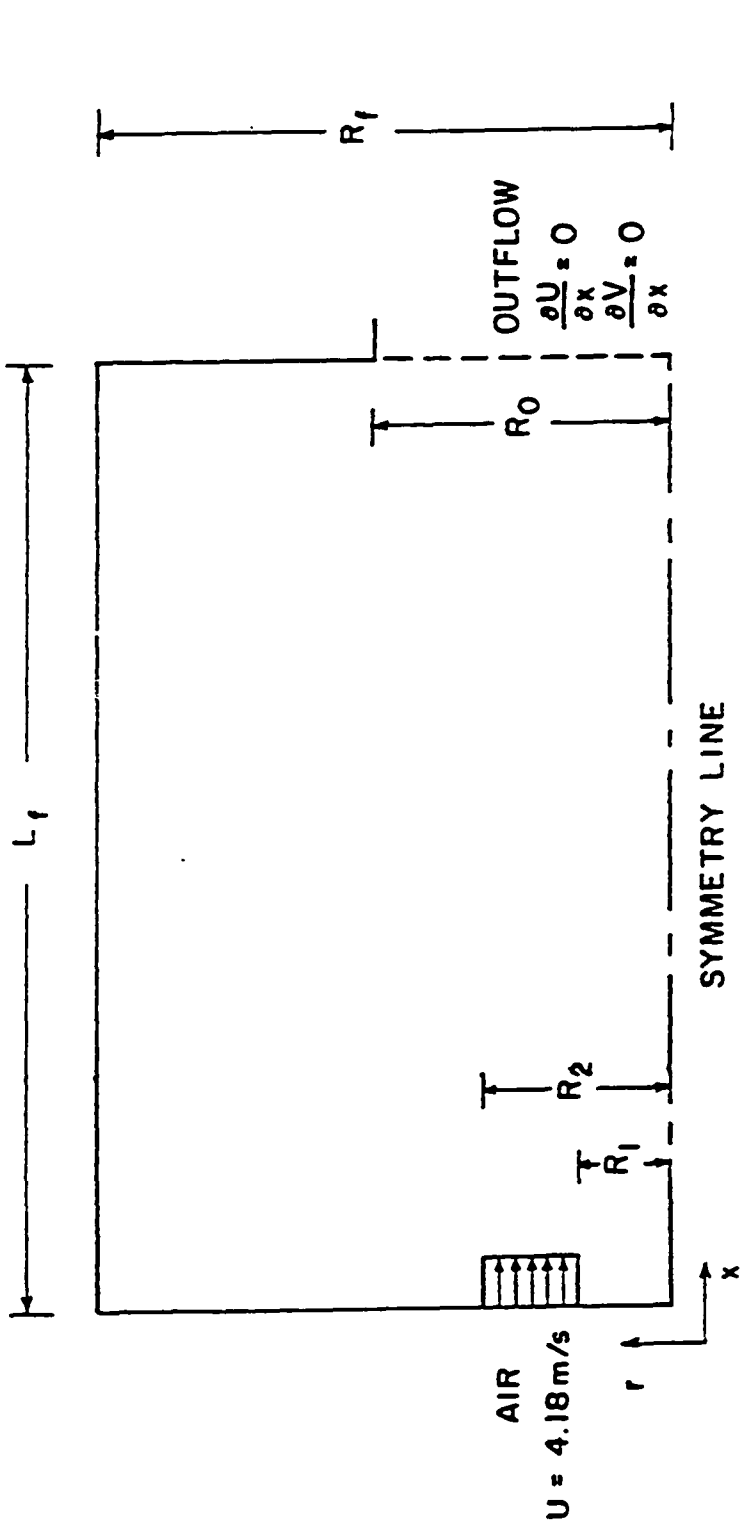

(mm)	
R_1	27
R_2	55
R_0	90
R_f	300
L_f	900

Fig. 3.1.4 Isothermal turbulent flow in an axi-symmetric geometry

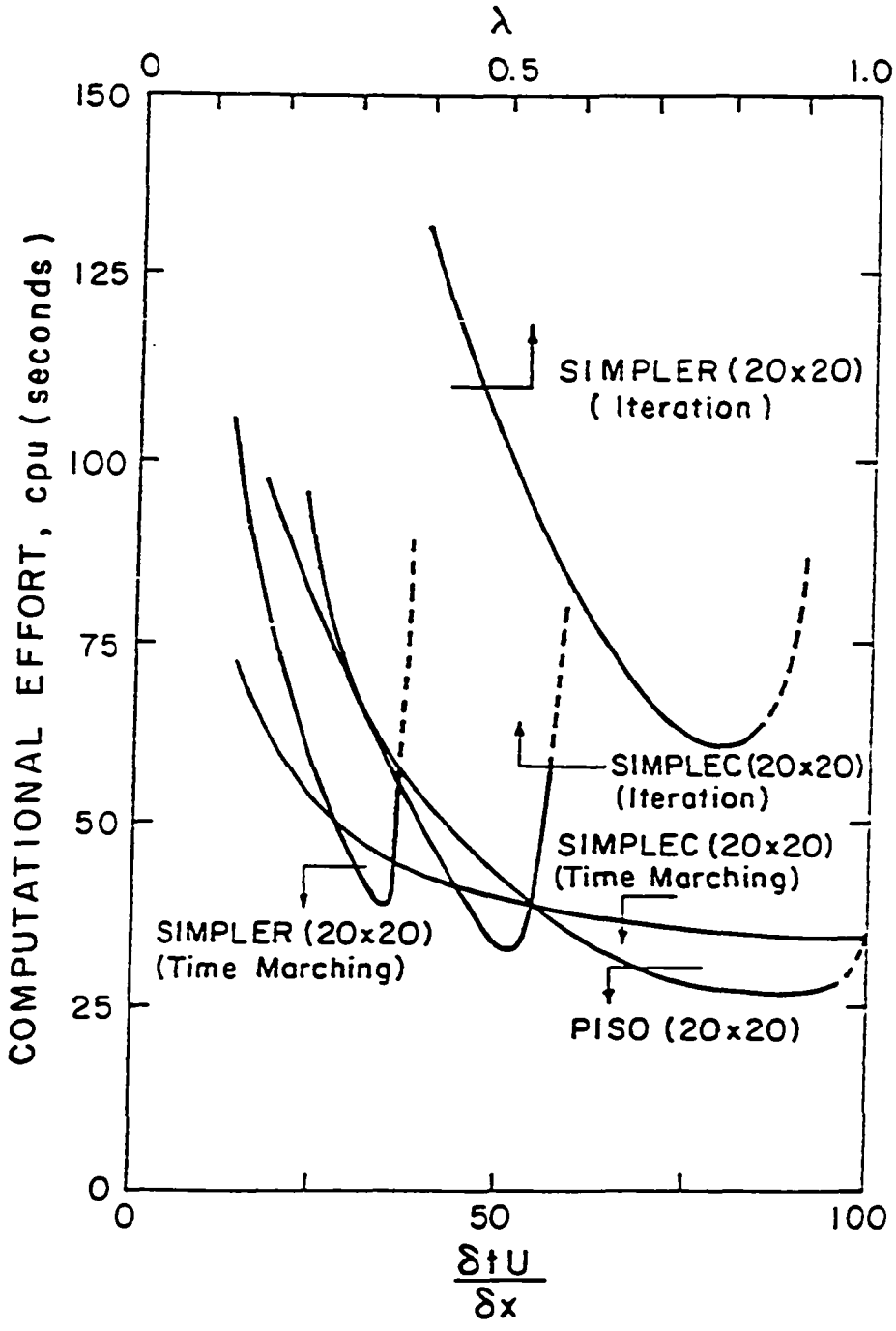

Fig. 3.1.5 Comparison of computational effort for the isothermal turbulent flow

While the comments pertaining to test problem 1 hold here, it should be remarked that in the PISO algorithm the appropriate splitting of the scalar variable equations (for k and ε) into implicit predictor and explicit corrector steps is found to be important in order to maintain a low computational effort.

TEST PROBLEM 3: Swirling, Reacting Flow in an Axi-Symmetric Furnace

The geometry of interes is shown in figure 3.1.6. Methane is injected through the inner nozzle and swirling primary air enters the furnace through the surrounding nozzle. Film cooling air is injected through a port immediately below the outer furnace wall. The inlet velocity of methane is adjusted to satisfy overall stoichiometry at inlet. The inlet tangential velocity of the primary air is characterized by the swirl number, S, defined as

$$S = \left. \frac{\int \rho\, u\, w\, r^2\, dr}{\int \rho u 2\, r\, R_c\, dr} \right|_{\text{inlet}} \qquad (3.1.32)$$

The furnace walls are assumed to be adiabatic and impermeable. The diffusion flame and infinite chemistry assumptions (i.e., fuel and oxygen cannot coexist at the same place and at the same time) are invoked. The flow is assumed to be laminar and steady.

With the aforementioned assumptions, a scalar variable m_{fx} can be defined as

$$m_{fx} = m_{fu} - \frac{m_{ox}}{s}\ , \qquad (3.1.33)$$

where m_{fx} satisfies the convection-diffusion equation with zero source term. The density ρ is calculated using the ideal gas law, i.e.,

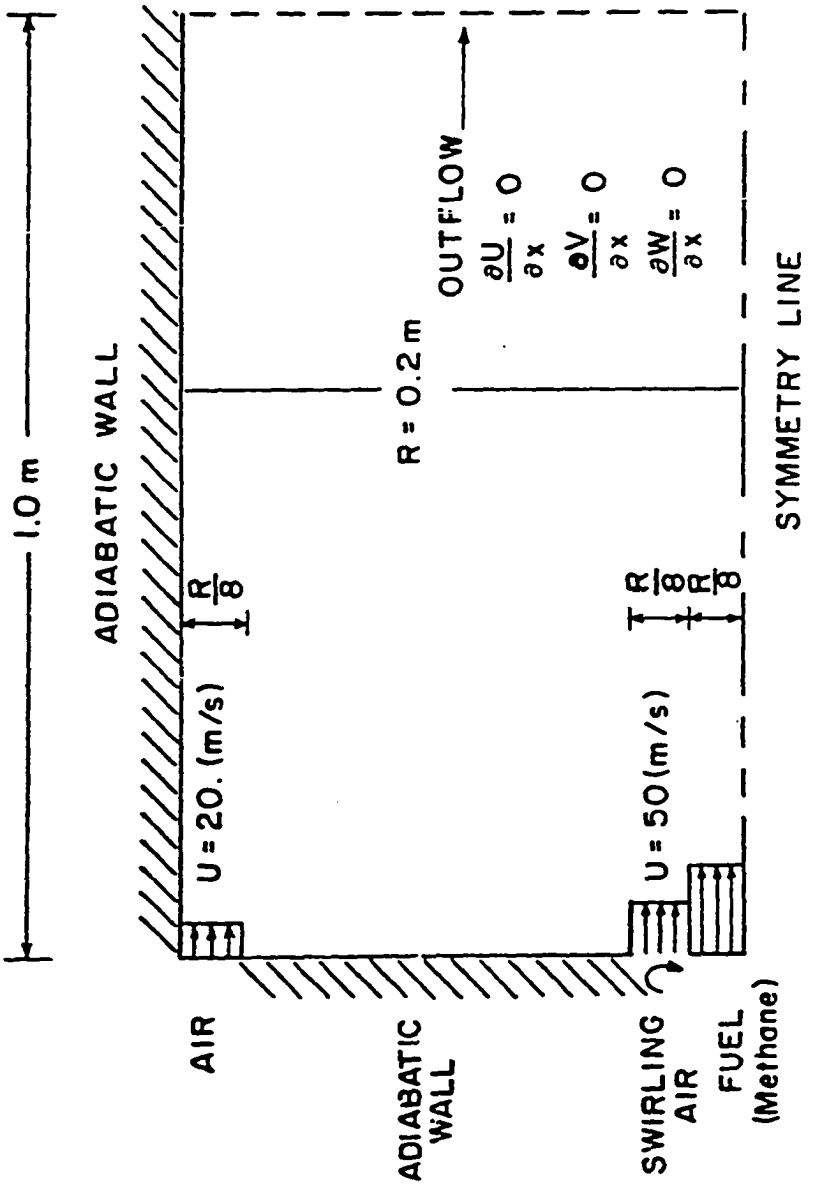

Fig. 3.1.6 Reacting swirling flow in an axi-symmetric furnace

$$\rho = \frac{p/RT}{(m_{fu}/W_{fu}) + (m_{ox}/W_{ox}) + (m_{pr}/W_{pr})} \quad . \qquad (3.1.34)$$

The momentum equations are coupled to the equations for the mass fractions and enthalpy (or temperature) through equation (3.1.34).

In view of the axi-symmetric nature of the problem $\frac{\partial p}{\partial \theta} = 0$. Thus, the tangential velocity equation has the same form as a scalar variable with the coupling between this variable and the momentum equations explicitly appearing as a source term $\frac{\rho w^2}{r}$ in the radial momentum equation. The strength of this coupling is dictated by the magnitude of the swirl number.

In Fig. 3.1.7, results are presented for a low swirl number s=0.04 and indicate quite clearly the superiority of the PISO algorithm for grid sizes of both 20x20 and 7x10. Thus, at low swirl numbers, when the direct coupling between w and the radial momentum equation is weak, PISO as in the earlier two test problems continues to exhibit good convergence properties despite a single predictor step for the scalar variables (w, T, m_{fx}) as recommended by Issa (1986) in the two-stage PISO scheme. The coupling between the scalar variables and the momentum equations, through equation (3.1.34), does not appear to have any adverse effect on the favorable performance of the PISO algorithm.

It should be noted that unlike the earlier two test problems, the SIMPLEC algorithm on the 20 x 20 grid, requires greater computational effort than the SIMPLER method in the iterative formulation and vice versa in the time marching formulation. Both algorithms exhibit poor convergence properties compared to the PISO method. While the smaller cpu time obtained with the SIMPLER

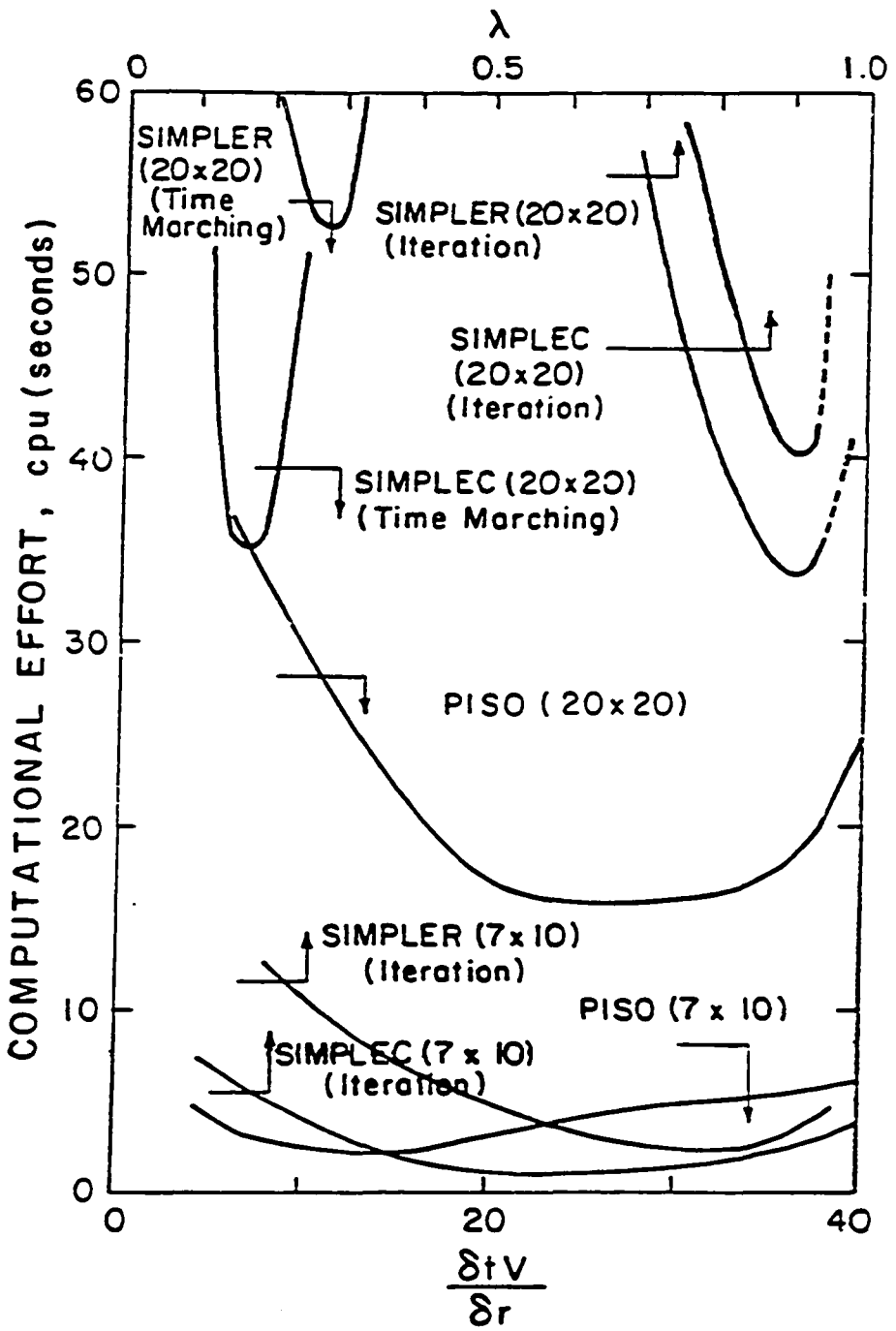

Fig. 3.1.7 Comparison of computational effort for reacting swirling flow in a furnace, swirl number S=0.04

iterative algorithm (compared to the SIMPLEC method) is in contrast with the observations in the earlier test problems, it is in keeping with the previous agrument that since the p-updating scheme in SIMPLER is more accurate but the u- and v-correction procedure involves a greater approximation when compared to the corresponding operations in the SIMPLEC algorithm, consistent superiority of one method over another is unlikely to be observed.

Figure 3.1.8 presents the results for the same problem but at very high swirl number (S=3.5) so that there is a strong coupling between the variable w and the other momentum equations through the source term. In this regard, the nature of the coupling is different to that at low swirl number where the primary coupling is through the density term or that in test problem 2 where the coupling of k and ε to the momentum equations is through the turbulent viscosity, μ_t term. Unlike the low swirl number case (Fig. 3.1.7), PISO does not exhibit very good convergence behavior requiring larger computing effort to obtain steady state solutions as compared to the iterative SIMPLER algorithm and requires nearly as much effort as the SIMPLEC algorithm. This seems to indicate that when the momentum equations are strongly coupled to a scalar variable (or tangential velocity) PISO algorithm does not show robust convergence behavior with reasonable solutions obtained only for small time steps and over a small range of Δt. To explain this behavior it should be noted that the velocity correction steps in the PISO algorithm are explicit type equations and therefore, not unconditionally stable. In view of the explicit nature of these equations, it is likely that PISO tends to become unstable as Δt is

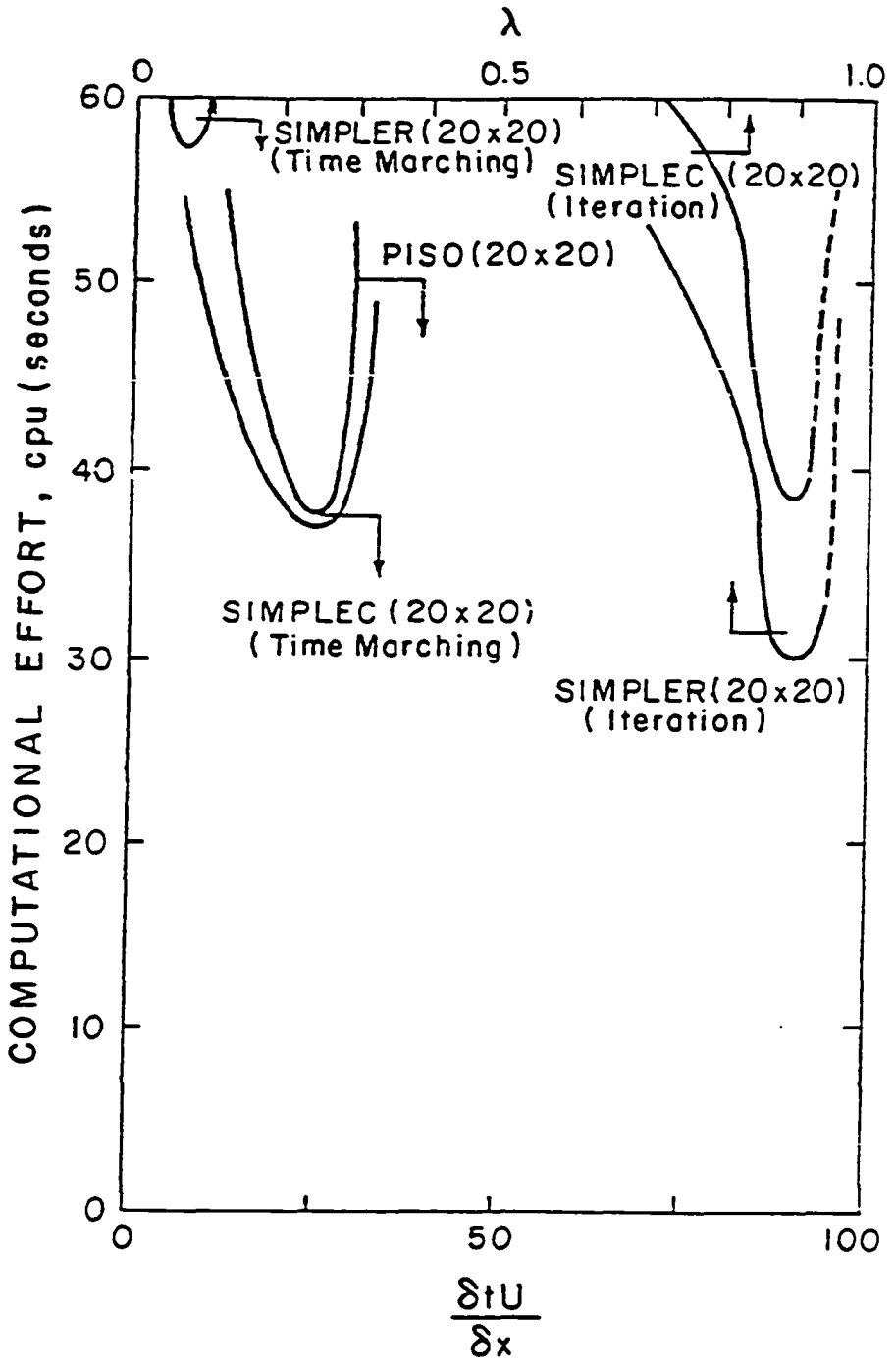

Fig. 3.1.8 Comparison of computational effort for reacting swirling flow in a furnace, swirl number S=3.5

increased leading to larger cpu seconds. To further substantiate this view, it is found that to obtain converged solutions with PISO, it is necessary to solve the implicit system of pressure equations as accurately as possible (both at the predictor and the corrector steps), since otherwise, errors in the p-solution grow rapidly with time steps. Since the solution to the system of equations is obtained by repeated sweeps of the Thomas algorithm, it is necessary to increase the number of sweeps of the Thomas algorithm while solving the p-equation. Failure to do so leads to poor results. These conclusions are further corroborated in the next test problem which deals with enclosure convection and where, the coupling between the scalar variable (temperature) and the momentum equations is solely responsible for the fluid motion.

TEST PROBLEM 4: Free Convection in an Enclosure

A schematic of the square enclosure considered with isothermal vertical walls and perfectly conducting horizontal walls is shown in Fig. 3.1.9. The flow is assumed to be laminar, two-dimensional and stationary. The working fluid is taken to be air and is assumed to satisfy the Boussinesq approximation. Results presented are for a Rayleigh number (Ra) of 10^4.

The dimensionless y-momentum equation, in this problem contains $Ra \cdot \theta$ as a source term where θ is the dimensionless temperature. As mentioned earlier, it is this coupling alone that is responsible for the convective motion. Results in Fig. 10 indicate, as expected (in view of the explicit type corrector steps and the inherent stability restrictions associated with these), the

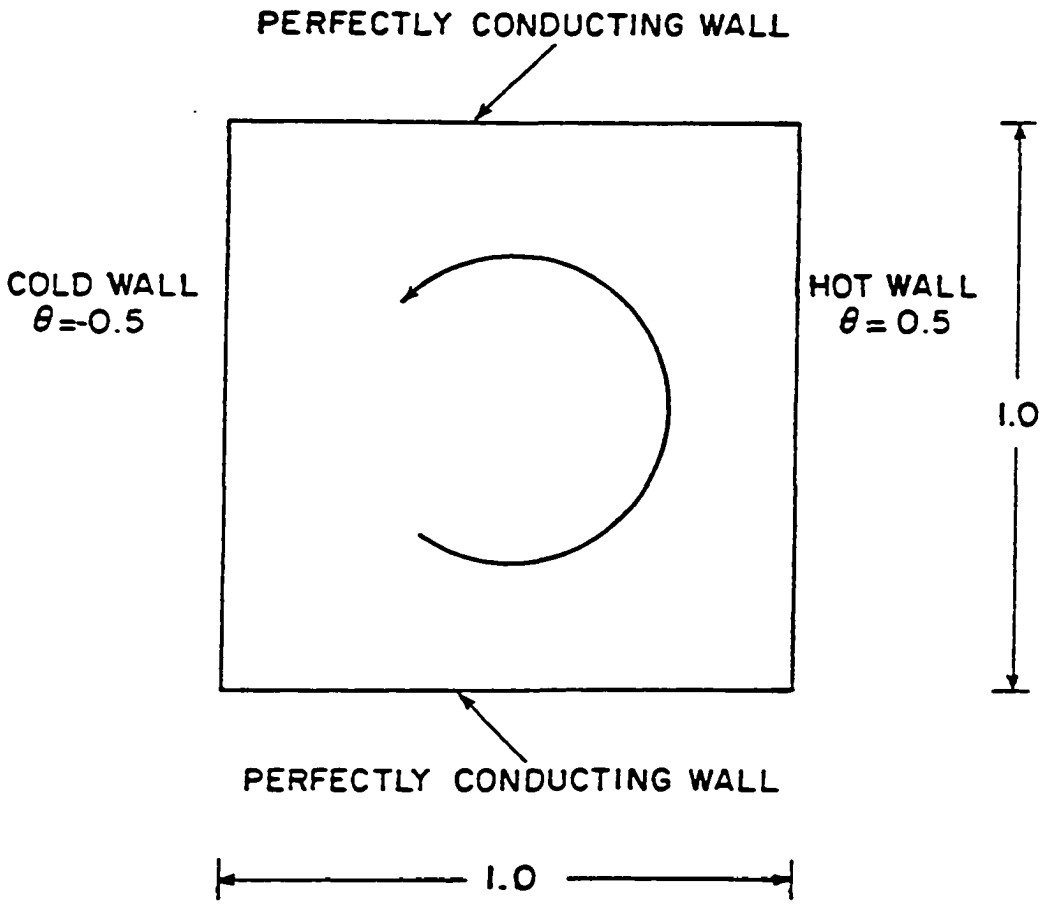

Fig. 3.1.9 Free convection in an enclosure

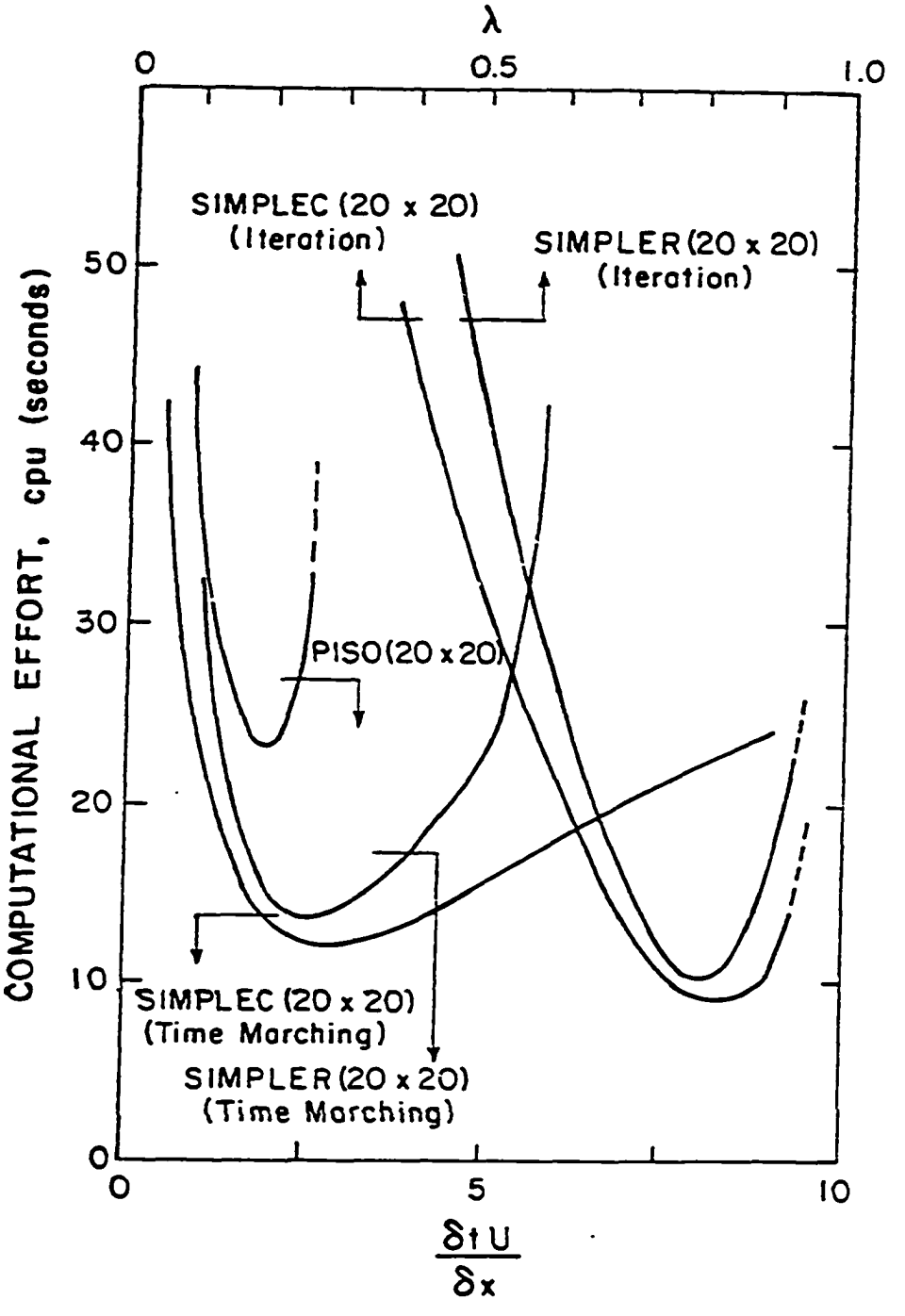

Fig. 3.1.10 Comparison of computational effort for free convection in an enclosure

larger computing effort necessary with the two stage PISO algorithm as compared to the SIMPLER and SIMPLEC methods. The convergence behavior of the SIMPLEC algorithm is noted to be slightly better than the SIMPLER method.

3.1.3 Concluding Remarks on Algorithm Comparisons

A comparative assessment has been made of the convergence behavior of the PISO, SIMPLER and SIMPLEC algorithms. The following conclusions may be drawn.

1. For problems in which the momentum equation is not coupled to a scalar variable, the PISO algorithm clearly demonstrates robust convergence behavior and, in general, requires less computational effort than the SIMPLER and SIMPLEC methods.
2. For the turbulent flow problem, in which the k-ε model for turbulence is invoked, it is necessary to have a two-step scheme (a predictor and a corrector step) for the scalar k and ε equations to ensure superior performance by the PISO method.
3. For scalar variables that are weakly linked to the momentum equations, say through the density term, the two stage PISO algorithm exhibits good convergence behavior compared to the other methods. However, for scalar variables that are strongly linked to the momentum equation, say through the source term as temperature, tangential velocity etc., PISO does not exhibit a robust behavior and gives acceptable results only for small time steps. Furthermore, to obtain converged solutions, it is

necessary at each time step of the PISO algorithm to obtain accurate solutions of the implicit system of pressure equations. The iterative formulations of the SIMPLER and SIMPLEC methods, in such problems, generally exhibit better behavior than the two-stage PISO method.

4. It is difficult to ascertain a clear superiority of SIMPLER over SIMPLEC and vice versa. In general, the iterative formulations of these methods are more robust than the corresponding time-marching formulations although exceptions exist. The time-marching SIMPLER algorithm, in particular, exhibits rather inconsistent behavior.

3.2 IMPROVED SOURCE TERM DECOMPOSITION FOR SWIRLING FLOW CALCULATIONS

Swirling flows are commonly encountered in pulverized coal combustor applications. The governing differential equations for these flows, as noted earlier, are the continuity and the Navier-Stokes equation, and in the numerical calculation of such flows, two factors have an important effect on the convergence characteristics of the numerical scheme. The first is the pressure-velocity coupling, and the method used to resolve this coupling. This issue has been addressed in the preceding section. The second is the coupling between the momentum equations through their respective source terms. Methods to efficiently resolve the source term coupling between the momentum equations have not been given the

same degree of attention. However, in swirling flows, the source terms, and in particular, the centrifugal term $\rho w^2/r$ in the radial momentum equation become important, and if the source term coupling is not properly addressed, rather poor convergence characteristics of the numerical scheme is noted. The objective of this section is to present a source term decomposition technique for the radial momentum equation which greatly enhances the convergence properties of the calculation method and thus reduces the computational time.

3.2.1 Governing Equations

The governing differential equations for steady, laminar, axisymmetric, incompressible flow can be written as

Continuity: $$\frac{\partial u}{\partial x} + \frac{1}{r}\frac{\partial (rv)}{\partial r} + \frac{1}{r}\frac{\partial w}{\partial \theta} = 0 \quad , \tag{3.2.1}$$

Axial momentum: $$\rho \vec{u} \cdot \nabla u = -\frac{\partial p}{\partial x} + \mu[\frac{\partial^2 u}{\partial x^2} + \frac{1}{r}\frac{\partial}{\partial r}(r\frac{\partial u}{\partial r})] \quad , \tag{3.2.2}$$

Radial momentum: $$\rho \vec{u} \cdot \nabla v = -\frac{\partial p}{\partial r} + \mu[\frac{\partial^2 v}{\partial x^2} + \frac{1}{r}\frac{\partial}{\partial r}(r\frac{\partial v}{\partial r})] - \frac{\mu v}{r^2} + \frac{\rho w^2}{r} \quad , \tag{3.2.3}$$

Tangential momentum: $$\rho \vec{u} \cdot \nabla w = \mu[\frac{\partial^2 w}{\partial x^2} + \frac{1}{r}\frac{\partial}{\partial r}(r\frac{\partial w}{\partial r})] - \frac{\mu w}{r^2} - \frac{\rho v w}{r} \quad . \tag{3.2.4}$$

In discretising the above equations, the control volume based finite difference procedure described by Patankar (1980) is used. In this procedure, the domain is subdivided into control volumes each associated with a grid point (Fig. 3.2.1). The momentum

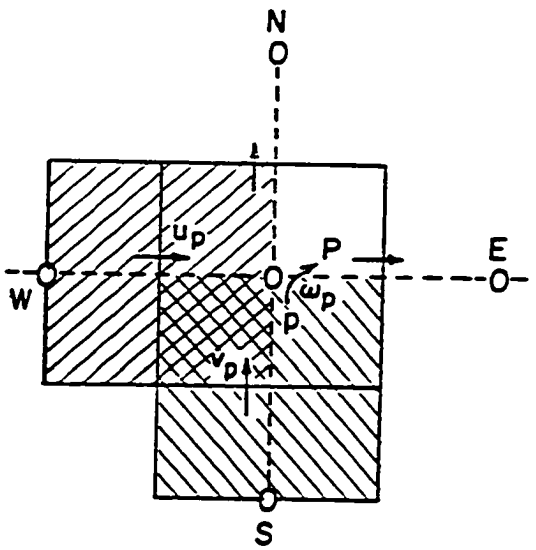

Fig. 3.2.1 Schematic of a control volume

equations are then integrated over each control volume, and by using Green's theorem and profile approximations in each coordinate direction, the axial, radial and tangential momentum equations can each be reduced to the following system of algebraic equations,

$$(a_P - S_P\Delta V_P)\phi_P = a_E\phi_E + a_W\phi_W + a_N\phi_N + a_S\phi_S + S_C\,\Delta V_P \qquad (3.2.5)$$

or $$\tilde{a}_P\phi_P = \Sigma\, a_{nb}\,\phi_{nb} + S_C\,\Delta V_P \quad , \qquad (3.2.6)$$

where ϕ represents either u, v or w, and a_P, a_E, a_W, a_N and a_S are the corresponding convection - diffusion coefficients that depend on the nature of the profile approximation made in each coordinate direction. The terms S_C and S_P arise from a source term linearisation as $S = S_C + S_P\,\phi_P$, and ΔV_P is the volume of the control volume for the grid point P. Equation (3.2.5) is re-written, in a more compact form, as equation (13.2.6) where the subscript nb refers to the four neighbors of the grid point P (i.e., E, W, N, and S in Fig. 3.2.1) and the summation is done over these four neighbors The system of algebraic equations (eqn. (3.2.6)) is solved iteratively. Generally, it is necessary to use an under-relaxation factor λ to obtain converged solutions. At high swirling rates, rather low values of λ's have to be used to prevent the solution from diverging.

The last two terms in eqns. (3.2.3) and (3.2.4) are the source terms of the radial and tangential momentum equation respectively. The most logical, and commonly adopted, decomposition of these source terms at any grid point P (see Fig. 3.2.1) are,

$$S_C = \frac{\rho_P (w_P^0)^2}{r_P} \quad , \quad S_P = - \frac{\mu_P}{r_P^2} \qquad \text{in the v-equation} \qquad (3.2.7)$$

$$S_C = \frac{\rho_P v_P^0 w_P^0}{r_P} \quad , \quad S_P = - \frac{\mu_P}{r_P^2} \qquad \text{in the w-equation} \qquad (3.2.8)$$

where superscript 0 denotes the current variable value in storage. As noted earlier, the decomposition in equation (3.2.7) can lead to poor convergence behavior and even divergence at high swirl rates. An improved source term decomposition method is suggested next.

The method proposed in this technical note uses a corrector form of the discretised tangential momentum equation,

$$\tilde{a}_P \, w_P = \Sigma \, a_{nb} \, w_{nb} - \frac{\rho_P w_P v_P}{r_P} \Delta v_P \qquad (3.2.9)$$

to express the source terms in the radial momentum equation. If, at any iteration, the available solution (in storage) of the implicit system of equations (3.2.9) is denoted by a superscript 0, then a correction to w can be written as,

$$w_P = \frac{\Sigma \, a_{nb} \, w_{nb}^0 - \frac{\rho_P \, w_P^0 \, v_P}{r_P} \, \Delta V_P}{\tilde{a}_P} \quad . \qquad (3.2.10)$$

If equation (3.2.10) is substituted for w_P in the discretised source term of the radial momentum equation, the right hand side of the equation below (eqn. 3.2.11) results. This expression has been written is in the desired linearized form of $S_C + S_P \, v_P$, i.e.,

$$S_C + S_P v_P = \left[\frac{\rho_P}{\tilde{a}_P^2 r_P}\left\{\left(\Sigma a_{nb} w_{nb}^0\right)^2 + \left(\frac{\rho_P w_P^0 v_P^0}{r_P}\Delta V_P\right)^2\right\}\right]$$

$$- \left[\frac{2\rho_P}{\tilde{a}_P^2 r_P}\left\{\left(\Sigma a_{nb} w_{nb}^0\right) \cdot \rho_P w_P^0 \Delta V_P\right\} + \frac{\mu_P}{r_P^2}\right] v_P \quad . \quad (3.2.11)$$

Thus, the first square-bracketed term in equation (3.2.11) is taken to be the S_C term, while the second square-bracketed term with the negative sign is the S_P term of the radial momentum equation.

It should also be noted, that in the calculation procedure described in Patankar (1980), the location of the axial and radial velocities are staggered, as shown in Fig. 3.2.1. This is done in order to avoid checkerboard velocity and pressure fields. Therefore, the storage location of the tangential and radial velocities are different, and to evaluate the tangential velocities on the right hand side of equation (3.2.11), it is necessary to interpolate. In obtaining the results shown in this section, it is found advantageous to stagger the location of w in the radial direction, so that w and v are stored at the same location. With this practice, interpolation is not necessary in evaluating the source terms, and this approach is, therefore, used in the present work.

3.2.2 Results and Discussions

The performance of the source term decomposition in equation (3.2.11) is examined by comparing the results with those obtained by using the conventional source term decomposition in equation (3.2.7). For this purpose, the test problem of isothermal flow in an axisymmetric sudden expansion (Fig. 3.2.2) is chosen. Slug flow is assumed at the inlet with a uniform swirl velocity characterized

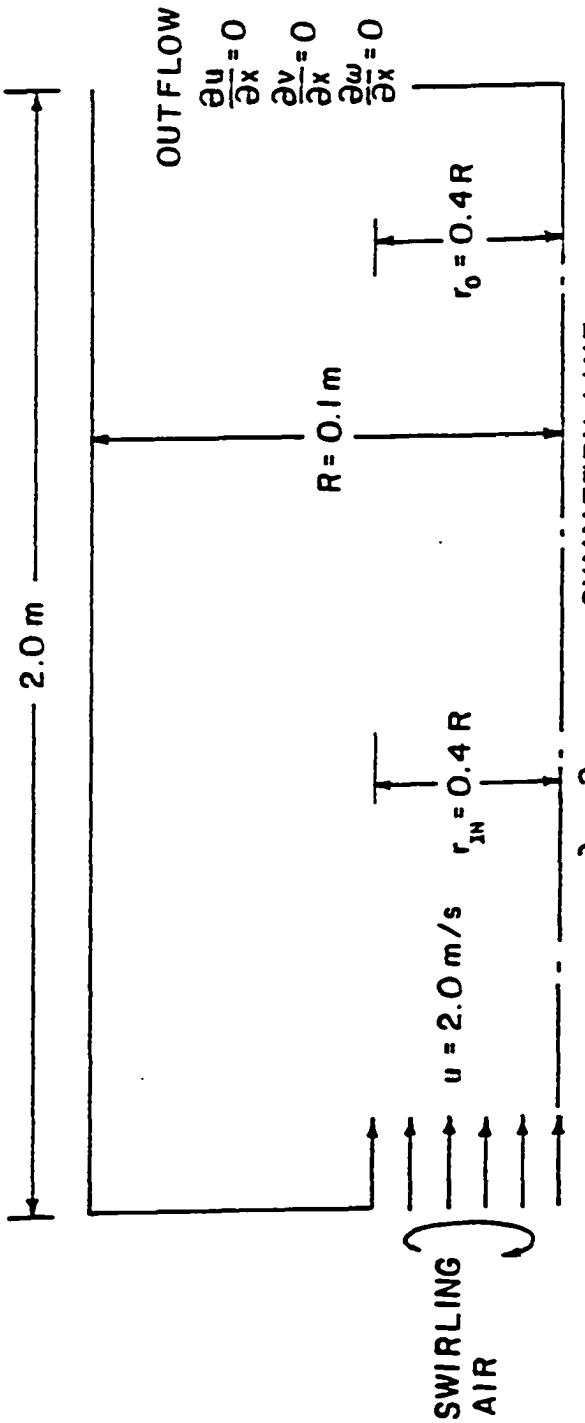

Fig. 3.2.2 Isothermal flow in an axisymmetric expansion

by a swirl number S defined as

$$S = [\int_0^{r_{IN}} \rho\, u\, w\, r^2\, dr / \int_0^{r_{IN}} \rho\, u^2\, r\, R_c\, dr]_{inlet} \quad , \qquad (3.2.12)$$

where r_{IN} is the inlet opening radius. Results are obtained for a low (S = 0.5) and a high (S = 2.0) value of the swirl number.

Calculations are made with a 10 x 30 grid on an IBM 3084 machine. Iterations are continued until the following residual convergence criterion is satisfied

$$[\, \|r_u\|^2 + \|r_v\|^2 + \|r_w\|^2]^{\frac{1}{2}} \leq 10^{-5} \quad , \qquad (3.2.13)$$

where r_u is the Eucledian norm of the residual for u, and is defined as

$$\|r_u\| = [\sum_{C\text{-}V} \{ \sum_{nb} a_{nb}\, u_{nb} + S_C\, \Delta V_p - \tilde{a}_p\, u_p \}^2]^{\frac{1}{2}}. \qquad (3.2.14)$$

The outer summation in the above equation is performed over all the control volumes in the domain.

Results are presented in Fig. 3.2.3 for S = 0.5, and in Fig. 3.2.4 for S = 2.0. The computational effort expressed as the number of iterations (shown on the vertical left axis), and the CPU time in seconds (shown on the vertical right axis) are plotted against the under-relaxation factor λ.

At low swirl rates (S = 0.5), both the conventional source term decomposition (eqn. (3.2.7)), and the source term decomposition recommended in this section (eqn. (3.2.11)) exhibit similar behavior (Fig. 3.2.3). However, at the higher swirl rate (S = 2.0), the advantages of the recommended source term decomposition (eqn. (3.2.11)) are clearly evident. A five fold decrease in computational effort is obtained with the source term decomposition

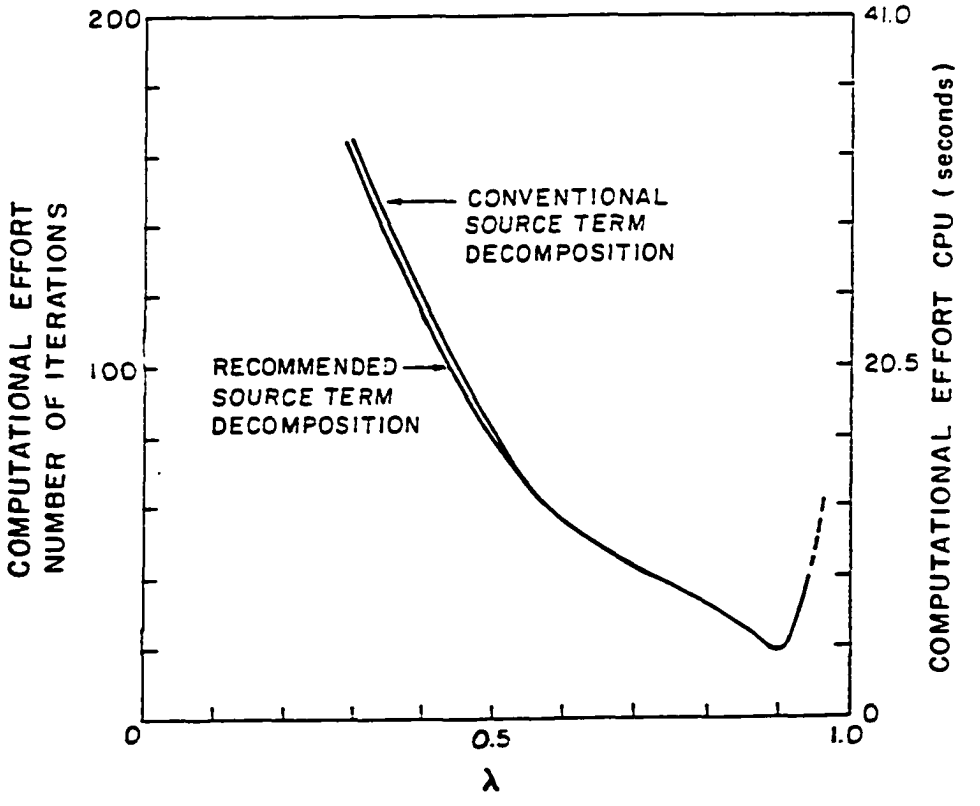

Fig. 3.2.3 Comparison of computational effort for swirl number S = 0.5

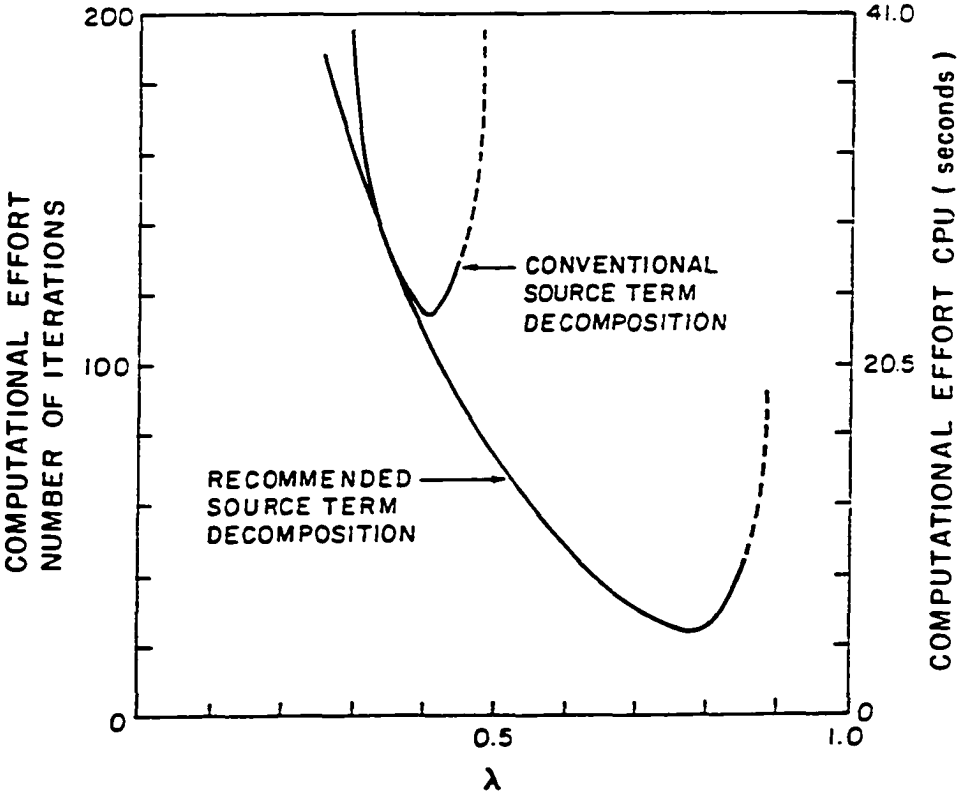

Fig. 3.2.4 Comparison of computational effort for swirl number S = 2.0

proposed in equation (3.2.11). More importantly, the solution algorithm exhibits stable convergent behavior over a wide range of under-relaxation factors (for λ nearly up to 0.8).

Based on the aforedescribed comparisons, it is recommended that in swirling flows the source term decomposition in equation (3.2.11) should be used. A considerable decrease in computational effort is obtained, if done so.

3.2.3 Concluding Remarks on Source Term Decomposition Method

A source term decomposition method is proposed, and shown to be computationally advantageous in highly swirling flows. The proposed method uses a corrector form of the tangential momentum equation to decompose the source terms of the radial momentum equation.

3.3 CONCLUDING REMARKS ON NUMERICAL ALGORITHM DEVELOPMENT

This chapter provides an evaluation of the relative performances of numerical algorithms to resolve pressure-velocity coupling such as PISO, SIMPLER and SIMPLEC. A source term decomposition method is developed, which is shown to be computationally advantageous in high swirling flows.

CHAPTER 4

GAS PHASE TURBULENT REACTIONS-MODELING OF NONEQUILIBRIUM EFFECTS

As mentioned in Chapter 1, the basic problem in modeling gaseous turbulent reactions lies in the proper closure of the turbulent correlation terms, that arise in time-averaging the non-linear chemical reaction source terms. Most turbulent combustion models circumbent this difficulty by ignoring the chemical kinetic aspects of the problem and model the reaction using turbulent mixing as the rate limiting step. In other words, chemical equilibrium is presumed. However, the fast chemistry assumption is not valid for many practical situations and nonequilibrium effects such as flame extinction or quenching, minor species formation and slow chemical reactions, play an important role. In such situations, both chemical kinetics and turbulent mixing should be considered.

In this chapter, a non-equilibrium turbulent reaction model is developed is to model flame extinction phenomena encountered in intensive, nonpremixed turbulent combustion. This model is called the modified perturbation model and is described later.

4.1 NON-EQUILIBRIUM MODELS FOR LOCAL FLAME QUENCHING IN INTENSIVE TURBULENT REACTIONS

In the modeling of non-premixed reacting flows, chemical

equilibrium is generally assumed leading to the popular "fast chemistry" models. In such models, a conserved scalar ξ is defined, and species mass fractions Y_i and enthalpy h can be shown to be instantaneously related to ξ alone, i.e., $Y_i(\xi)$, $h(\xi)$. Therefore, if the time-averaged value ξ and the variance $\overline{\xi''^2}$ are computed using balance equations, the time averages for other scalar quantities can be simply determined as mentioned in section 2.1,

$$\bar{Y}_i = \int_0^1 Y_i(\xi)\ p\ (\xi)\ d\xi \qquad (4.1)$$

where $p(\xi)$ is an assumed probability density function for ξ.

However, it is well known that most non-premixed flames are characterized by local non-equilibrium effects (Brzustowski, 1980; Kalghatgi, 1981), and for realistic predictions, the fast chemistry model should be extended to account for local quenching and non-equilibrium behavior. The primary objective of this section is to present a simple model to predict the departure from equilibrium in turbulent non-premixed flames.

A number of models have been proposed that incorporate non-equilibrium or local quenching effects. Peters and co-workers (Peters and Williams, 1983; Janica and Peters, 1982) have assumed that the turbulent non-premixed flame is made up of an ensemble of laminar flamelets subjected to the effects of stretch and strain due to the turbulent flow field. They further assume that when the local rate of strain, characterized by a scalar dissipation rate x, exceeds a critical value x_q, local quenching occurs. However, considerable uncertainty exists regarding the value of x_q and how it should be calculated. Liew et al. (1984) have also assumed a

stretched laminar flamelet to represent the microscopic element in the turbulent flame. However, their model has provisions for the incorporation of realistic chemistry, with local conditions at any point described by any one of a family of flamelets whose members are distinguished from each other by the value of x at the maximum temperature x_{max}, and therefore in each flamelet

$$Y_i = Y_i(\xi, x_{max}) \tag{4.2}$$

The functional relationship in equation (4.2) can be obtained, for example, from measurements. Time averaged values are calculated by assuming statistical independence of ξ and x_{max} and assuming that for $x_{max} > x_q$ equation (4.2) is replaced by the frozen mixing relationship. In the work of Liew et al. (1984), only a single value of $x_{max} = 0$ corresponding to undisturbed flamelet burning is chosen from the range of possible values for x_{max} (between 0 and x_q) and experimental data of Michell et al. (1980) is used to describe $Y_i = Y_i(\xi,0)$. Comparisons have been reported with the open jet flame data of Hassan et al. (1980).

Chakravarty et al. (1984) have formulated a quenching criterion based on the notion of significant premixing at the base of the flame. Extinction is assumed to occur when the volumetric interdiffusion rate between adjacent burnt and unburnt Kolmogorov vortices exceeds the rate of chemical reaction.

Bilger (1979), in order to predict non-equilibrium effects, has derived an equation for the average departure from equilibrium of a species, y_i. This equation has a positive source term representing the production of non-equilibrium material due to mixing and a negative source term w_i due to chemical reaction. Bilger

(1980) has used the method for predicting the non-equilibrium behavior in ozone/NO_x reactions in photochemical smog and in hydrogen-air combustion. For these two reactions, Bilger has expressed the chemical reaction source term as

$$\dot{w}_i = - \rho k y_i^n \tag{4.3}$$

Thus, with n = 1 (Bilger, 1980), the calculation of mean chemical reaction term $\overline{\dot{w}_i}$ is straightforward and the need for additional modeling of covariances and triple correlations (Borghi and Dutoya, 1979) is obviated. However, equation (4.3) will apply only for a limited number of reaction systems, and in general, the problem of specifying w remains.

In this chapter, the perturbation method of Bilger is extended by proposing an approximate, but simple, method to calculate the time-averaged source term in the perturbation species equation y_i. Calculations have been made using this method for the elliptic, reacting flow (natural gas-air nonpremixed flame) configuration experimentally studied by Lewis and Smoot (1981).

4.2 MODIFIED PERTURBATION MODEL

The steady state governing equations for species mass fraction Y_i, with the assumption of equal molecular diffusivity, can be written as

$$\rho u_\beta \frac{\partial Y_i}{\partial x_\beta} - \frac{\partial}{\partial x_\beta} \left(\rho D \frac{\partial Y_i}{\partial x_\beta} \right) = \dot{w}_i \tag{4.4}$$

Following Bilger (1979, 1980), the mass fraction Y_i is first expressed as

$$Y_i = Y_i^e(\xi) + y_i \tag{4.5}$$

where Y_i^e is the equilibrium value and y_i is the departure of the species from equilibrium. Substituting eqn. (4.5) into eqn. (4.4) leads to

$$\rho\, u_\beta \frac{\partial y_i}{\partial x_\beta} - \frac{\partial}{\partial x_\beta}\left(\rho\, D \frac{\partial y_i}{\partial x_\beta}\right) = \dot{w}_i + \rho\, D \frac{\partial \xi}{\partial x_\beta}\frac{\partial \xi}{\partial x_\beta}\frac{d^2 Y_i^e}{d\xi^2} \tag{4.6}$$

The source term S_y (right hand side of eqn. (4.6)) is made up of the chemical reaction rate $\dot{w}_i$ and the production of non-equilibrium species due to mixing. Time averaging both sides of the equation results in

$$\overline{\rho\, u_\beta} \frac{\partial \bar{y}_i}{\partial x_\beta} - \frac{\partial}{\partial x_\beta}\left(\rho\, D_t \frac{\partial \bar{y}_i}{\partial x_\beta}\right) = \bar{\dot{w}}_i + \tfrac{1}{2}\,\rho\, \overline{x \frac{d^2 Y_i^e}{d\xi^2}} \tag{4.7}$$

where the scalar dissipation rate is defined as

$$x = 2\, D \frac{\partial \xi}{\partial x_\beta}\frac{\partial \xi}{\partial x_\beta} \tag{4.8}$$

In obtaining eqn. (4.7) from eqn. (4.6), the commonly invoked assumption that the turbulent scalar flux $\overline{u'_\beta\, y'_i}$ can be modeled with a gradient hypothesis is made, i.e., $-\overline{u'_\beta\, y'_i} \sim D_t \frac{\partial y_i}{\partial x_\beta}$, where D_t is the turbulent diffusion coefficient and is calculated based on the two equation (k-ε) model for turbulence.

In this section, instead of specifying $\dot{w}_i$ by using eqn. (4.3) (as in Bilger, 1980) or by a more complicated form involving covariances and triple correlations (as in (Borghi and Dutoya, 1979)), a somewhat different approach is adopted. For fast reactions $Y_i = Y_i(\xi)$, and Bilger (1976) has shown that $\dot{w}_i$ can be written as

$$\dot{w}_i = - \rho D \frac{\partial \xi}{\partial x_\beta} \frac{\partial \xi}{\partial x_\beta} \frac{d^2 Y_i}{d\xi^2} = - \tfrac{1}{2} \rho \chi \frac{d^2 Y_i}{d \xi^2} \qquad (4.9)$$

However, in a later paper, Bilger (1977) has empirically demonstrated the validity eqn. (4.9) for moderately fast reactions. Further verification of eqn. (4.9) is provided by the data of Fenimore and Fraenkel (1981) who determined the formation of fixed-nitrogen species in diffusion flames.

If eqn. (4.9) is used, the source term in eqn. (4.7) can be expressed as

$$\overline{S}_y = \overline{\tfrac{1}{2} \rho \chi \left(\frac{d^2 Y_i^e(\xi)}{d\xi^2} - \frac{d^2 Y_i(\xi)}{d\xi^2} \right)}$$

$$= \int_0^\infty \int_{\frac{1}{2}}^1 \overline{\rho \chi} \left(\frac{d^2 Y_i^e(\xi}{d\xi^2} - \frac{d^2 Y_i(\xi)}{d\xi^2} \right) p_{\xi\chi} (\xi,x) \, d\xi \, dx \qquad (4.10)$$

It is common to assume that x and ξ are statistically independent (Peters and Williams, 1983; Liew et al., 1984; Bilger, 1979), and therefore $p_{\xi,x}(\xi,x) = p_\xi(\xi) \, p_x(x)$. Equation (4.10) thus becomes

$$\overline{S}_y = \tfrac{1}{2} \overline{\rho} \, \overline{\chi} \int_0^1 \left(\frac{d^2 Y_i^e}{d\xi^2} - \frac{d^2 Y_i(\xi)}{d\xi^2} \right) p_\xi (\xi) \, d\xi \qquad (4.11)$$

If the functional relationships $Y_i^e(\xi)$ and $Y_i(\xi)$ were known, S_y can be determined by assuming the probability distribution function $p_\xi(\xi)$. A Gaussian distribution is assumed for $p_\xi(\xi)$ as described in section 2.1.

The equilibrium distribution $Y_i^e(\xi)$ is well known and is given by

$$Y_i^e(\xi) = H(\xi - \xi_s) \, Y_{i,1} \, (\xi - \xi_s)/(1 - \xi_s) \qquad (4.12)$$

where H is the Heaviside function and $Y_{i,1}$ denotes the Y_i value in the fuel stream ($\xi = 1$). If no chemical reactions occur, conditions are described by inert mixing and the mass fraction $Y_i^f(\xi)$ is given by

$$Y_i^f(\xi) = Y_{i,1} \cdot \xi \tag{4.13}$$

Both the $Y_i^e(\xi)$ and $Y_i^f(\xi)$ distributions are shown in Fig. 4.1.

The $Y_i(\xi)$ distribution is governed by kinetic considerations but must lie between the $Y_i^e(\xi)$ and $Y_i^f(\xi)$ distributions. Below a lower limit for ξ (ξ_ℓ) and above an upper limit (ξ_u), no chemical reaction is expected to occur since in very lean or very rich mixtures a steady deflagration wave cannot be maintained. At stoichiometry, from chemical kinetics consideration alone, chemical equilibrium must exist. If for $\xi_\ell \leq \xi \leq \xi_s$ and $\xi_s \leq \xi \leq \xi_u$, a linear $Y_i \sim \xi$ relationship is assumed then the $Y_i(\xi)$ distribution is completely specified as

$$\begin{aligned}
Y_i(\xi) &= Y_{i,1}\, \xi && \text{for } 0 \leq \xi < \xi_\ell \\
Y_i(\xi) &= Y_{i,1}\, \xi_\ell\, (\xi_s - \xi)/(\xi_s - \xi_\ell) && \text{for } \xi_\ell \leq \xi < \xi_s \\
Y_i(\xi) &= Y_{i,1}\, \xi_u\, (\xi - \xi_s)/(\xi_u - \xi_s) && \text{for } \xi_s \leq \xi < \xi_u \\
Y_i(\xi) &= Y_{i,1}\, \xi && \text{for } \xi_u \leq \xi < 1
\end{aligned} \tag{4.14}$$

The $Y_i(\xi)$ distribution is shown by dotted lines in Fig. 4.1. Using eqns. (4.12) and (4.14), the time averaged source term S_y (eqn. 4.11)) can be evaluated as

$$\begin{aligned}
\bar{S}_y = \tfrac{1}{2}\, \rho\, \bar{\chi}\, [&(s_{e_1} - s_{e_2})\, p_\xi\, (\xi_s) + (s_{n_2} - s_{n_1})\, p_\xi\, (\xi_u) - \\
&(s_{n_2} - s_{n_3})\, p_\xi\, (\xi_s) - (s_{n_4} - s_{n_3})\, p_\xi\, (\xi_\ell)]
\end{aligned} \tag{4.15}$$

where s_{e_1}, s_{e_2}, s_{n_1}, s_{n_2}, s_{n_3} and s_{n_4} are the various slopes of

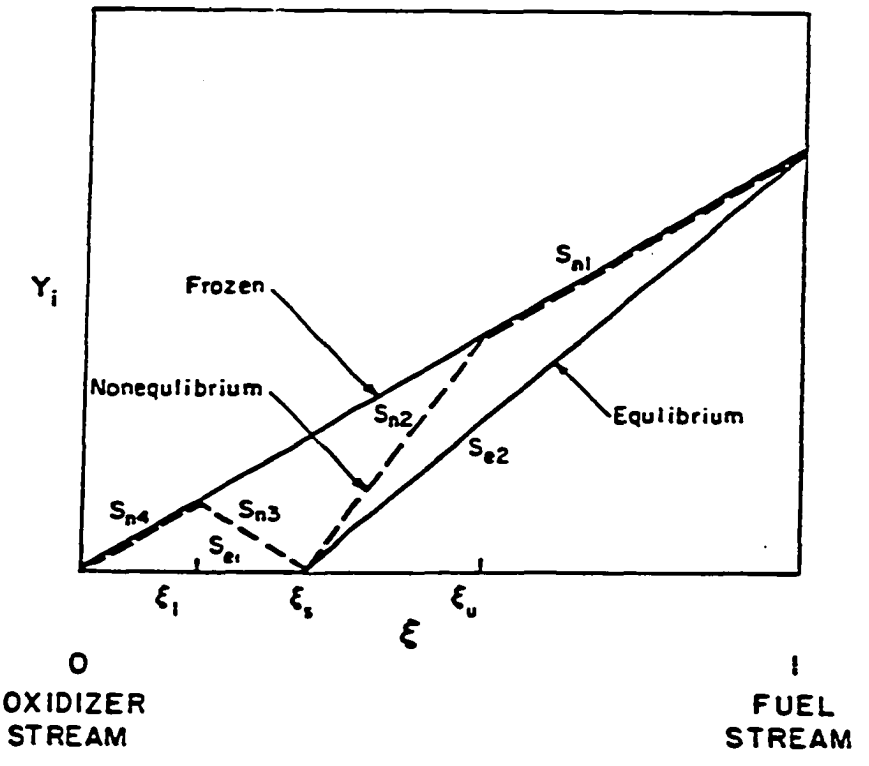

Fig. 4.1 Frozen, equilibrium and nonequilibrium $Y_i \sim \xi$ distribution

the straight line segments in Fig. 4.1. , i.e.,

$$s_{e_1} = Y_{i,1}/(1 - \xi_s),\ s_{e_2} = o$$

$$s_{n_1} = s_{n_4} = Y_{i,1},\ s_{n_2} = Y_{i,1}\ \xi_u/(\xi_u - \xi_s),$$

$$S_n = - Y_{i,1}\ \xi_\ell/(\xi_s - \xi_\ell) \qquad (4.16)$$

For x, balance equations proposed by Borghi and Dutoya (1979) and Launder and Elgobashi (1981) can be solved. However, rather limited testing of these proposals have been made and therefore, the introduction of an additional modeled equation is unwarranted. Rather, $\overline{x}$ is obtained from the two equation moel of turbulence as (Liew et at., 1984; Chakravarty et al., 1984)

$$\overline{x} = C_{g_2}\ \overline{\xi''^2}\ k/\varepsilon \qquad (4.17)$$

where $C_{g_2} = 2.0$

Some additional comments should be made on the features of the model. If $\overline{\xi} = \xi_s$, increasing the scalar dissipation rate from $\overline{\xi''^2_1}$ (curve 1 in Fig. 4.2) to $\overline{\xi''^2_2}$ (curve 2), results in a portion of the curve falling below the lower limit ξ_ℓ leading to higher $\overline{S_y}$ values and lower flame temperatures. Further increases to $\overline{\xi''^2_3}$ (curve 3) extends the curve to beyond ξ_u thus promoting the non-equilibrium behavior. However, for $\overline{\xi} = \xi_{shift}$ (nearly mid-way between ξ_ℓ and ξ_u), the $\overline{\xi''^2_2}$ curve (curve 4) falls between the lower and upper limits, and thus compared to curve 2, the probability of burning and therefore the flame temperature is higher. However, compared to curve 1, curve 3 yields lower flame temperature because of smaller $p_\xi(\xi)$ values. This conforms with the behavior reported by

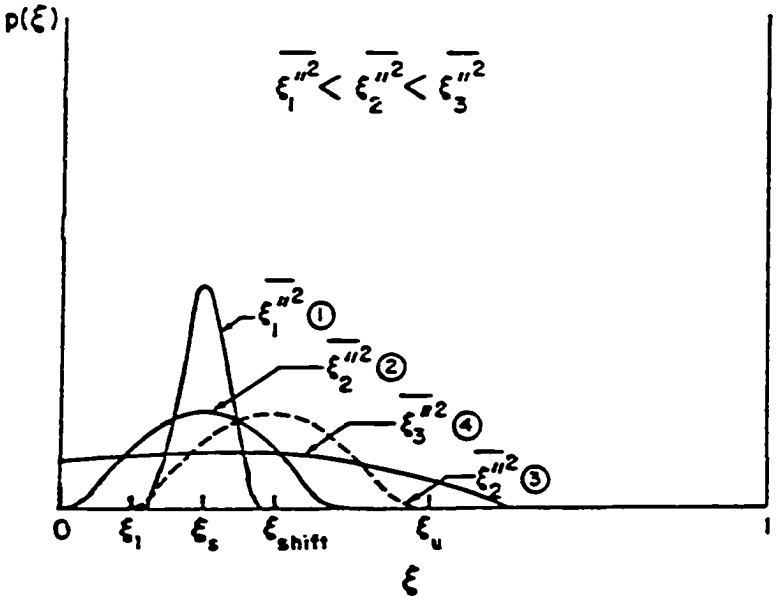

Fig. 4.2 Possible distributions for p(ξ)

Liew et al. (1984) where, with increasing scalar dissipation rate ($\sim \overline{\xi''^2}$), the peak temperature decreases and occurs at a higher value of ξ (= ξ_{max}). At a critical value of the scalar dissipation rate x_q, extinction occurs. Liew et al. (1984) report a value of 0.19 for ξ_{max} at $x = x_q$.

To complete the model, the lower and upper limits ξ_ℓ and ξ_u have to be specified. Although determination of universal values or functions for ξ_ℓ and ξ_u is not straightforward, reasonable choices may be made using empirical inputs and the concept of flammability in premixed flames, since, even for non-premixed systems, the formation of locally flammable mixtures of fuel and air is required for reaction. In the absence of stretching effects ($x = 0$), the lower and upper limits of flammability (0.025 and 0.1 for the natural gas-air flame of interest in this study) are logical choices for ξ_ℓ and ξ_u. However, for turbulent flows, the flame is subjected to stretching effects; the influence of stretching, based on arbuments and the study reported by Liew et al. (1984), is to increase ξ_ℓ and ξ_u. In (Liew et al., 1984), a value of 0.19 is reported as the ξ value at which quenching or frozen mixing occurs. Therefore, in this study sensitivity studies have been made byr ξ_u in the range of 0.2 - 0.4 and for ξ_ℓ in the range of 0.03 - 0.035.

Fig. 4.3 plots the expected distributions for $\overline{S_y}$ (eqn. (4.15)) and $\overline{y_i}$ as a function of $\overline{\xi}$. This behavior can be better understood by examining the state of a fuel packet along its trajectory. As $\overline{\xi}$ decreases from 1 (at the inlet), non-equilibrium effect increases. At $\overline{\xi} = \xi_u$, $\overline{S_y}$ has a local peak due to the contribution from the second term in eqn. (4.15). As the fuel packet approaches the

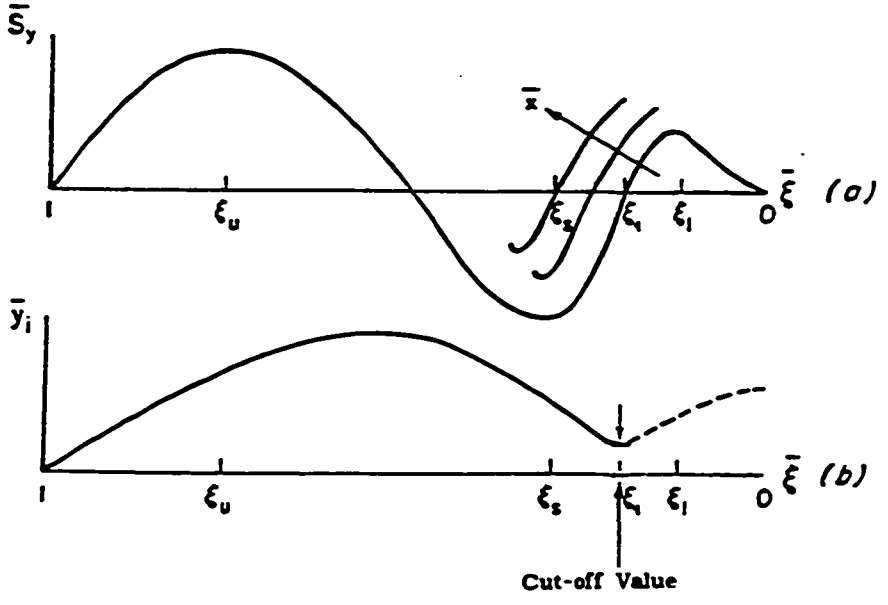

Fig. 4.3 Expected distributions for $\bar{S}_y$ and $\bar{y}_i$ as a function of ξ

flame front and $\overline{\xi}$ approaches ξ_s, the first term (positive) and the third term (negative) in eqn. (4.15) become increasingly important and the net effect is that $\overline{S}_y$ decreases to zero and attains a negative peak at ξ_s. Negative $\overline{S}_y$ values reduce $\overline{y}_i$ from a positive maximum $\overline{y}_{i,max}$ as expected when the fuel packet approaches the flame front. Beyond $\overline{\xi} = \xi_s$, the fourth term in eqn. (4.15) becomes increasingly dominant and $\overline{S}_y$ becomes positive at $\overline{\xi} = \xi_1$ attaining a positive local maximum at $\overline{\xi} = \xi_\ell$. This triggers an increase in $\overline{y}_i$. However, past the flame front a significant increase in $\overline{y}_i$ of the nearly - burnt fuel packet is physically unrealistic but, if x is sufficiently high, $\overline{S}_y$ (for $\overline{\xi} > \xi_1$) may be large enough (due to the fourth term in eqn. (4.15)) to yield high $\overline{y}_i$ predictions. Therefore, it is assumed that for $\overline{\xi} > \xi_1$, the mean source term is represented only by the first and third terms in eqn. (4.15). This is tantamount to the assumption that beyond the flame front, say in the slow recirculation region in the upper corner of the combustor, production of net non-equilibrium fuel species y_i due to inert mixing does not occur.

4.3 SOLUTION SCHEME

The solution scheme of the governing equations for turbulent diffusion flames using equilibrium fast chemistry models have been described in a number of earlier references (see (Bilger, 1976)) for example) and therefore a detailed discussion is not provided here. Turbulence is modeled using the two-equatin (k-ε) model for turbulence and radiation effects have been neglected. Equations solved are those of the time averaged axial and radial velocities

$(\bar{u},\bar{v})$, kinetic energy of turbulence (k) and its dissipation rate (ε), time averaged mixture fraction ($\bar{\xi}$) and its variance ($\overline{\xi''^2}$) and the time averaged departure from equilibrium of the fuel species ($\bar{y}_i$). Each of these equations can be expressed in the form

$$\nabla \cdot (\bar{\rho}\ \bar{y}\ \bar{\phi}) = \nabla \cdot (\bar{\Gamma}_\phi\ \nabla\ \bar{\phi}) + \bar{S}_\phi \qquad (4.18)$$

where ϕ represents the general dependent variable, and Γ_ϕ and S_ϕ are the effective diffusion coefficient and the source term respectively for ϕ. The solution technique is also described in detail in Chapter 2.

The mean equilibrium mass fraction for the fuel species Y_i^e can be calculated from $\bar{\xi}$, $\overline{\xi''^2}$ and $p(\xi)$ by

$$\bar{Y}_i^e = \int_0^1 Y_i^e(\xi)\ p\ (\xi)\ d\xi \qquad (4.19)$$

where $p(\xi)$, as mentioned earlier, is assumed to be Gaussian with mean $\bar{\xi}$ and variance $\overline{\xi''^2}$. The mean non-equilibrium value is obtained by adding y_i to equation (4.19). The mean non-equilibrium value for other major species is obtained by defining a mean reactedness as

$$\bar{r} = (\bar{Y}_i - \bar{Y}_i^f) / (\bar{Y}_i^e - \bar{Y}_i^f) \qquad (4.20)$$

A 20 x 20 non-uniform mesh is used in most of the calculations. Based on preliminary calculations, the grid point distribution is arranged to be denser in regions of large gradients. Results on this mesh compare will with those of a finer mesh and overall conservation is satisfied to less than 1%.

4.4 RESULTS AND DISCUSSION

As mentioned earlier, predictions have been obtained for the experimental configuration studied by Lewis and Smoot (1981). A schematic of this configuration is shown in Fig. 4.4.

The centerline oxygen mole fraction predictions are shown in Fig. 4.5 together with the measured values and the axial distance along which a visible flame was observed. As may be noted, the predictions with the non-equilibrium model exhibit reasonable agreement with the data while the corresponding fast chemistry equilibrium predictions significantly underestimate the centerline oxygen mole fraction. The experimentally observed O_2 penetration to the centerline, and the inability of the fast chemistry equilibrium models to correctly predict this has been noted and reported earlier (Liew et al., 1984; Smith and Smoot, 1981). The present non-equilibrium model, however, correctly predicts the penetration of the oxygen mole fraction to the centerline. Also, a sharp decrease in the O_2 mole fraction is predicted in the region of the experimentally observed visible flame as expected.

Sensitivity studies for the choice of ξ_u and ξ_ℓ in the range of $\xi_u = 0.2 - 0.4$ and $\xi_\ell = 0.03 - 0.035$ have been made and shown in Fig. 4.5. Significant differences in the results are not noted and is due to the fact that an increase in ξ_u is associated with a decrease in the slope S_{n_2}. These two effects are counteracting, and partly explain the lack of sensitivity of the results to the ξ_u value in the 0.2 - 0.4 range. Similar argument may be made for ξ_ℓ value in the 0.03 - 0.035 range.

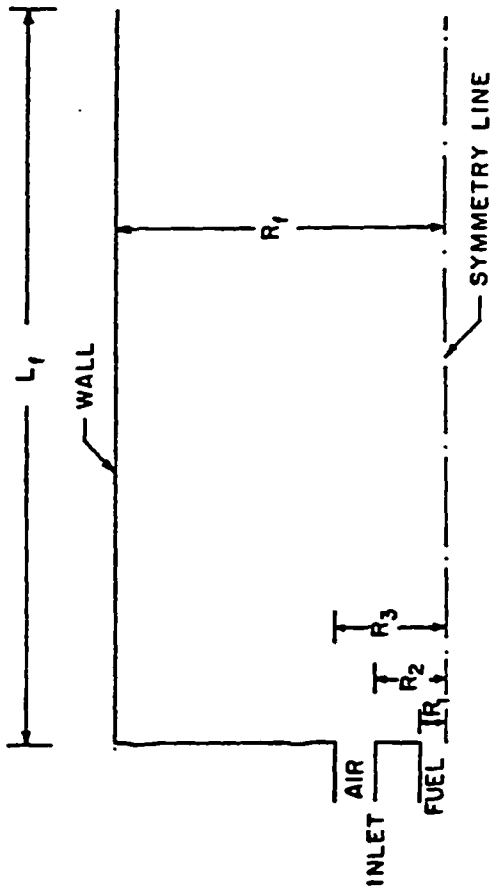

(cm)	
R_1	0.8
R_2	1.3
R_3	2.85
R_1	10.15
L_1	152.4

Fig. 4.4 Experimental configuration

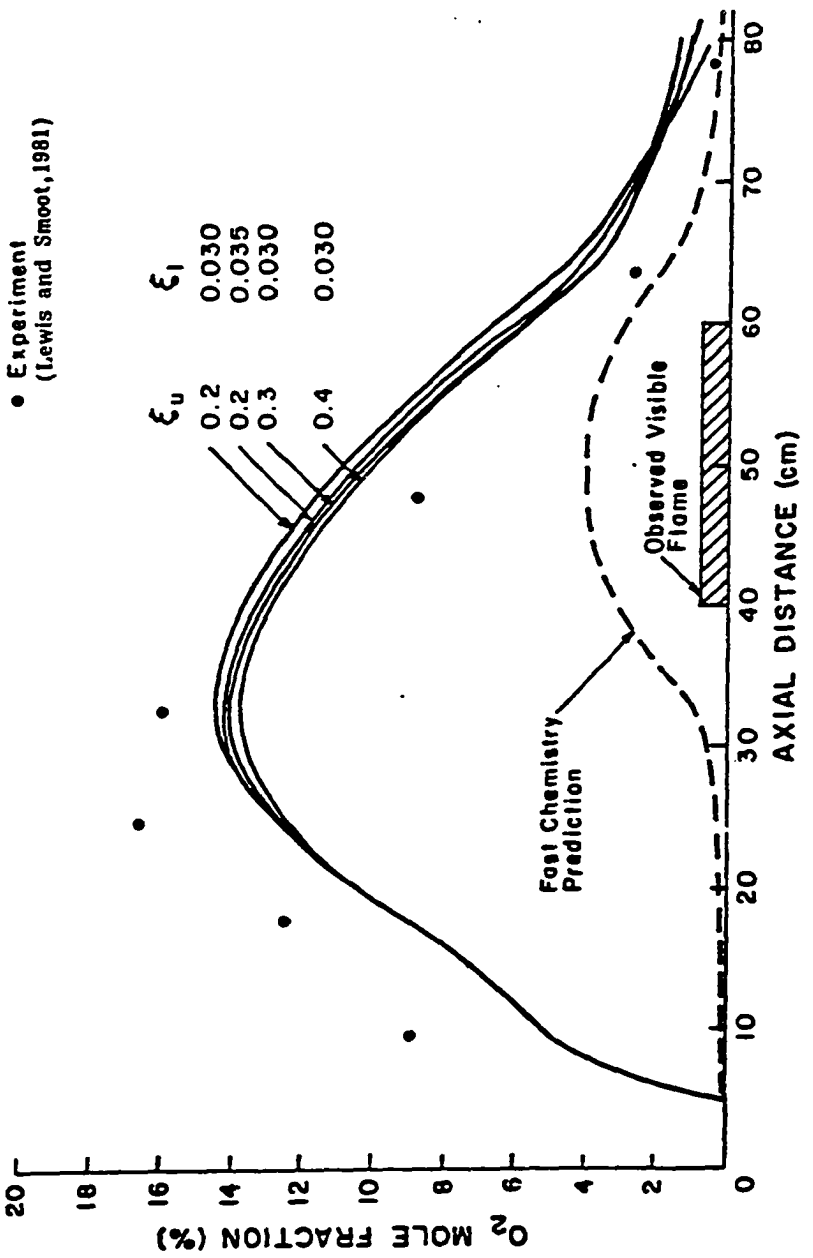

Fig. 4.5 Centerline O_2 mole fraction

Figs. 4.6 and 4.7 respectively present the radial distributions of O_2 and CO_2 mole fractions at different axial locations. In regions where non-equilibrium effects are important, the predictions with the perturbation model outlined in this section agree well with measurements. Fast chemistry equilibrium predictions exhibit significantly larger discrepancies. In other regions where local extinction effects are not important, both the non-equilibrium and equilibrium predictions exhibit similar behavior.

Fig. 4.8 shows the non-equilibrium predictions of the mixture fraction. As in Figs. 4.6 and 4.7, the predicted and measured values agree well with each other.

4.5 CONCLUDING REMARKS ON THE FLAME QUENCHING MODEL

A model for predicting the non-equilibrium behavior in turbulent non-premixed flames is presented. This model solves a differential equation for y_i which is the departure of species y_i from equilibrium. A simple method is presented for calculating the mean chemical reaction rate $\dot{w}_i$ which appears in the equation for y_i. Results obtained with this model are compared with experimental data and exhibit good agreement. Fast chemistry equilibrium predictions, however, do not compare will with the data particularly in regions where non-equilibrium effects are important.

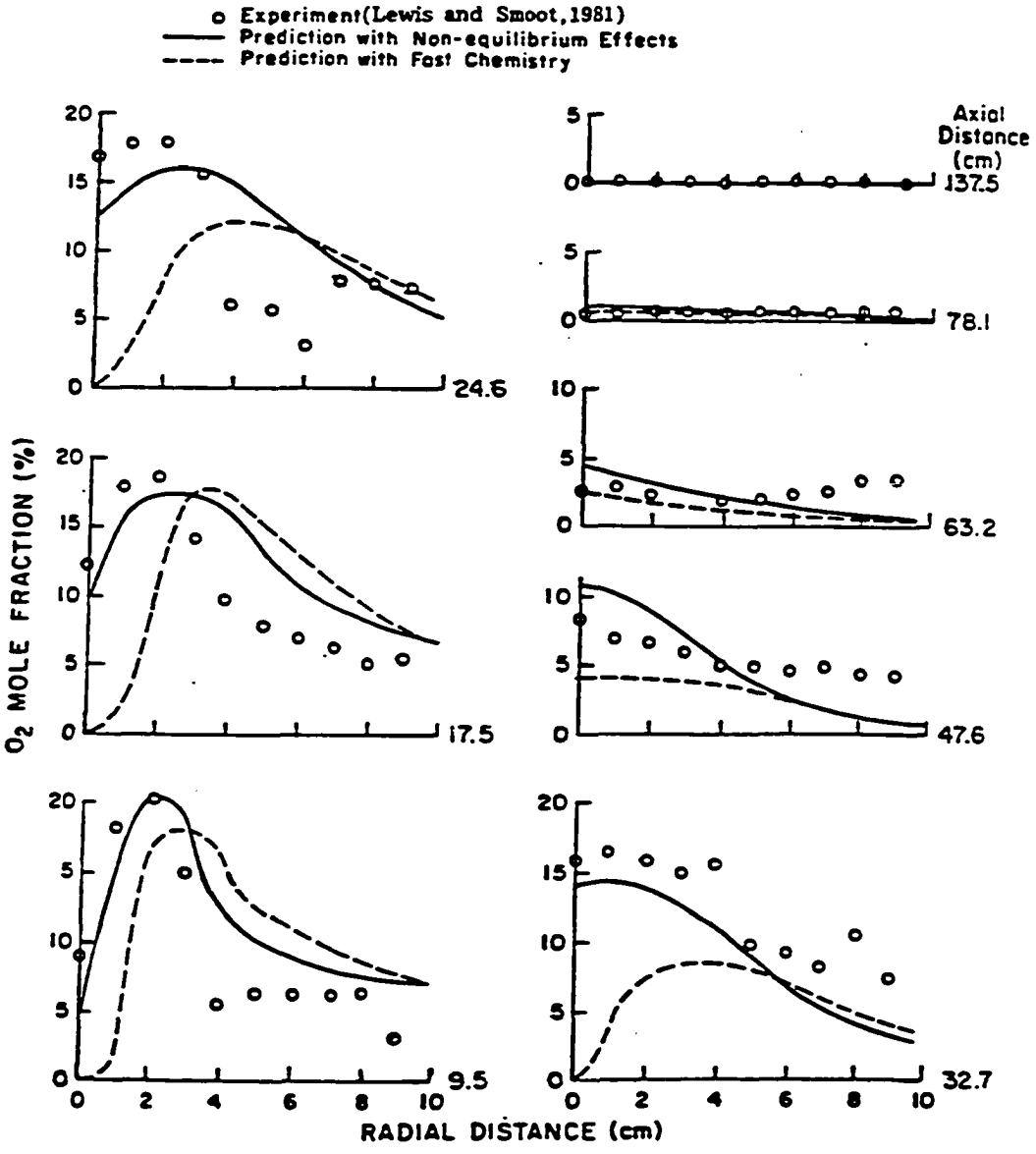

Fig. 4.6 Radial distributions of O_2 mole fraction

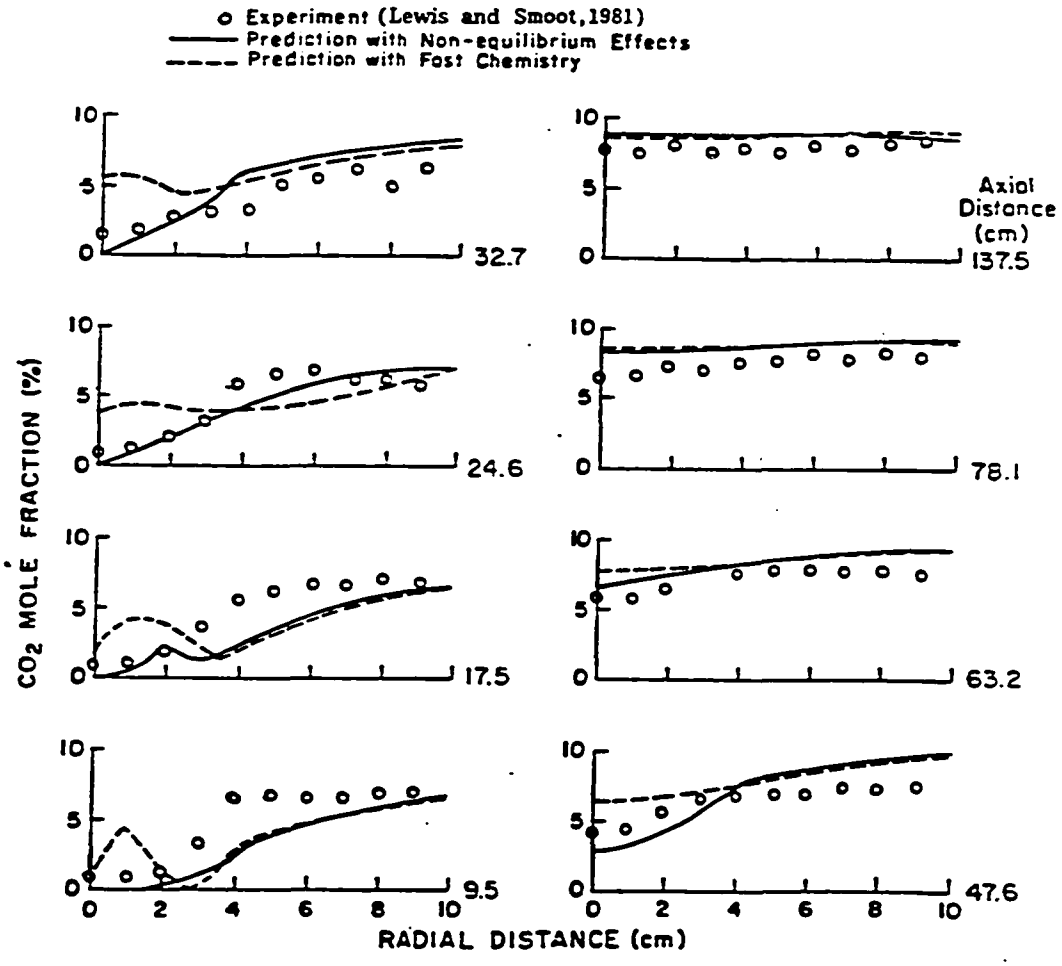

Fig. 4.7 Radial distributions of CO_2 mole fraction

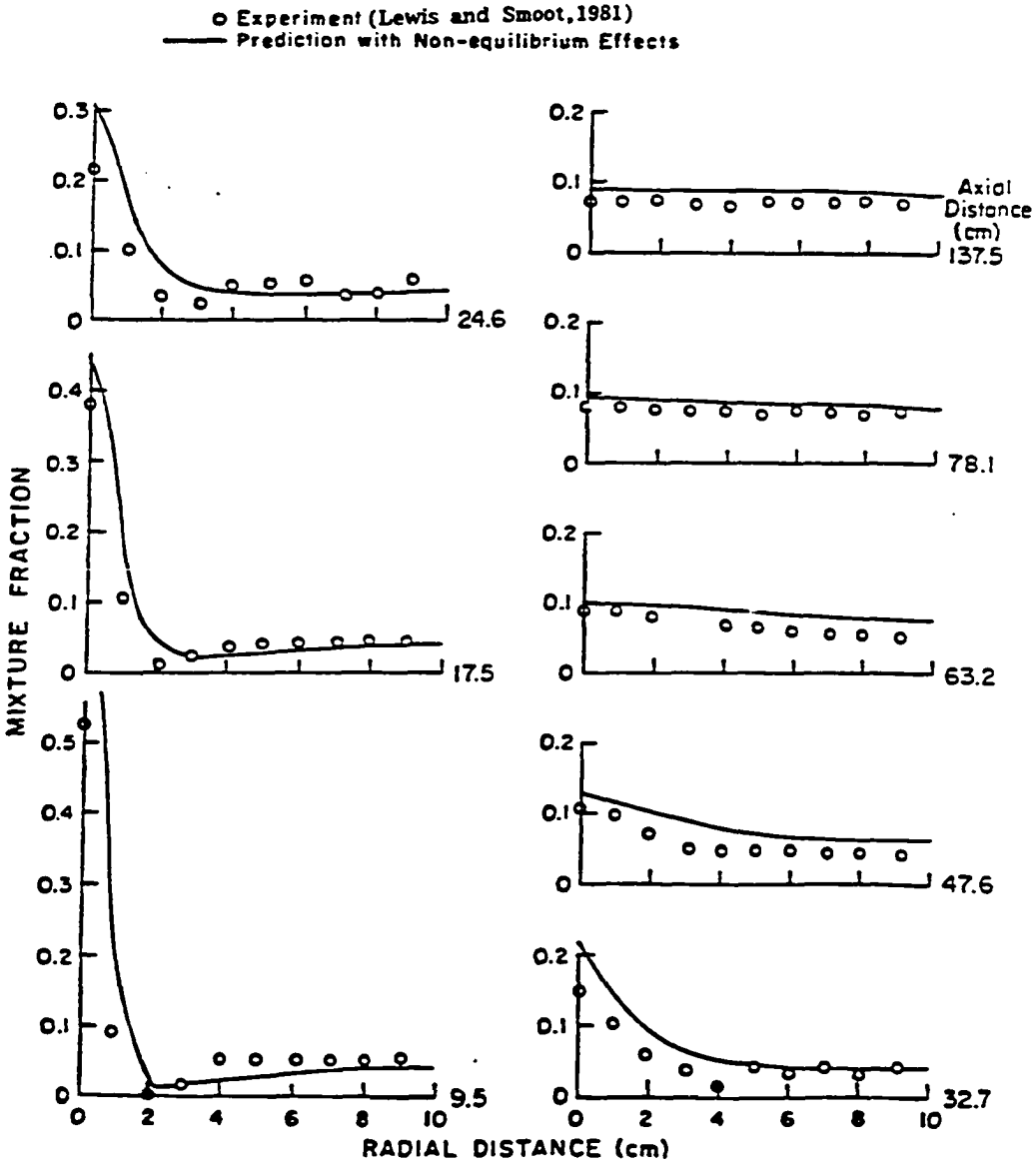

Fig. 4.8 Radial distribution of mixture fraction

CHAPTER 5

EVALUATION AND DEVELOPMENT OF PARTICLE DISPERSION MODELS

Two phase combustion such as pulverized coal or droplet spray combustion is commonly encountered in combustion equipment. The motion of the particle or droplet phase is dictated both by the mean velocity and the turbulence of the gas phase. For realistic predictions, the interaction between the particle phase and the gas phase turbulence must be accurately modeled. The primary emphasis of this chapter is to examine the modeling of particle dispersion in a turbulent, confined and recirculating (or elliptic) flow field as encountered in a typical furnace or combustor geometry.

As noted by Smoot (1981), the approach commonly adopted for modeling particle dispersion is heavily based on empiricism. The models proposed by Lockwood et al. (1980) and Smith et al. (1981) are typical examples of such empirical models. In both these models, the dispersion of particles due to turbulence is assumed to be a diffusional process and expressed as a gradient of either the mean velocity (Lockwood et al., 1980) as in the Boussinesq approximation for Reynolds stresses, or the gradient of the particle bulk number density (Smith et al., 1981). The models, quite clearly, are less than satisfactory, since the basic assumption of relating the dispersion of particles to mean gradients is not well-founded. Further, both models contain empirical constants and there is considerable uncertainty about the suitable values of these constants.

Despite these drawbacks, the models have had some measure of success in correctly predicting the general trends, although significant local differences between predicted and measured profiles have been noted (Fletcher, 1980; Fletcher, 1983). An alternative method has been proposed by Yuu et al. (1978), Dukowicz (1980) and Gosman and Ioannides (1981) in which a stochastic approach towards modeling particle dispersion is used. Unlike the empirical approaches, the instantaneous equation for particle motion is solved with the instantaneous turbulent quantities obtained by random or stochastic sampling.

Faeth and associates have extensively used the stochastic approach and evaluated it for parabolic flows (Shuen et al., 1983 a, b, c; Solomon et al., 1985 a, b, c; and Zhang et al., 1985) by comparing the results of the stochastic method with two other two phase flow models, both of which ignore the turbulent dispersion of particles. However, no comparisons with the empirical models for particle dispersion (Lockwood et al., 1980; Smith et al., 1981) have been made.

The stochastic approach has not been widely used for elliptic flows, with the authors aware of only four recent studies (Gosman and Ioannides, 1981; Boysan et al., 1986; Boyd and Kent, 1986; Truelove, 1986) where this approach has been used in combustion or furnace geometries. In none of these studies, has the performance of the stochastic method been compared with the other models for particle dispersion.

The objective of this chapter is to evaluate the performance of the stochastic model for particle dispersion in a turbulent,

confined and recirculating (or elliptic) flowfield as encountered in most combustion equipment. Results obtained with the stochastic model will be compared with two other models for turbulent dispersion of particles (Lockwood et al., 1980; Smith et al., 1981). Two sets of experimental data for isothermal flows (Memmott, 1977, Leavitt, 1980) and one set of data for reacting flow (Michel and Payne, 1980) will be used in making the performance evaluations.

5.1 MATHEMATICAL MODELS

In solving for the coupled system of equations for the gas and particles, an Eulerian-Langrangian formulation is adopted, in which the gas phase equations are solved in an Eulerian framework and the particle equations are solved in Lagrangian coordinates. The gas-particle coupling is resolved through additional source terms in the gas phase equations. A consecutive calculation procedure is adopted, in which the time-averaged gas phase equations are first solved followed by the solution of the particle equations. The additional source terms in the gas phase equations due to the particles are calculated and the solution for the gas phase equations again obtained. This process is repeated until convergence.

Gas Phase Equations

The dependent variables characterizing the mean gas flow are the velocity components $(\bar{u},\bar{v})$, pressure (p), enthalpy $(\bar{h})$ and the mass fractions of the chemical constituents, $(\bar{m}_{fu}, \bar{m}_{ox}, \bar{m}_{CO_2},$

$\overline{m}_{H_2O}$). The steady-state governing differential equations for these dependent variables can be expressed as

$$\partial(\overline{\rho u_i}\bar{\phi})/\partial s_i = \partial(\Gamma_{eff,\phi}\, \partial\bar{\phi}/\partial x_i)\partial x_i + S_\phi + S_{\phi,p} \qquad (5.1)$$

where u_i represents the mean velocity components, ϕ is the mean dependent variable, $\Gamma_{eff,\phi}$ is the effective diffusion coefficient, ρ is the mean density, and S_ϕ and $S_{\phi,p}$ are the source terms and the additional source terms due to passage of the particles, respectively.

Turbulence is modeled using the high Reynolds number version of the two-equation (k-ε) model for turbulence (Launder and Spalding, 1972). This requires the solution of the kinetic energy of turbulence k and its dissipation rate ε. Governing differential equations of the same form as equation (5.1) can be derived for both k and ε. As recommended by Launder and Spalding (1972), the presence of the near-wall viscous sub-layer is resolved through the use of wall functions.

For reacting flows (pulverized coal combustion is considered in this chapter), additional models for radiation heat transfer and combustion have to be introduced. In this chapter, the four-flux model for radiation (Gosman and Lockwood, 1974) has been used. This model has been shown to be satisfactory for furnace applications (Smith et al., 1981; Khalil et al., 1975). The combustion of volatiles released from the particles is likely to occur after mixing with the surrounding gases and at a rate determined not by chemical considerations but by the turbulence dissipation rate in the gas phase. The phenomenological model proposed by Magnussen

and Hjertager (1976) is adopted here, by which, the source term S_ϕ in equation (5.1) for the fuel mass fraction m_{fu}, is expressed in the "eddy breakup" form of Spalding (1971) as

$$S_{fu} = \text{minimum of } \left| \rho A \bar{m}_{fu}\, \varepsilon/k,\ \rho A(\bar{m}_{ox}/s)(\varepsilon/k),\right.$$
$$\left. \rho A' m_{pr}/(1+s)(\varepsilon/k) \right| \qquad (5.2)$$

where s is the stoichiometric mass ratio, and A and A' are empirical constants. Gas properties are calculated from the functional relationships given by Svehla (1963).

Particle Equations

For isothermal flows, the equations for particle motion characterize the particle behavior. These equations can be expressed as

$$du_p/dt = \alpha\ (u_g - u_p) \qquad (5.3)$$

$$dv_p/dt = \alpha\ (v_g - v_p) \qquad (5.4)$$

where u and v are the axial and radial velocities, and subscripts p and g refer to the particle and gas phases, respectively. The term α is defined as

$$\alpha = 18\ \mu_g\ C_D\ Re_p\ /\ 24\ \rho_p\ d_p^{\,2} \qquad (5.5)$$

where Re_p is the particle Reynolds number defined as

$$Re_p = \rho_g \left| \vec{u}_g - \vec{u}_p \right| d_p\ /\ \mu_g \qquad (5.6)$$

and C_D is the drag coefficient which is specified according to the expression given by Wallis (1969).

The velocities in equation (5.3)-(5.6) are instantaneous quantities. Since, only time-averaged gas phase quantitites are solved for, it is logical to attempt the solutions of the time-averaged forms of equations (5.3)-(5.4) which may be expressed as

$$d\bar{u}_p/dt = \bar{\alpha}\,(\bar{u}_g - \bar{u}_p) + \overline{\alpha'(u_g' - u_p')} \tag{5.7}$$

$$d\bar{v}_p/dt = \bar{\alpha}\,(\bar{v}_g - \bar{v}_p) + \overline{\alpha'(v_g' - v_p')} \tag{5.8}$$

The second term, on the right-hand side of equations (5.7)-(5.8), represents the dispersion of the particles due to turbulence in the gas-phase, and it is the modeling of this term that is of primary interest in this chapter. The three models considered in this study are described later.

For pulverized coal combustion, additional equations have to be resolved for the particle temperature and combustion of the particle. The particle temperature is described by the equation

$$m_p c_p dT_p/dt = \pi\, d_p\, Nu\, k_g(T_g - T_p) - H(dm_p/dt) + L(\, dm_p/dt) + Q_r \tag{5.9}$$

The terms on the right side of the above equation represent heat transfer to or from the particle through convection, char reaction, volatilization and radiation. Char reaction is suppressed until volatilization is complete and is described, as suggested by Baum and Street (1971), by

$$dm_p/dt = -\, K_T\, \pi\, d_p^{\,2}\, p\, \bar{F}_{ox} \tag{5.10}$$

where K_T is the overall rate coefficient, p is the pressure, and F_{ox} is the oxygen volume fraction at the particle surface. The calculation of volatile release from the particle is again based on the recommendation of Baum and Street (1971),

$$\begin{aligned} dx_v/dt &= \min\,(Q_p/L,\ B) \quad && \text{for } T_p > 600^{\circ}K \\ dx_v/dt &= 0 && \text{for } T_p < 600^{\circ}K \end{aligned} \tag{5.11}$$

where x_v is the fraction of volatile mass released, Q_p is the particle heating rate and B is a maximum devolatilization rate equal to 30 s^{-1}. The modeling of the gas phase combustion of volatiles was described earlier. For particle swelling during devolatilization, the recommendation of Anson et al. (1971) and Smoot and Pratt (1979) are implemented.

Turbulent Dispersion of Particles

In this section three models for the turbulent dispersion of particle are described. The first two models are commonly employed in the comprehensive modeling of two-phase elliptic flows and will be referred to as Model 1 and Model 2 in this study. Both these models solve the time-averaged equation for particle motion (equation (5.7) and (5.8)) and thus require closure for the fluctuating term correlations appearing in equations (5.7) and (5.8). The third model, called the stochastic model, solves the instantaneous equations for particle motion (equations (5.3) and (5.4)) and requires the prescription of the instantaneous gas phase velocities u_g and v_g.

Model 1: Lockwood et al. (1980) have proposed that the effects of turbulent dispersion of particle be incorporated by defining diffusional particle valocities $u_{p,diff}$ and $v_{p,diff}$ due to gas phase turbulence and rewriting equations (5.7) and (5.8) as

$$d\bar{u}_p/dt = \{ 18\ \mu_g C_D/(24\ \rho_p\ d_p^2)\}(\bar{\rho}_g|\vec{\bar{u}}_g-\vec{\bar{u}}_p-\vec{\bar{u}}_{p,diff}|d_p/\mu_g)$$
$$(\bar{u}_g-\bar{u}_p-\bar{u}_{p,diff}) \qquad (5.12)$$

$$d\bar{v}_p/dt = \{ 18\ \mu_g C_D/(24\ \rho_p\ d_p^2)\}(\bar{\rho}_g|\vec{\bar{u}}_g-\vec{\bar{u}}_p-\vec{\bar{u}}_{p,diff}|d_p/\mu_g)$$
$$(\bar{v}_g-\bar{v}_p-\bar{v}_{p,diff}) \qquad (5.13)$$

The diffusional velocities are related to the gas phase turbulence through

$$\bar{u}_{p,diff} = c_1 \left|\overline{u'^2}\right| \text{ and } \quad v_{p,diff} = c_2 \left|\overline{v'^2}\right| \qquad (5.14)$$

where the turbulence intensities are estimated with the aid of Boussinesq hypothesis:

$$\overline{u'^2} = - c_3\ 2\mu_t/\bar{\rho}_g\ (d\bar{u}_g/dx) + \tfrac{2}{3}\ k,$$
$$\overline{v'^2} = - c_4\ 2\mu_t/\bar{\rho}_g\ (d\bar{v}_g/dy) + \tfrac{2}{3}\ k, \qquad (5.15)$$

The constants c_1, c_2, c_3 and c_4 are specified empirically.

Model 2: In tis model (Smith et al., 1981), equations (5.7) and (5.8) are first solved without the turbulent dispersion terms; thus, the computed particle velocities are those that correspond only to the mean gas motion and are denoted by $\vec{u}_{pc}$ ($= \vec{i}\ u_{pc} + \vec{j}\ v_{pc}$). The total particle velocity is obtained by adding a turbulent diffusional velocity $\vec{u}_{p,diff}$ to $\vec{u}_{pc}$ i.e.,

$$\vec{u}_p = \vec{u}_{pc} + \vec{u}_{p,diff} \qquad (5.16)$$

The diffusional velocity is approximated by a gradient diffusion law:

$$\dot{m}''_p = \rho_p^b \vec{u}_{p,diffy} = - \Gamma_p \nabla \rho_p^b = - (\nu_p^t/\sigma_p^t) \nabla \rho_p^b \qquad (5.17)$$

where ρ_p^b is the bulk particle density, Γ_p is the turbulent particle diffusivity and ν_p^t and σ_p^t are the turbulent particle kinematic viscosity and the turbulent particle Schmidt number, respectively. The relationship proposed by Melville and Bray (1979) is normally used for ν_p^t,

$$\nu_p^t / \nu_g^t = [\ 1 + (t_*/t_L)\ ]^{-1} \qquad (5.18)$$

where t_* is the particle relaxation time and t_L is the Lagrangian time scale for the gas phase turbulence. For σ_p^t, a value of 0.35 has been recommended by Fletcher (1983). The particle bulk density is obtained from the particle number density n_p^b which is calculated by solving an Eulerian equation of the form similar to equation (5.1) (Fletcher, 1980). This model is the most commonly adopted approach for incorporating the effects of turbulence on particle dispersion (Fletcher, 1980; Smith et al., 1981; Smoot, 1981; Fletcher, 1983; Hill, 1983).

Stochastic model: In the stochastic model (Gosman and Ioannides, 1981; Shuen et al., 1983 a,b,c,), equations (5.3) and (5.4) are solved directly in their instantaneous forms. Thus the need to model fluctuating term correlations in equations (5.7) and (5.8) is eliminated. Instead, the particle is assumed to interact with a succession of eddies as it traverses the flow. The properties in each eddy are assumed to be uniform but change randomly from one eddy to the next. Since equation (5.3) and (5.4) are solved in their instantaneous form, instantaneous eddy properties are requir-

ed. These are obtained by assuming isotropic turbulence and making a stochastic selection from the Gaussian velocity probability distribution function with mean u_g and variance 2k/3. Both u_g and k are obtained from the gas phase calculations.

The particle is assumed to interact with the eddy if its displacement within the eddy is smaller than a characteristic eddy size ℓ_e, and the time of interaction is smaller than the characteristic eddy life time t_e. Conventional expressions for the eddy size and life time are (Gosman and Ioannides, 1981).

$$\ell_e = c_\mu^{3/4} \, k^{3/2}/\varepsilon \quad , \quad t_e = \ell_e/(2k/\varepsilon)^{1/2} \quad . \tag{5.19}$$

Since the specification of eddy size is important, the expression for ℓ_e proposed by Driscoll (1982) has also been used in this study. This expression is a modification of the dissipation length scale in equation (5.19),

$$\ell_e = (c_{d_1} + c_{d_2} \; / \; Re_\lambda \;) \; k^{3/2} \; / \; \varepsilon \tag{5.20}$$

where $c_{d_1} = 0.166$, $c_{d_2} = 5.12$ and Re_λ is Reynolds number based on the Taylor microscale defined as $Re_\lambda = (20/)3^{1/2} \; k/(\nu_g \; \varepsilon)^{1/2}$. A third choice for the eddy size is that given in Williams (1985) and deduced dimensionally on the notion that the average rate of spectral transfer of energy is the same as the average rate of dissipation of turbulent kinetic energy. The expression for ℓ_e is

$$\ell_e = (2 \; k/3)^{3/2} \; / \; \varepsilon \tag{5.21}$$

An important consideration and one that has been recognized Gosman and Ioannides, 1981; Faeth, 1986) is that of specifying the correct instantaneous particle conditions at the inlet. The importance of the inlet particle fluctuation terms can be noted from the

reported measurements of Shuen et al. (1983, b) in a particle laden jet. Since, in general, inlet particle fluctuation measurements are not reported, an alternative approach to predicting these terms has to be devised.

In this study a relatively simple approach has been developed to predict the particle fluctuation terms at the inlet of the furnace. The calculation domain is extended upstream of the inlet to include a certain length of inlet pipe carrying the particle-air mixture. Since, the cross-stream particle fluctuations dictate the particle dispersion in the radial direction, calculations in the inlet pipe are done by the stochastic method outlined above for v_p and w_p. Fully developed turbulent gas flow is assumed in the pipe with $v_g = w_g = 0$, and $u_p = u_g$. Eddy size information is obtained from the experimental data for mixing length (Davies, 1972). To calculate instantaneous eddy properties, a Gaussian pdf is assumed with the mean value obtained from the assumption of fully developed pipe flow and the variance from the assumption of 10% turbulent intensity in the pipe. At the entrance to the pipe, for each particle size group, a mass weighted radial location is calculated assuming uniform radial distribution of particles and stochastic calculations for this particle size group are initiated from its mass-weighted location and continued to the end of the inlet pipe (which coincides with the inlet to the furnace). The computed particle velocities at the end of the inlet pipe are computed for each particle size group and are used to characterize the particle condition at each radial location at the combustor inlet.

5.2 SOLUTION PROCEDURE

The particle field is modeled as a set of representative particle trajectories. Five or six particle size groups are assumed and trajectory calculations are initiated from the grid points at the entrance to the domain. The particle number flow rate along each trajectory is assumed to be a constant.

The solution to the Lagrangian particle equations is obtained by a forward integration process. Since the particle equations for a dependent variable ψ can be linearized and expressed as

$$d\psi/dt = A - B\psi \ , \tag{5.22}$$

the forward integration (explicit) results in

$$\psi_{n+1} = \psi_n \, e^{-B\delta t} + A/B \ (1 - e^{-B\delta t}) \tag{5.23}$$

where n and n + 1 denote the beginning and end of the time increment δt. This equation has been used in the present calculations. Gas velocities at each particle location are interpolated from the neighboring velocity values stored along the control volume faces.

As mentioned earlier, the converged results are obtained by consecutive solutions of the gas phase and particle equations. After every solution of the particle equations, the gas phase source terms $S_{\phi,p}$ due to the passage of particles is computed and used in the very next solution of the gas phase equations. This process is repeated until changes in consecutive solutions are smaller than a pre-specified tolerance.

It is clear that the overall calculation process is extremely computer intensive, and the mesh size used should reflect a balance between accuracy and economy. A nonuniform 20 x 20 mesh is used in

the gas phase calculations and is found to satisfy overall conservation to less than 1%. The final mesh size and distribution of mesh points for each configuration is obtained after performing calculations on successively finer grids and accepting the mesh to be final if the solutions compare will with the solutions on a much finer mesh.

5.3 RESULTS AND DISCUSSION

Three sets of measurements have been chosen to make performance evaluations. The first two sets (Memmott, 1977; Leavitt, 1980) correspond to isothermal, two-phase flow in a cylindrical combustor geometry shown in Fig. 5.1. Experimental conditions for these measurements are also shown in the figure. The third set of data was obtained by Michel and Payne (1980) for pulverized coal flame in a rectangular geometry which, in this study, has been replaced by a cylindrical geometry with the same equivalent diameter. This practice is justified, in view of the large expansion ratio of the furnace, and Lockwood and Salooja (1983) have made the same assumptions with satisfactory results.

It should be noted that in the configurations considered, the nearfield of the inlet is characterized by strong adverse and radial pressure gradients, and radial velocities. Thus the injected particles clearly experience the flow field ellipticity.

Sensitivity tests

The sensitivity of the stochastic method to the number of stochastic calculations, tangential velocity fluctuation, eddy size

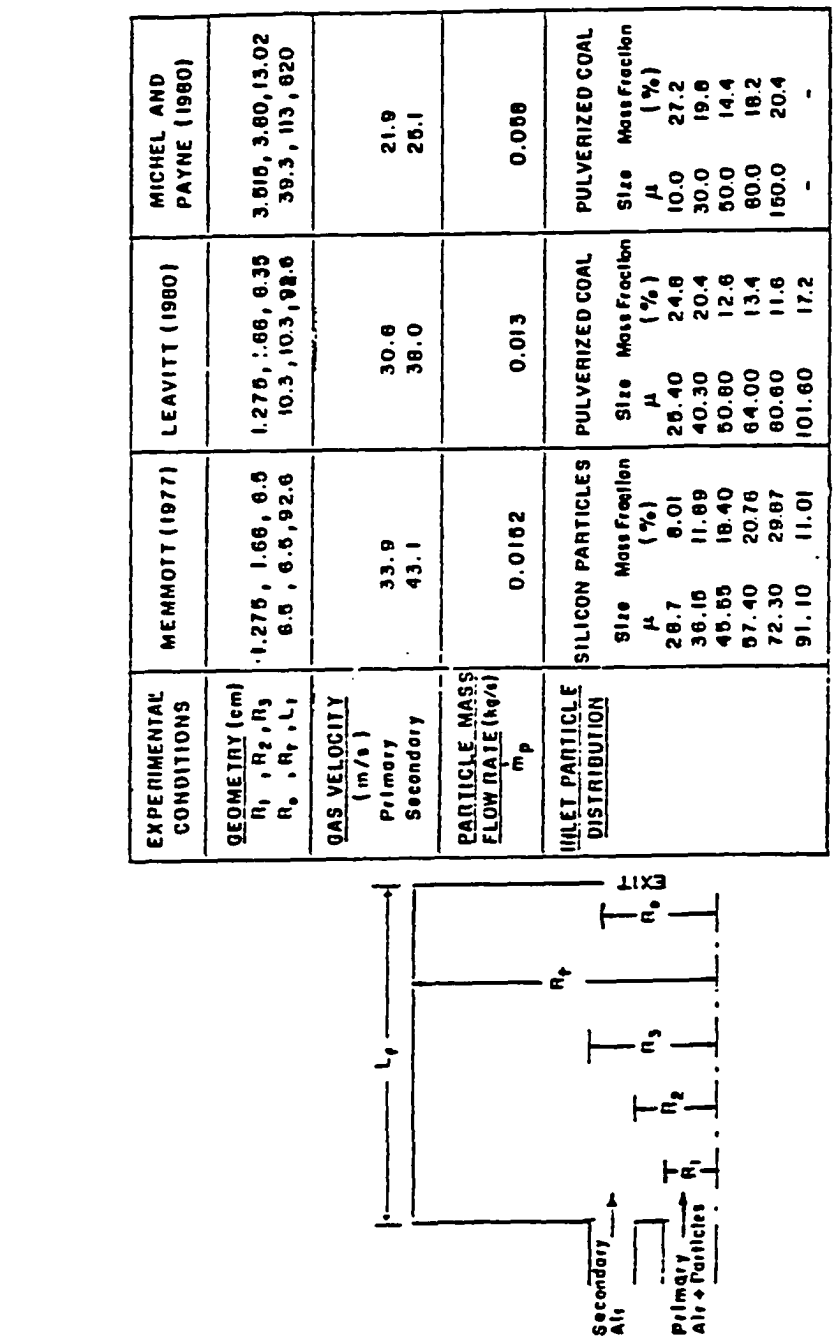

EXPERIMENTAL CONDITIONS	MEMMOTT (1977)	LEAVITT (1980)	MICHEL AND PAYNE (1980)
GEOMETRY (cm) R_1, R_2, R_3	1.275, 1.66, 6.5	1.275, 1.66, 6.35	3.810, 3.60, 13.02
R_e, R_f, L_f	6.5, 6.5, 92.6	10.3, 10.3, 98.6	39.3, 113, 620
GAS VELOCITY (m/s)			
Primary	33.9	30.6	21.9
Secondary	43.1	38.0	25.1
PARTICLE MASS FLOW RATE (kg/s) $\dot{m}_p$	0.0182	0.013	0.058
INLET PARTICLE DISTRIBUTION	SILICON PARTICLES	PULVERIZED COAL	PULVERIZED COAL
	Size μ / Mass Fraction (%)	Size μ / Mass Fraction (%)	Size μ / Mass Fraction (%)
	28.7 / 8.01	26.40 / 24.8	10.0 / 27.2
	36.15 / 11.89	40.30 / 20.4	30.0 / 19.8
	45.55 / 18.40	50.80 / 12.8	50.0 / 14.4
	57.40 / 20.78	64.00 / 13.4	80.0 / 18.2
	72.30 / 29.87	80.60 / 11.6	150.0 / 20.4
	91.10 / 11.01	101.60 / 17.2	- / -

Fig. 5.1 Schematic of the furnace configuration studied and experimental conditions

prescription, and the inlet dissipation rate are described in this section. The number of stochastic calculation for each particle size group and starting location is an important factor in controlling the overall computational cost. This consideration is particularly important for the computer intensive calculation of elliptic flows. Therefore, a sensitivity test is performed, and results are obtained with 5, 20, 40, 100 and 200 stochastic calculations for each particcle size group and starting location and compared with the isothermal data of Memmott (1977). In performing these calculations, the approach described earlier for computing the inlet particle fluctuations is not used, and the effect of tangential gas phase fluctuations is ignored. The turbulent energy dissipation rate is specified as recommended by Smoot and Smith (1985),

$$\varepsilon_{IN} = C_{\mu}^{0.75} \, k^{1.5} \, / \, (0.25 \, D_e) \qquad (5.24)$$

It can be seen (Fig. 2) that the predictions with 20, 40, 100 and 200 stochastic calculations per particle size group and starting location agree well with each other and also with the measured values. With 5 stochastic calculations per particle size group and starting location, local discrepancies are noted. Therefore, it appears that 20 stochastic calculations per representative particle trajectory are sufficient for elliptic, isothermal flows. This observation is also verified for reacting flows.

It should be pointed out that the measured particle mass flux profiles are typically characterized by a rapid initial decay followed by a long tail. In the region of rapid decay, a small uncertainty associated with the radial location translates into a

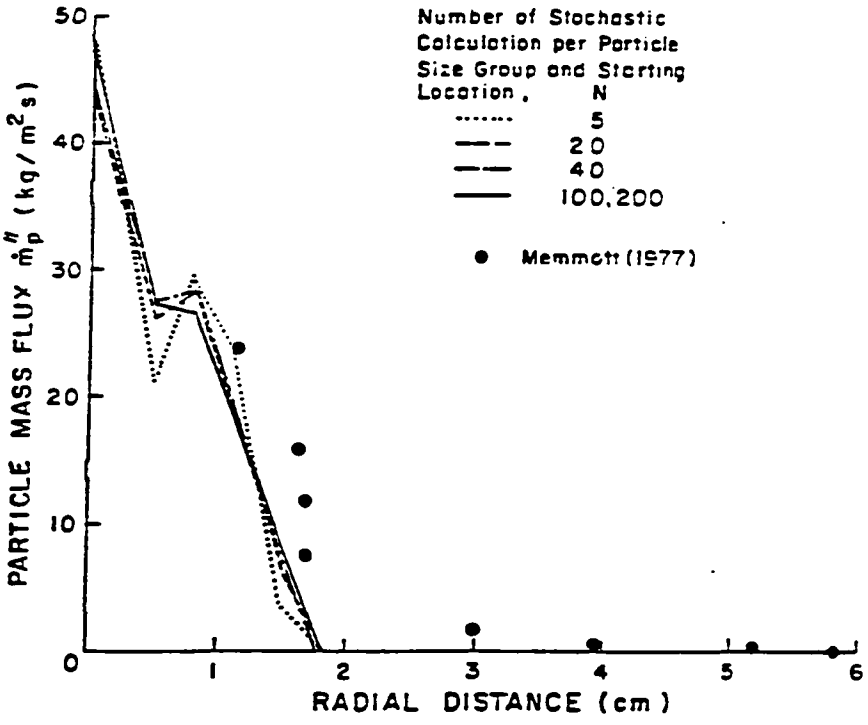

Fig. 5.2 Effect of number of stochastic calculations per particle size group and starting location

substantially larger error in the particle mass flux. Data shown in this study have been obtained with a suction prove, and in view of the uncertainty associated with the exact location of the probes center, comparison between predictions and measurements should be made with this in mind. Therefore, in this study, good agreement implies that the predictions correctly reproduce the measured trends.

In the stochastic model, the effect of the tangential gas phase velocity fluctuations w_g' ($w_g = 0$) can be handled with relative ease, but the importance of this effect on the two-dimensional trajectory predictions is not clearly known. Therefore calculations have been made with and without the tangential gas phase velocity fluctuation w_g' and the results compared in Fig. 5.3. In performing the calculations with w_g', the particle velocity equations (equations (5.3) and (5.4)) are rewritten as

$$du_p/dt = \alpha\ (u_g - u_p) \tag{5.25}$$

$$dv_p/dt = \alpha\ (v_g - v_p) + w_p^2/r \tag{5.26}$$

$$dw_p/dt = \alpha\ (w_g' - w_p) - v_p\ w_p/r \tag{5.27}$$

Since two dimensional trajectory calculations are being performed, equation (5.27) is solved only to calculate w_p^2/r appearing in equation (5.26). It is through this term that the effect of w_g' on the radial dispersion of particles is incorporated.

From Fig. 5.3 it can be seen that tangential gas phase velocity fluctuation reduce the mass flux values in the vicinity of the centerline; away from the centerline, the effects are negligible. To explain this it should be noted that since w_p is relatively small, the w_p^2/r term assumes importance only in the vicinity of the

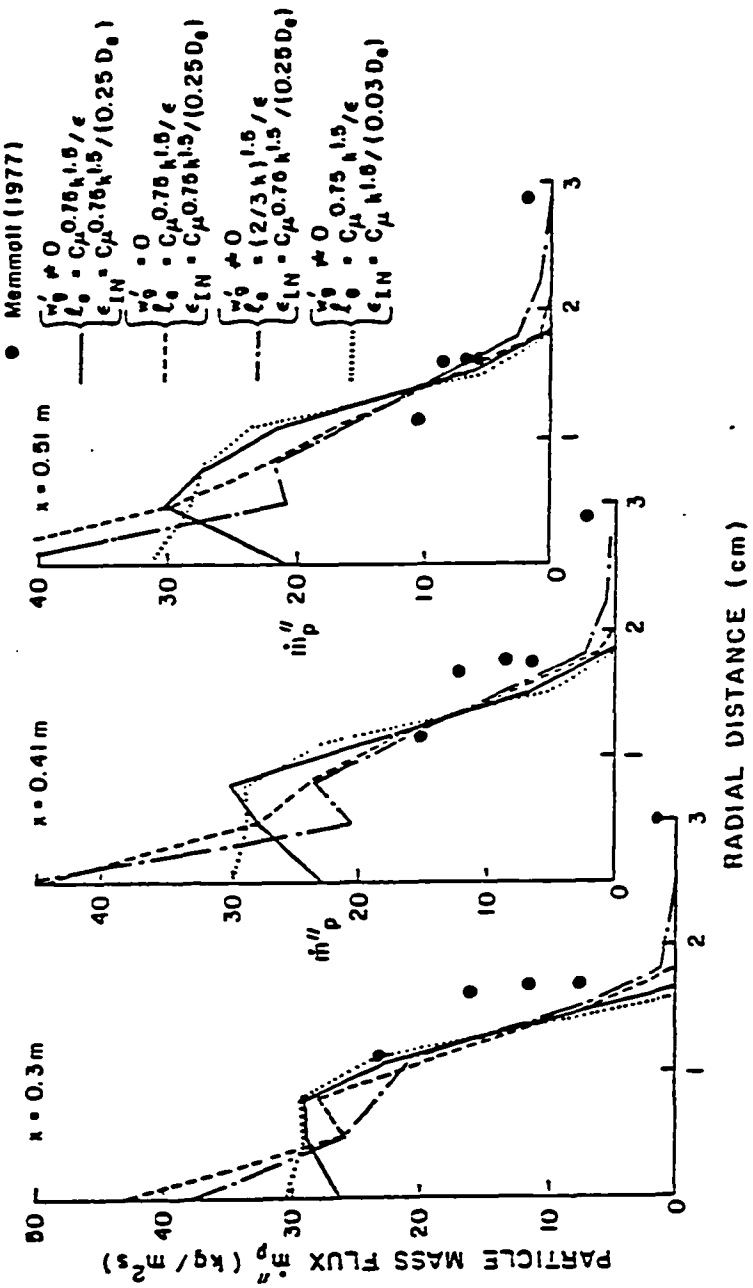

Fig. 5.3 Effect of tangential gas phase velocity fluctuations (w_g'), eddy size (ℓ_e), and inlet dissipation rate (ε_{IN}).

centerline where r also has a small value. Although centerline measurements are not available for this study, extrapolation of measured radial particle flux distributions appear to validate the lower centerline fluxes computed with the inclusion of w'_g.

Figure 5.3 also shows the effect of the eddy size (equations (5.19), (5.20) and (5.21)) on the particle dispersion. The eddy size given by equation (5.21) is only 10% or so greater than that predicted by equation (5.19) and the corresponding predictions for particle dispersions are nearly identical (solid line). When equation (5.21) is used, the computed eddy size is nearly 3 times larger, and therefore the predicted profiles (dash-dot lines) exhibit the measured trends of greater particle dispersion away from the centerline. Increase in centerline particle flux is also noted since, at the inlet, the particles are injected at the mass-weighted radial location, and the larger eddies disperse more particles towards the centerline. Since there is considerable uncertainty about the inlet gas phase dissipation rate ε_{IN}, its effect on particle dispersion is determined by using two commonly recommended expressions. The first is equation (5.24), recommended by Smoot and Smith (1985), and the second is the higher value of ε_{IN} recommended by Khalil et al. (1975) and Syed and Sturgess (1980) and given by

$$\varepsilon_{IN} = c_\mu \, k^{1.5} / (0.03 \, D_e) \quad . \tag{5.28}$$

It can be seen from Fig. 5.3 that the higher inlet dissipation rate (dotted line) increases centerline paticle flux, but except close to the centerline, compares well with the predictions using equation (5.24) (solid line).

It should be noted that although the centerline particle mass flux appears to be quite sensitive to the effects of tangential gas phase fluctuation, eddy size and inlet dissipation rate, the particle mass flow rate in view of the smaller cross-sectional area near the centerline, is less sensitive than the centerline particle flux. Results reported in the remaining study include the effect of tangential gas phase fluctuation and use equation (5.19) for ℓ_e and equation (5.24) for ε_{IN}.

The effect of specifying the particle velocity fluctuations at the inlet, using the simple stochastic approach described earlier for computing the radial particle velocity fluctuations in a lead-in inlet pipe, is shown in Figs. 5.4 and 5.5. Quite clearly, the effects are significant, and for realistic predictions with the stochastic method, the inlet particle velocity fluctuations must be included.

Model Evaluation

In this section the predictions for particle dispersion using Models 1 and 2 and the stochastic model will be compared with each other.

Isothermal Flow: Since Model 2 has been the most populaar approach heretofore, isothermal flow predictions has been obtained using Model 2 and the stochastic method. In view of the uncertainty associated with the value of σ_p^t in Model 2, predictions have been obtained using the recommended value of 0.35 (Fletcher, 1983) and 0.2.

Figure 5.4 shows the comparison between the predictions and the data of Memmott (1977) at two axial locations. Predictions using Model 2 exhibit a steep radial decay in particle flux with near zero values beyond r = 2.0 cm. The measurements, however, indicate a greater level of the radial dispersion of particles with the particle flux gradually decaying to zero at r = 4.0 cm. Predictions using the stochastic method exhibit these measured trends and, quite clearly, provide more realistic simulations than those obtained using Model 2. Both choices of σ_p^t yield nearly similar radial profiles with somewhat greater radial dispersion predicted at the lower σ_p^t value.

The validity of the simple stochastic method used for predicting the inlet particle velocity fluctuations may be noted by comparing $(\sqrt{v_p'^2}/u_p)_{inlet}$ predicted in this study (the overbar denotes ensemble average) with the measurements in Shuen et al. (1983, b). The two values agree well with each other, and although the two flow conditions in the two inlet pipes are somewhat different, the same order of magnitude of the two values indicates the validity of the approach.

The stochastic approach incorporating the stochastic calculation of the inlet conditions and 20 stochastic calculation per particle size group and starting location takes nearly 3.4 times more computing effort than the computations with Model 2. However, this increase in the computational effort, quite clearly, is offset by the more realistic simulations of particle dispersion profiles.

Fig. 5.5 shows the comparison of predictions with the data of Leavitt (1980) and observed trends are consistent with those in

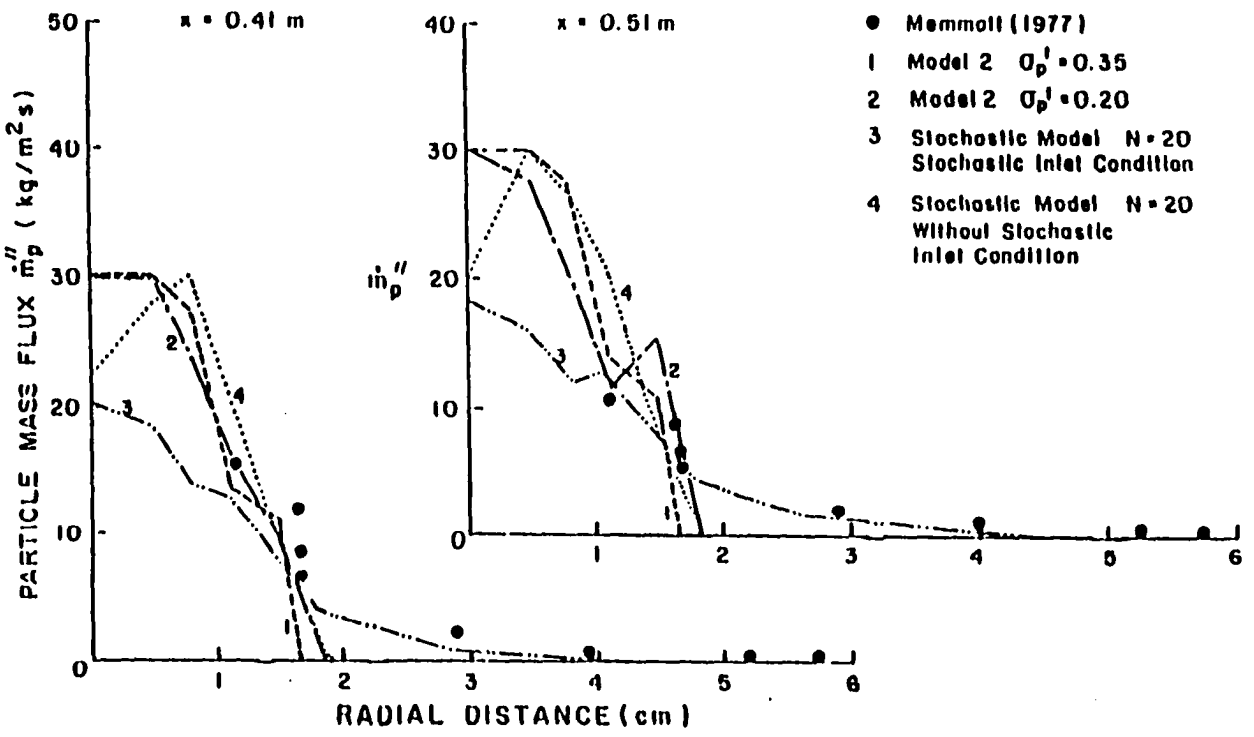

Fig. 5.4 Model evaluation, isothermal flow data of Memmott (1977)

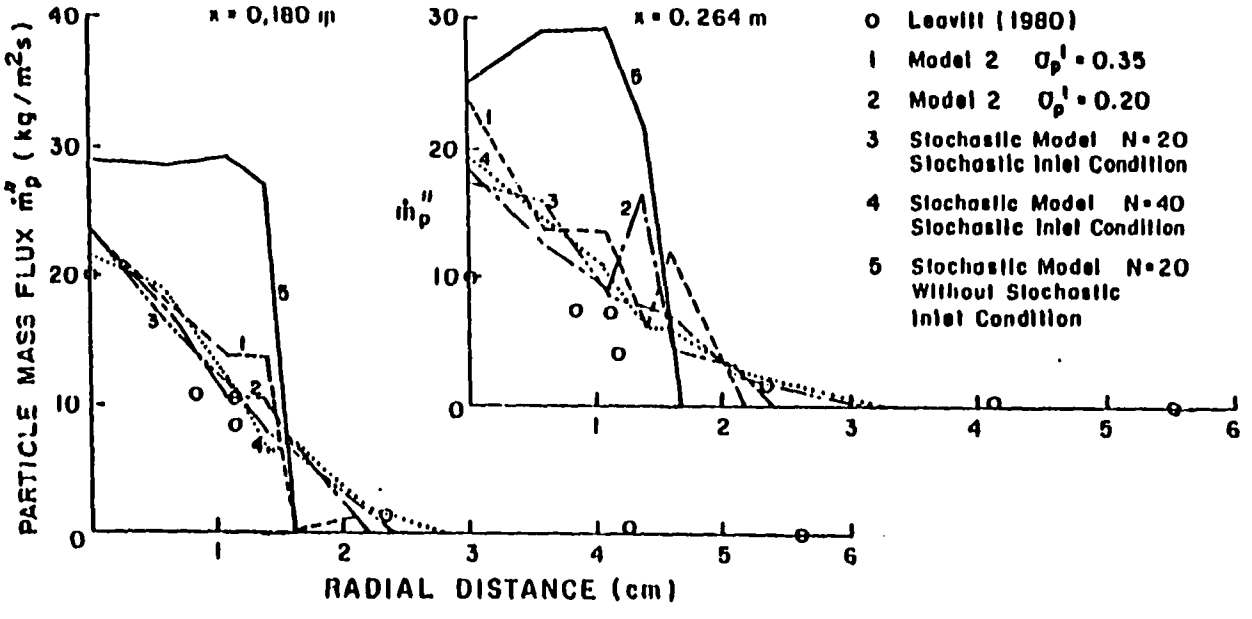

Fig. 5.5 Model evaluation, isothermal flow data of Leavitt (1980)

Fig. 5.4. Model 2 profiles exhibit rather non-uniform behavior. These nonuniformities can be reduced by increasing the number of particle starting locations and particle size groups but the radial dispersion of particles is always underpredicted when Model 2 is used. Further, increasing the particle size groups and starting locations for Model 2, leads to significant increases in computational effort.

Reacting Flow: Pulverized coal combustion predictions using Model 1, Model 2 and the stochastic method are compared with the A1 flame data of Michel and Payne (1980). Model 1 predictions compare rather poorly with the measured values, while the solutions obtained using Model 2 do not agree with the measurements beyond X of 2.0 meter. Model 2 predictions with $\sigma_p^t = 0.2$ exhibit a sharper decay than those with $\sigma_p^t = 0.35$, and are therefore not shown in the figure.

Predictions with stochastic method appear to agree well with the measured values. The axial distribution without inlet particle velocity fluctuations exhibit satisfactory agreement with the data, but the radial distributions (not shown) indicate local differences between predictions and measurements, and again point to the importance of incorporating tangential and radial particle velocity fluctuations at the inlet.

In Fig. 5.2, the sensitivity of the stochastic predictions to the number of stochastic calculations per particle size group and starting location was presented for isothermal flows. For a reacting flow, Fig. 6 shows the effect of increasing the number of

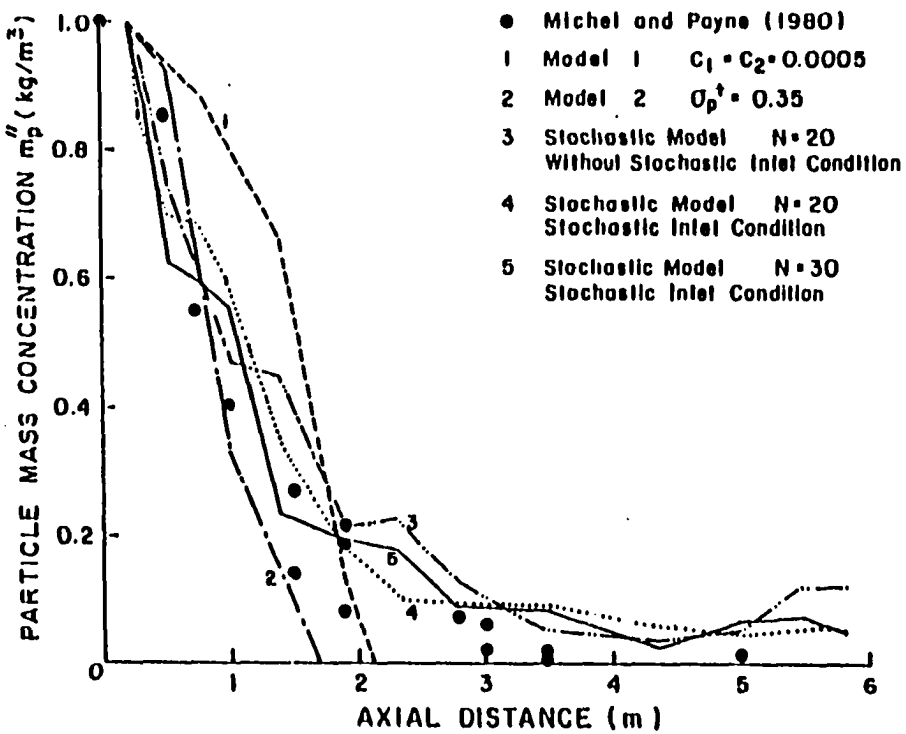

Fig. 5.6 Model evaluation, reacting flow data of Michel and Payne (1980)

stochastic calculation per size group and starting location from 20 to 30. The predicted profiles, again, show close agreement to each other.

As for isothermal flows, stochastic calculations with inlet particle velocity fluctuations, require nearly 3 times greater computational effort than the calculations with Model 2.

Radial distributions of particle concentration at different axial distances, ranging from 0.1 m to 3.5 m from the inlet, are presented in Fig. 5.7. Predictions using the stochastic method and Model 2 are presented. Quite clearly, at all axial locations, the stochastic method provides predictions in better agreement with the measured values. As for isothermal flows, the radial profiles predicted using Model 2 exhibit non-uniform behavior.

5.4 CONCLUDING REMARKS

A comparison between the stochastic model and two gradient models for the dispersion of particles due to turbulence in an isothermal or reacting elliptic flow field has been made. Predictions of the gradient models are characterized by a more rapid decay in the radial dispersion of particles compared to the measured trend and the predicted profiles exhibit rather non-uniform behavior. Predictions with the stochastic model show good agreement with the measured values in both isothermal and reacting environments, but require the correct specification of the inlet cross stream particle velocity fluctuations. The stochastic method requires greater computing effort, but is recommended in view of the more physically realistic simulations.

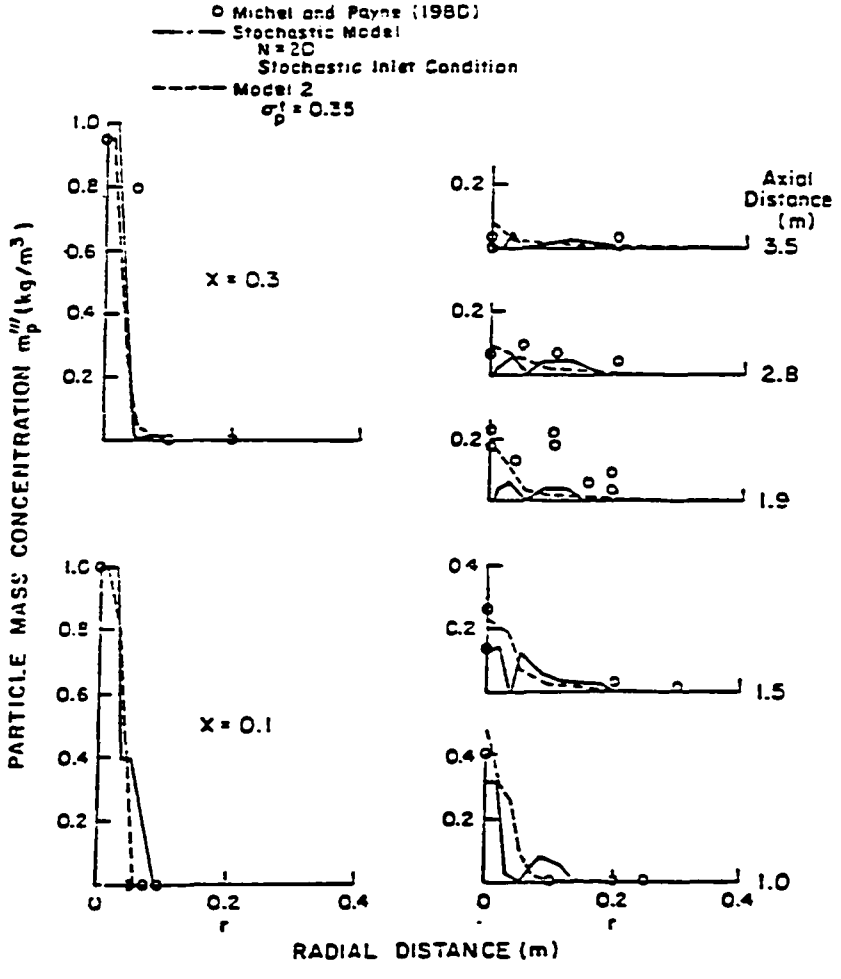

Fig. 5.7 Radial distribution of particle mass concentration

CHAPTER 6

COMPREHENSIVE COMPUTER CODE FOR PULVERIZED COAL COMBUSTION

The purpose of this chapter is to evaluate the comprehensive computer code for the prediction of pulverized coal combustion in a two-dimensional axi-symmetric geometry. The basic methodology and models have already been described in detail in chapters 2 and 5. Therefore, only a brief summary is presented in section 6.1 for completeness. The evaluation of the comprehensive computer code is based on comparison with IFRF experimental data (Michel and Payne, 1980) using West German bituminous Saar coal.

6.1 MATHEMATICAL MODELS AND SOLUTION PROCEDURE

In solving for the coupled system of equations for the gas and particles, an Eulerian-Lagrangian formulation is adopted, in which the gas phase equations are solved in an Eulerian framework and the particle equations are solved in Lagrangian coordinates. The gas-particle coupling is resolved through additional source terms in the gas phase equations as recommended by Crowe et al. (1977).

The dependent variables characterizing the mean gas flow behavior such as mean velocities are solved by a control volume based finite difference procedure (Patankar, 1980). The two equation (k-ε) model is used for turbulence closure (Launder and Spalding, 1972). A phenomenological eddy breakup model proposed by

Magnussen and Hjertager (1976) is employed to account for coal-off gas turbulent combustion. The model is characterized, as mentioned in section 2.1, by the neglect of turbulent fluctuation of dependent variables such as species mass fraction and temperature. The reason for selecting this combustion model is because of the partial premixed burning of coal-off gas since coal-off gas release occurs in the near burner low temperature region (Lockwood and Salooja, 1983). Since models for the general case of partially premixed turbulent reactions are not available, the aforementioned eddy breakup model is employed. The eddy breakup model constants are chosen based on the recommendation of Lockwood and Salooja (1983).

For radiation, the four flux model (Gosman and Lockwood, 1974) is used. Gas properties are calculated from the functional relationships given by Svehla (1963). The Lagrangian particle calculations are initiated for each particle size group and radial statar-ing locations at the inlet to the furnace by a forward integration procedure.

To model the effect of turbulence on particle dispersion, an improved version of the stochastic model proposed by Gosman and Ioannides (1981) is employed. As described, in detail, in the previous chapter, this improvement is centered around the development of a suitable technique for correctly predicting the inlet instantaneous cross-stream particle velocities. As in the previous chapter, five particle size groups and four starting locations are employed and 20 stochastic iterations are performed for each particle size group and starting location.

For coal particle devolatilization and char reaction, the empirical models based on the recommendation of Baum and Street (1971) are employed. The heat of particle reaction is assigned entirely to the particle phase.

As mentioned in chapter 2, a consecutive calculation procedure is adopted for obtaining converged results, in which, the time-averaged gas phase equations are first solved, followed by the solution of the particle equations. After every solution of the particle equations, the coupling source terms due to the passage of particles is computed and used as additional source terms in the very next solution of the gas phase equations. This process is repeated until changes in major gas phase variables such as enthalpy and velocities are smaller than a specified tolerance. Typically 30 consecutive calculations of gas and particle phase equations are needed.

In this chapter, predictions are obtained and compared with four sets of experimental data reported by Michel and Payne (1980). In one of the four cases the flame is detached from the burner while in other three cases an attached flame is obtained. The experiments were conducted whose configuration is shown in Fig. 5.1 and the experimental conditions for the four cases are given in Table 6.1. The furnace used in these investigations has a square cross section, but is modeled with an equivalent cylinderical geometry as discussed in Chapter 5.

Table 6.1 Experimental conditions of IFRF data (Michel and Payne, 1980)

	A1	A2	B1	B3
Primary				
Velocity (m/s)	21.9	30.8	40.7	29.7
Temperature (k)	423	588	463	623
Burner Dia (mm)	70.3	107.1	703	132
Coal Mass Flow (kg/hour)	212	220	212	220
Secondary				
Velocity (m/s)	25.1	25.1	9.6	12.5
Temperature (k)	763	763	773	743
Burner Dia (mm)	260	260	399	342
Flame State	Attached	Attached	Detached	Attached

6.2 RESULTS AND DISCUSSION

A1 Flame

The first set of measurements by Michel and Payne (1980) correspond to the A1 flame and provide detailed temperature and species concentration profiles along the radial direction at several axial locations. As shown in Table 6.1, an attached coal flame is obtained in this case.

Figure 6.1 shows comparisons of measured and predicted centerline gaseous temperature profiles together with predicted particle temperature profile. In Fig. 6.2, the radial profiles of gaseous temperature at axial locations of 0.5 m, 1.0 m, 1.9 m and 3.5 m are shown. In general, comparisons between predictions and measurements are in good agreement. The discrepancy between gas and particle temperature is believed to be due to the effect of assigning the entire heat of particle reaction to the particle phase.

Fig. 6.3 shows comparisons of measured and predicted O_2 and CO_2 profiles along the centerline, together with the measured CO profile. In addition, the prediction of O_2 reported by Hill (1983) is included for comparison purposes. The predicted trend of O_2 profile is in good agreement with the measured value. The predicted CO_2 profile shows considerable deviation from the measured values with a peak in the profile occurring at an axial location of 1.5 m. The overestimation of CO_2 level is attributed to the lack of modeling CO prediction, considering the total mass of carbon atom balance together with the CO concentration level on Fig. 6.3.

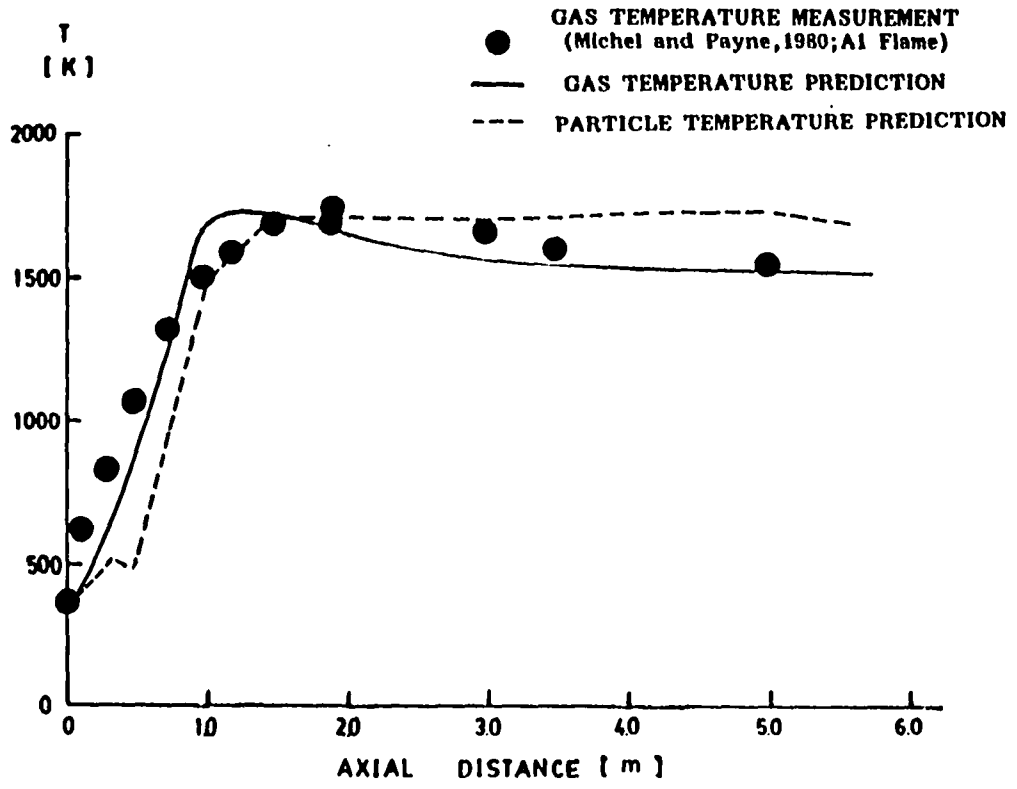

Fig. 6.1 Comparison of gas and particle temperature profiles along the centerline (A1 flame)

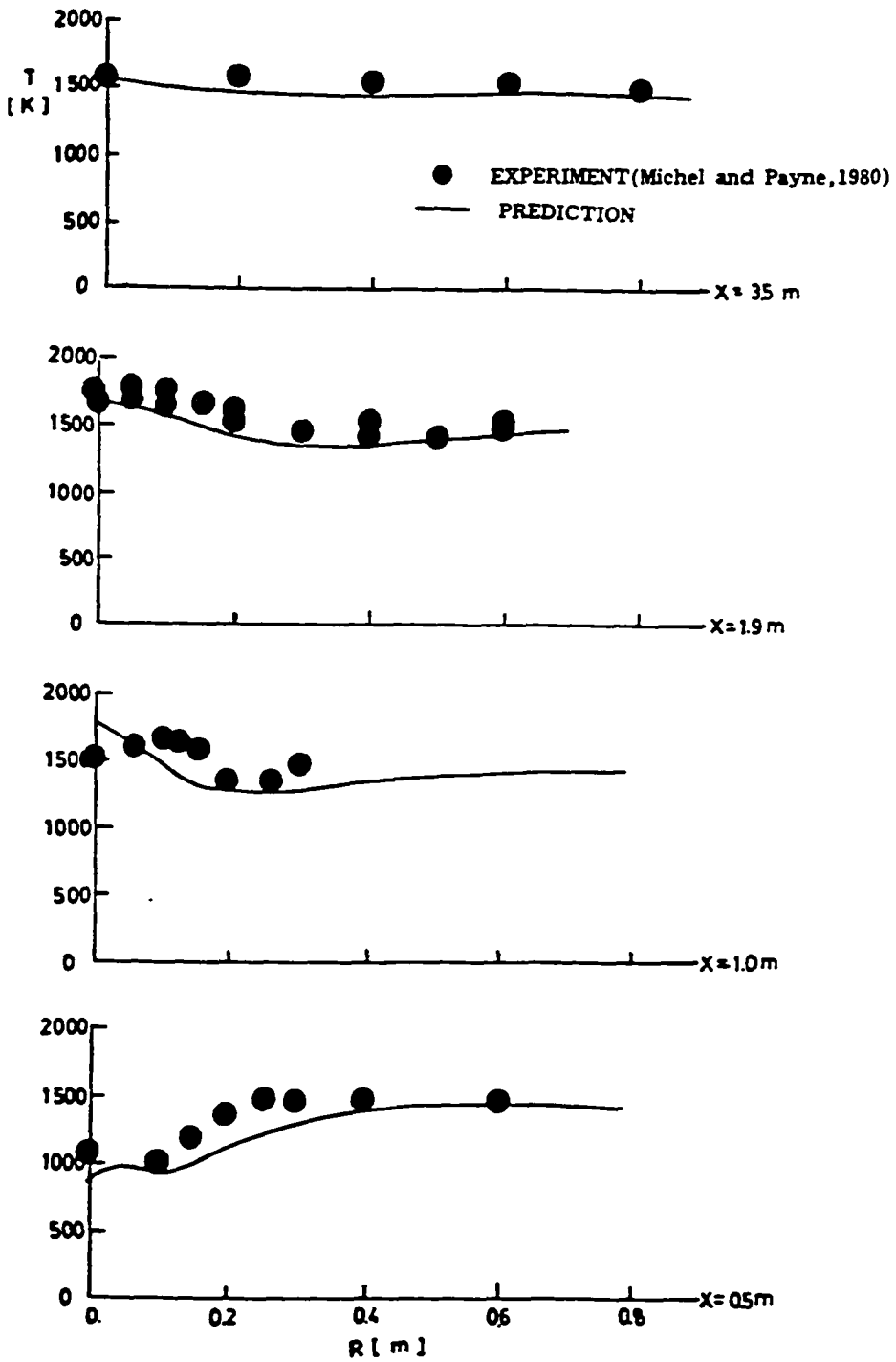

Fig. 6.2 Comparison of radial gas temperature profiles (Al flame)

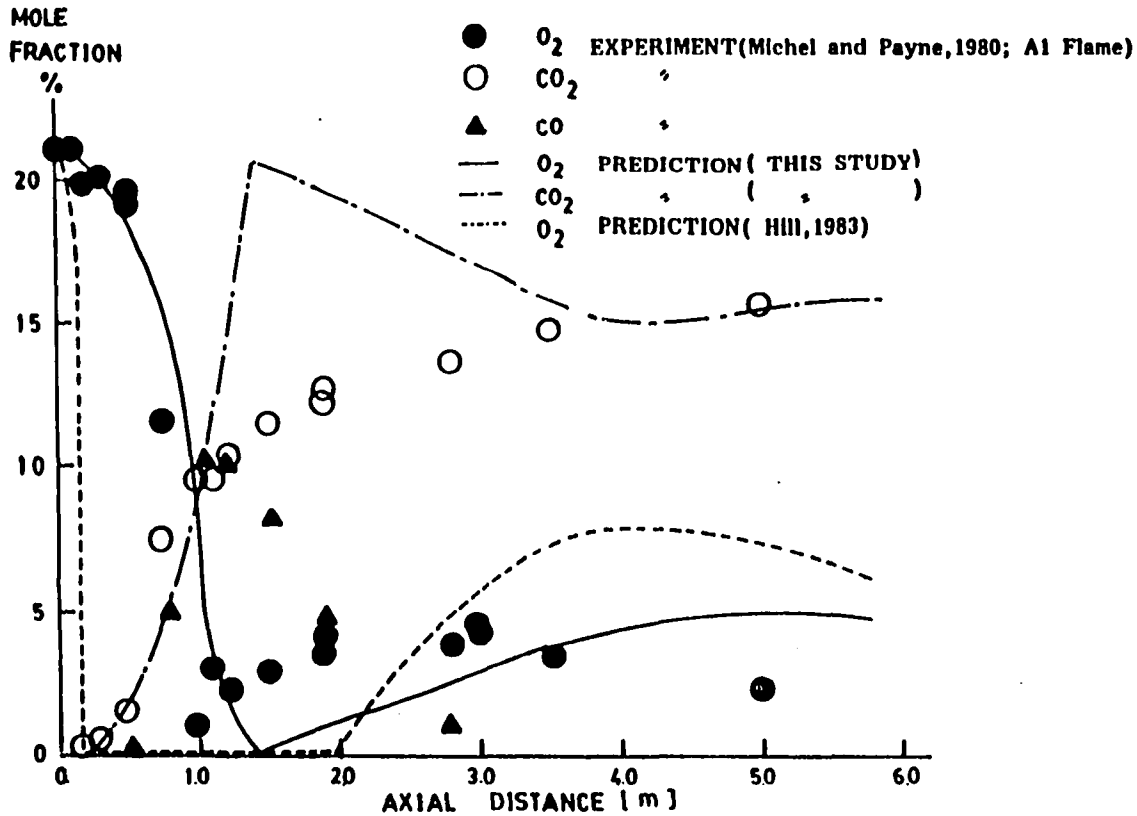

Fig. 6.3 Comparison of species concentration profiles along the centerlin (A1 flame)

The predicted O_2 profile by Hill (1983) shows a sharp decay in the near burner region and rather poor agreement with the measured trend. Hill (1983) has employed a number of different models, compared to this study; these include the conserved scalar method for coal-off gas combustion, an empirically based gradient model for turbulent particle dispersion and devolatilization model proposed by Ubhayakar et al. (1976). Therefore, any quantitative evaluation of individual model performances and comparison of models used by Hill (1983) and in the present work is not feasible.

The O_2 and CO_2 profiles are also shown in Fig. 6.4 and 6.5, respectively. The predicted O_2 levels overestimate the measured values for $R > 0.2$ m. Similar trends are observed in the prediction of Hill (1983) which are not shown here. One possible explanation is that the inlet air flow rate may have been overestimated or the coal flow rate underestimated. As a consequence of O_2 overprediction, the CO_2 profile is correspondingly underestimated for $R \geq 0.2$ m.

A2 Flame

The measurements of A2 flame provide temperature and species concentration only along the centerline. This is again an attached flame but with different primary stream flow conditions. Fig. 6.6 and 6.7 show comparisons between measured and predicted temperature and species profiles. These trends are similar to those of A1 flame described above. In general, agreement is good, considering the fact that the production and destruction of CO is not modeled.

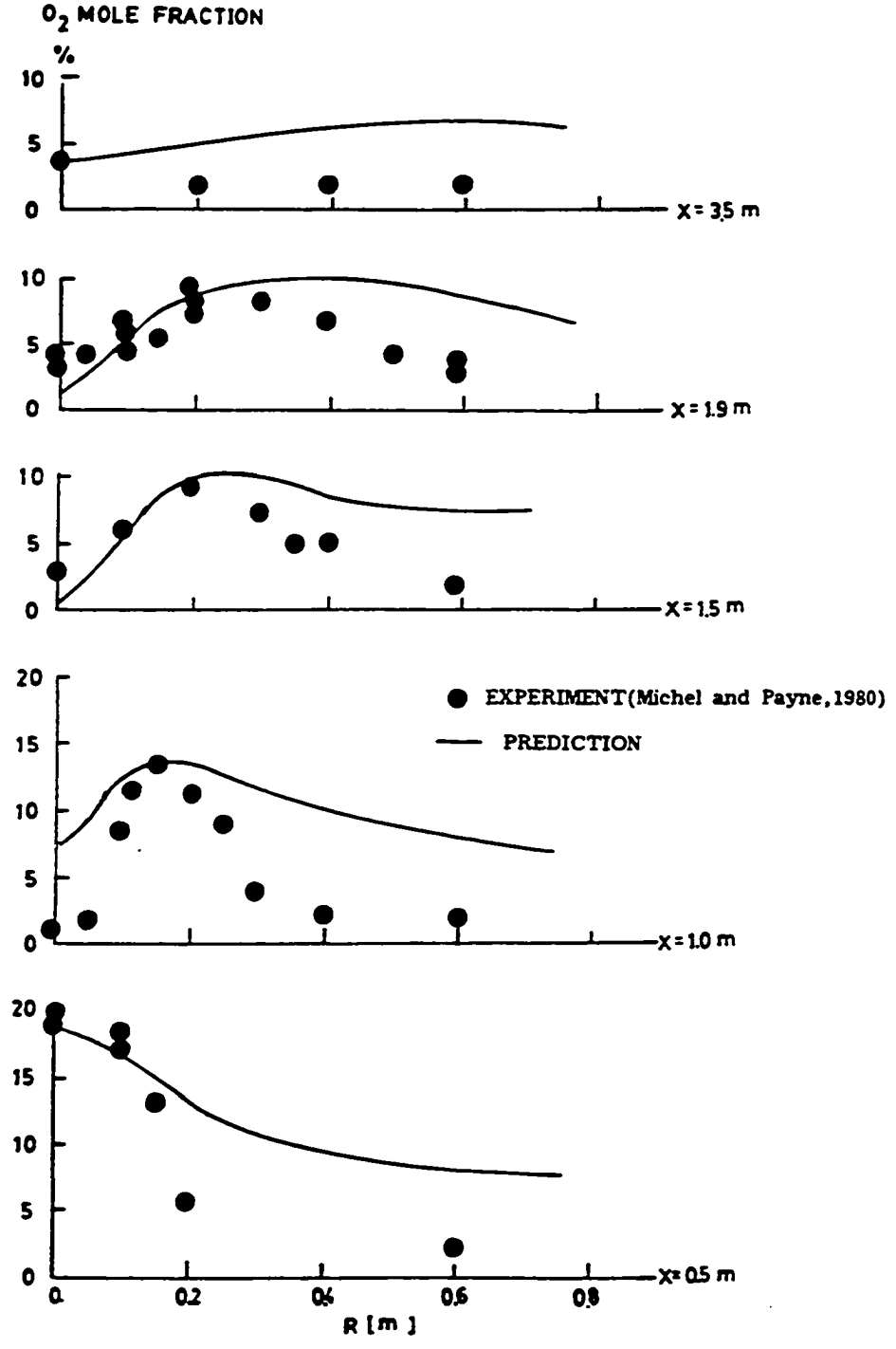

Fig. 6.4 Comparison of radial O_2 concentration profiles (A1 flame)

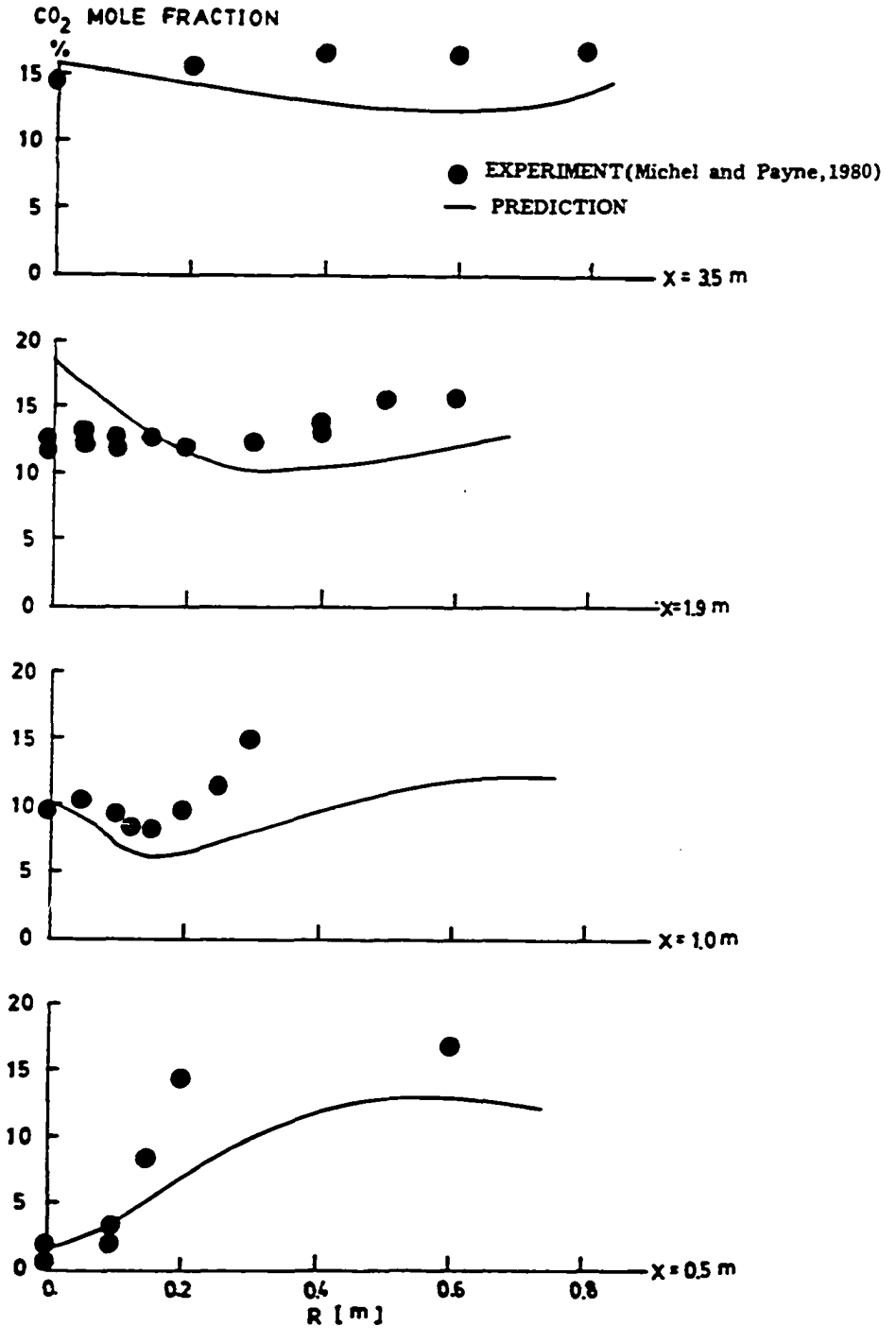

Fig. 6.5 Comparison of radial CO_2 concentration profiles (A1 flame)

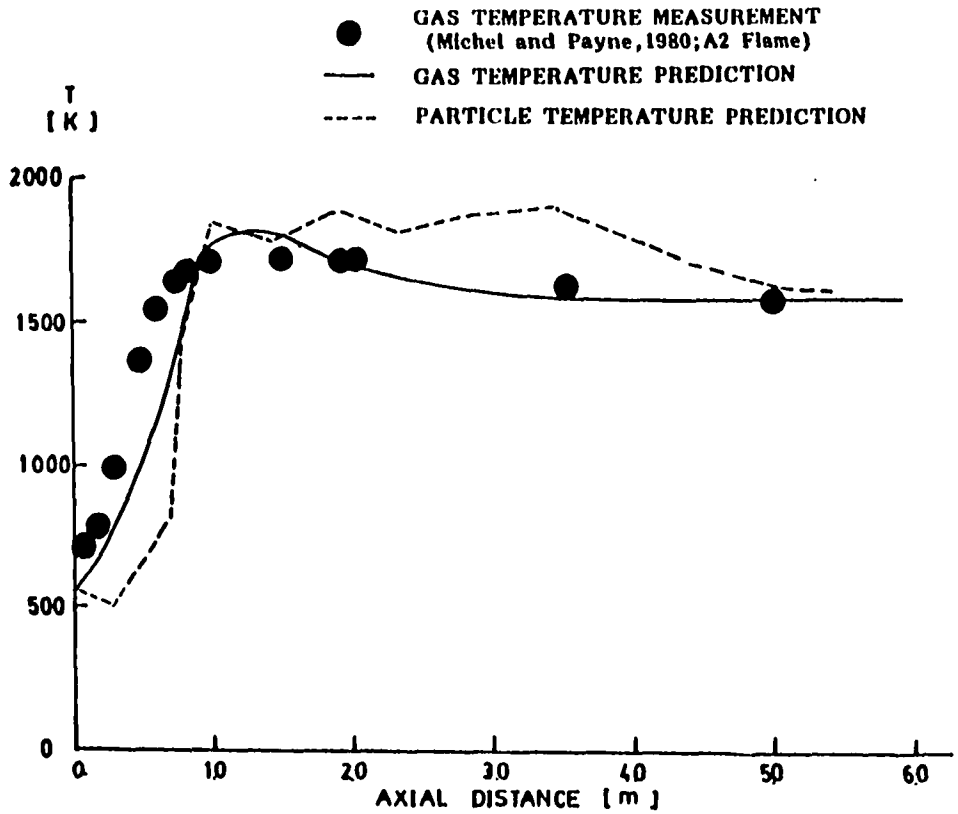

Fig. 6.6 Comparison of gas and particle temperature profiles along the centerline (A2 flame)

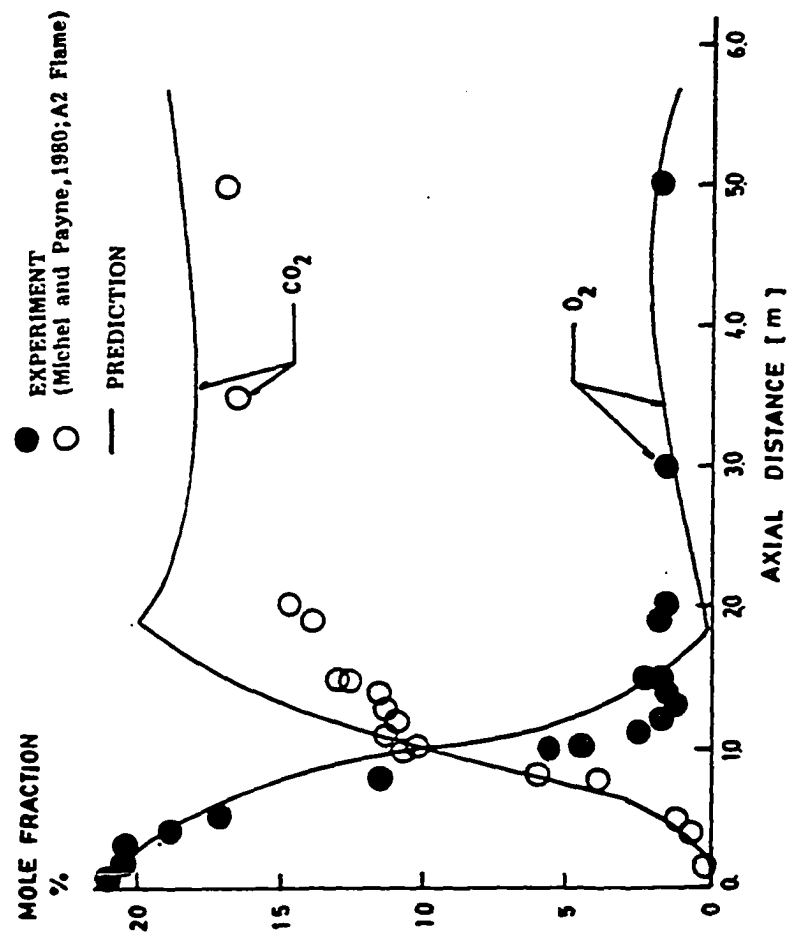

Fig. 6.7 Comparison of species concentration profiles along the centerline (A2 flame)

B1 Flame

The measurements of B1 flame again provide detailed temperature and species concentrations along the radial direction at several axial locations. As shown in Table 6.1. this case has a higher primary velocity which causes flame lift-off. Fig. 6.8 and 6.9 show predicted and measured gas phase temperature profiles together with the predicted centerline particle temperature profile. In the lift-off region, up to 1.0 meter from the inlet, significant deviations between measured and predicted values are noted, and can be attributed to the fact that local quenching effects have not been included.

Comparisons of species concentration profiles are illustrated in Figs. 6.10-13, which also indicate the importance of flame quenching modeling in the near inlet nozzle field. However, the overall trends are in good agreement with each other. The prediction of O_2 centerline profile by Hill (1983) is also presented in Fig. 6.10, and as for the A1 flame larger differences from the measured trend, compared to the differences in the present study, are noted.

Flame B3

The measurements of attached B3 flame again provide temperature and species concentration profiles only along the centerline as in A2 flame. Comparisons are presented in Figs. 6.14 and 6.15. Trends similar to those observed earlier are obtained.

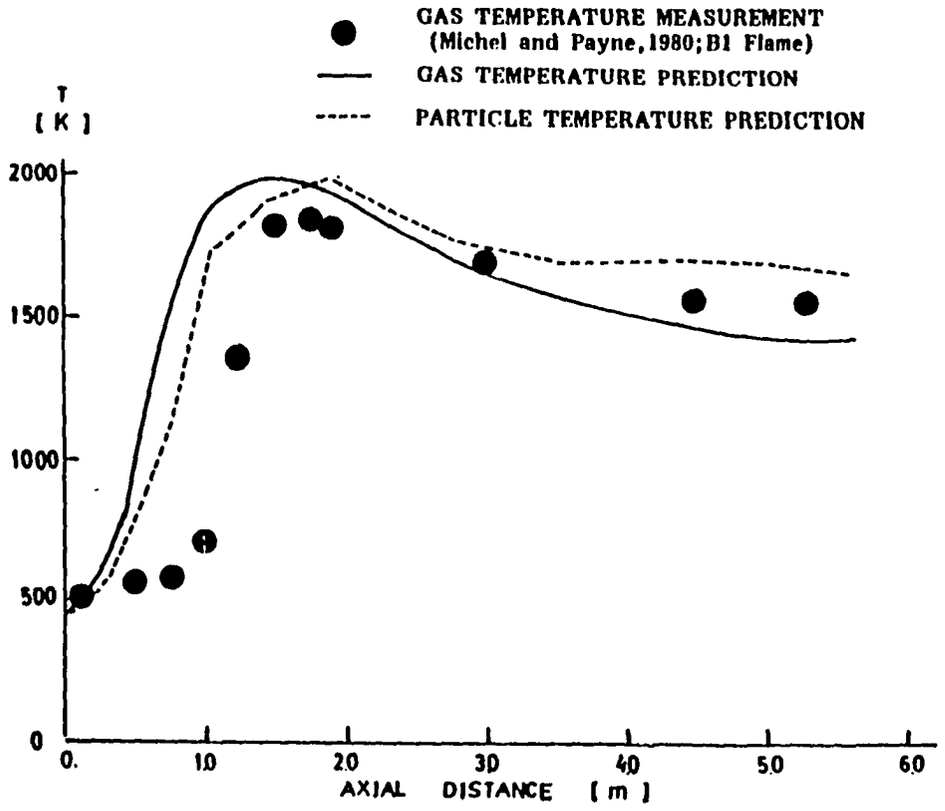

Fig. 6.8 Comparison of gas and particle temperature profiles along the centerline (B1 flame)

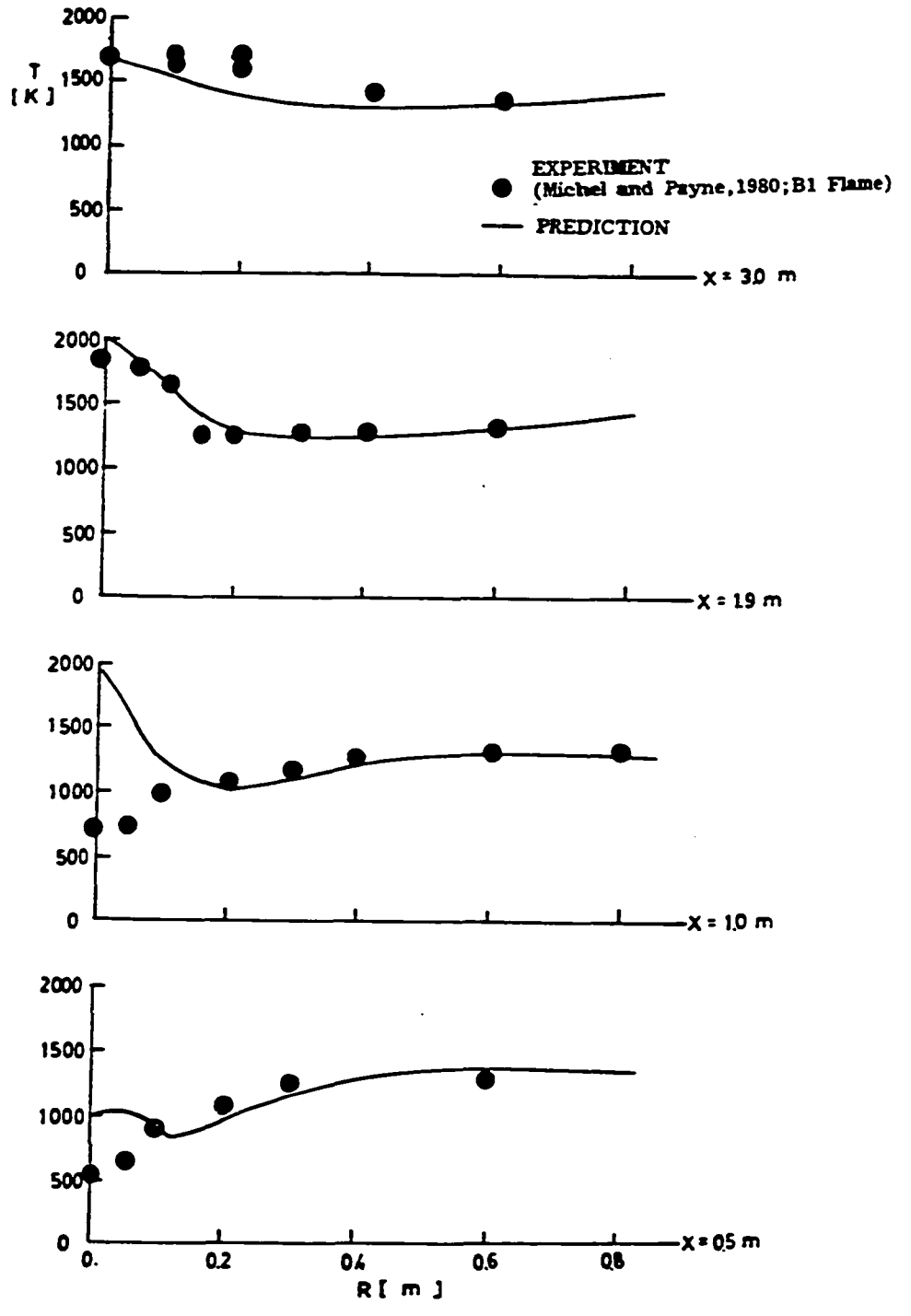

Fig. 6.9 Comparison of radial temperature profiles (B1 flame)

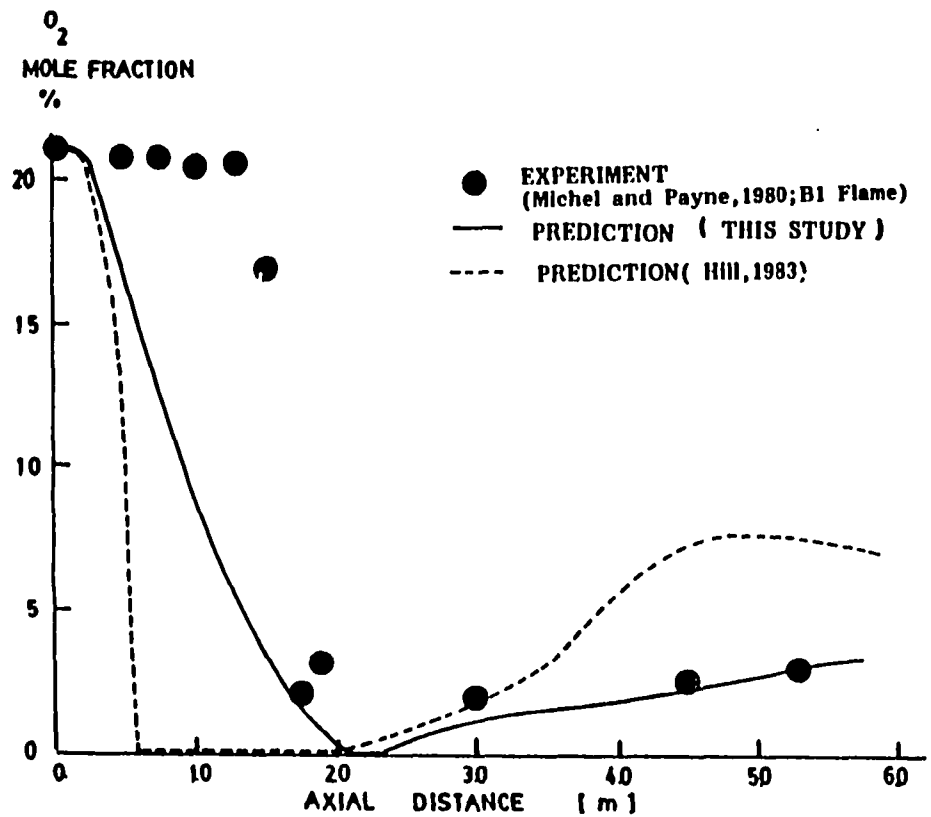

Fig. 6.10 Comparisons of O_2 concentration profiles along the centerline (B1 flame)

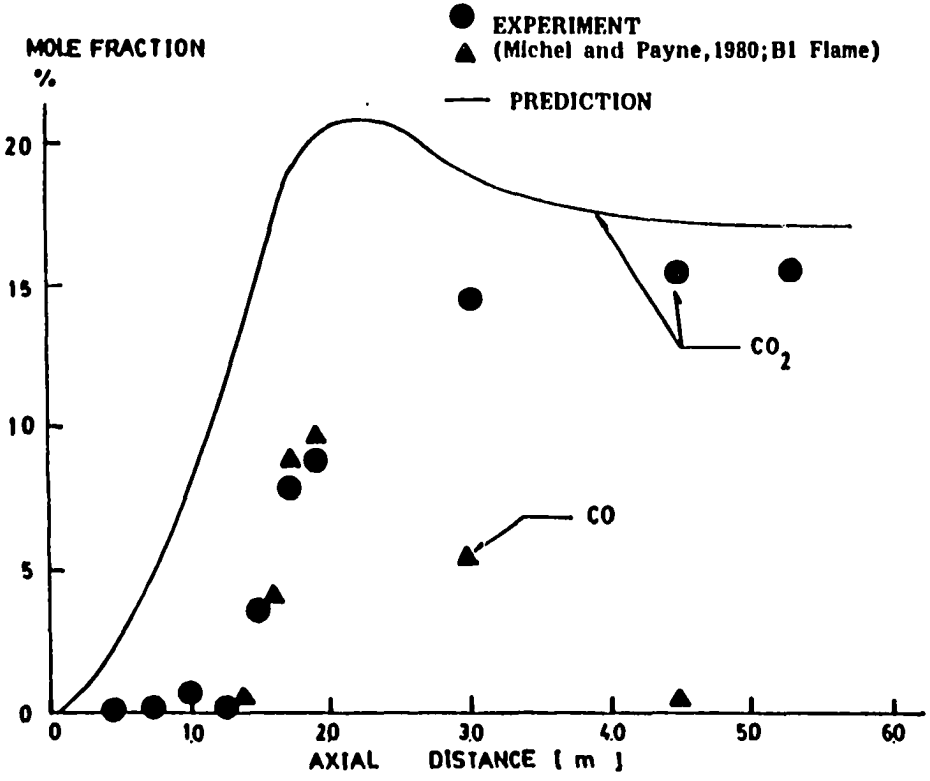

Fig. 6.11 Comparison of CO_2 concentration profiles along the centerline (B1 flame)

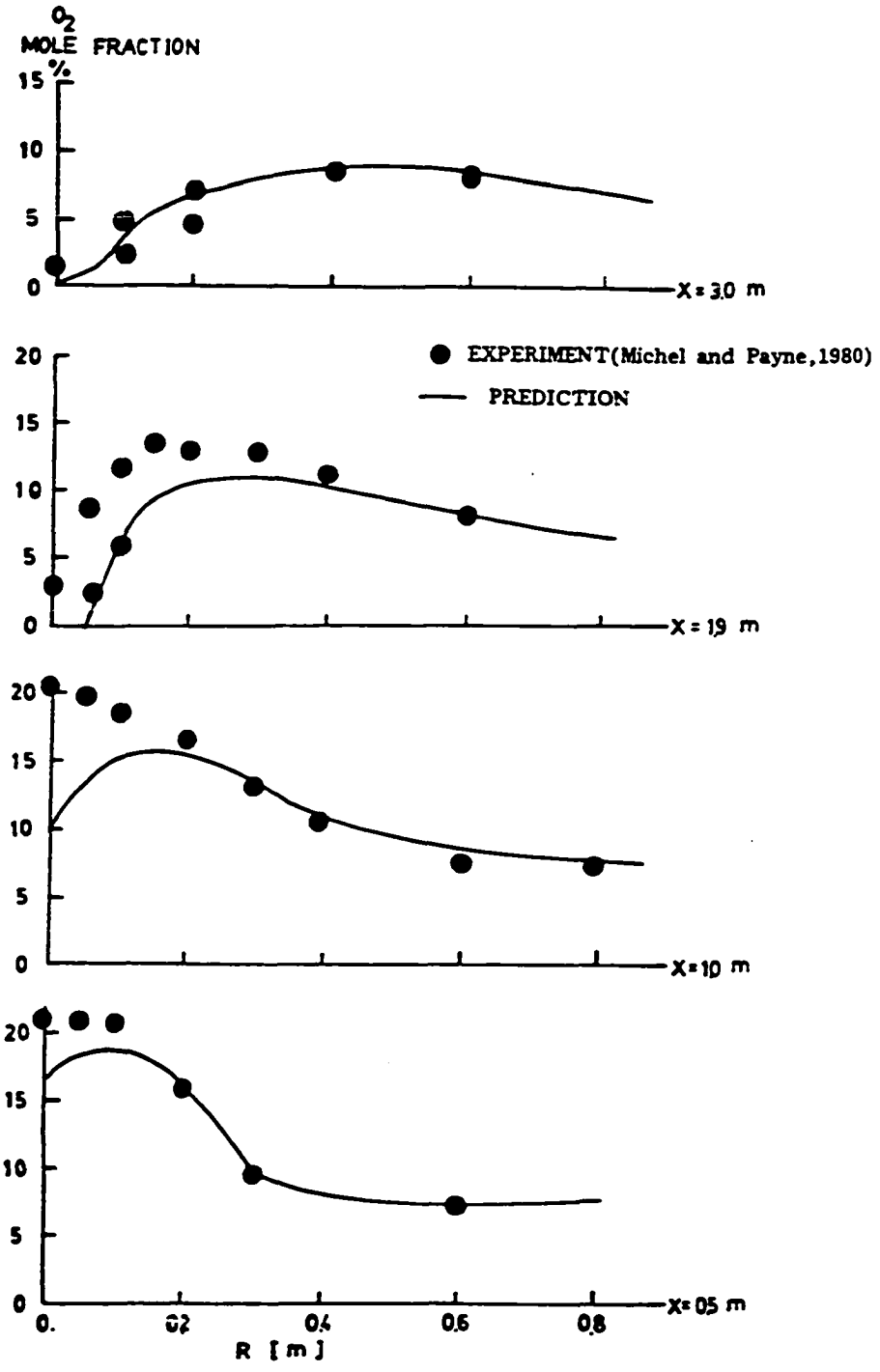

Fig. 6.12 Comparison of O_2 radial concentration profiles (B1 flame)

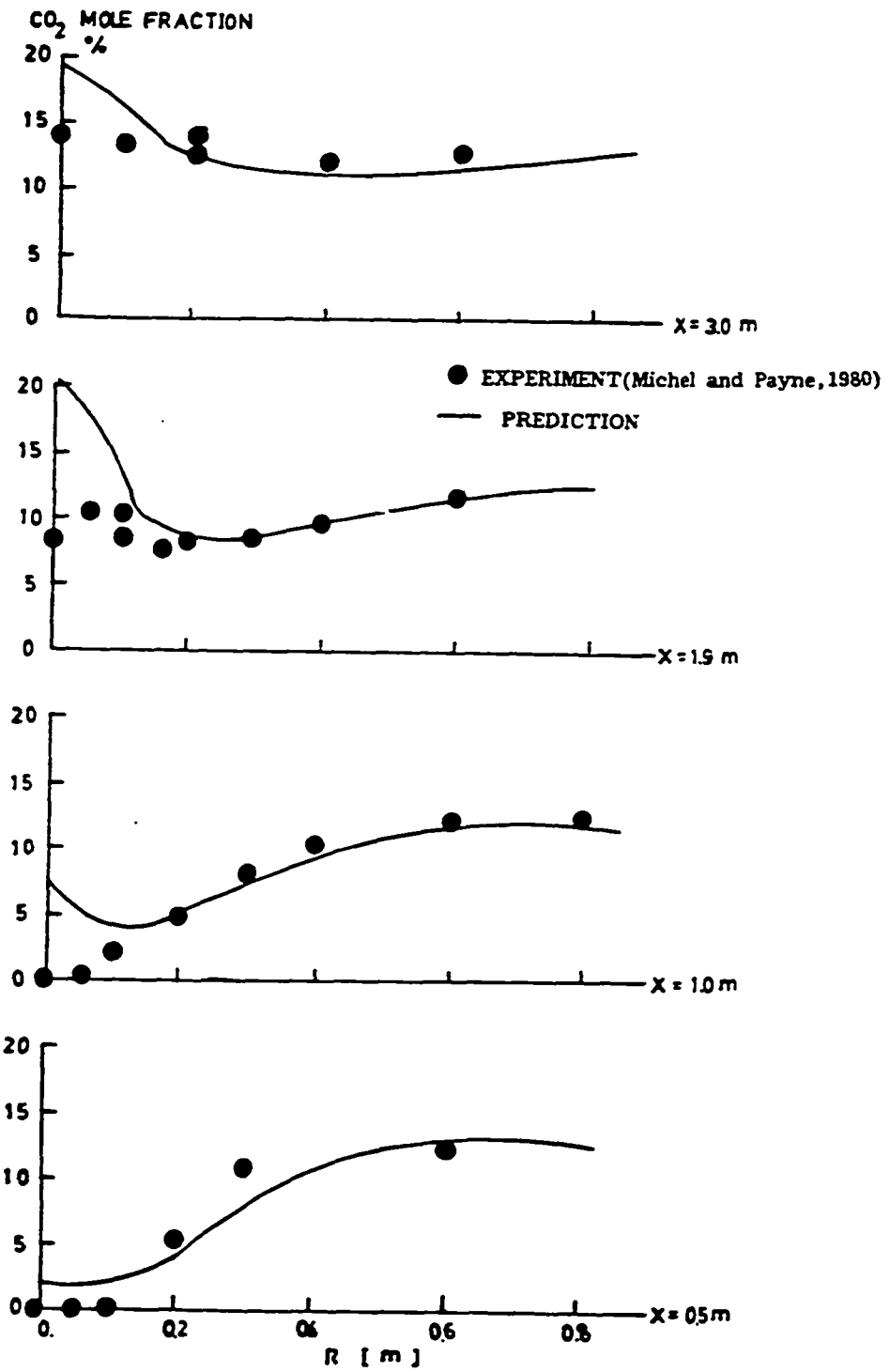

Fig. 6.13 Comparison of CO_2 radial concentration profiles (B1 flame)

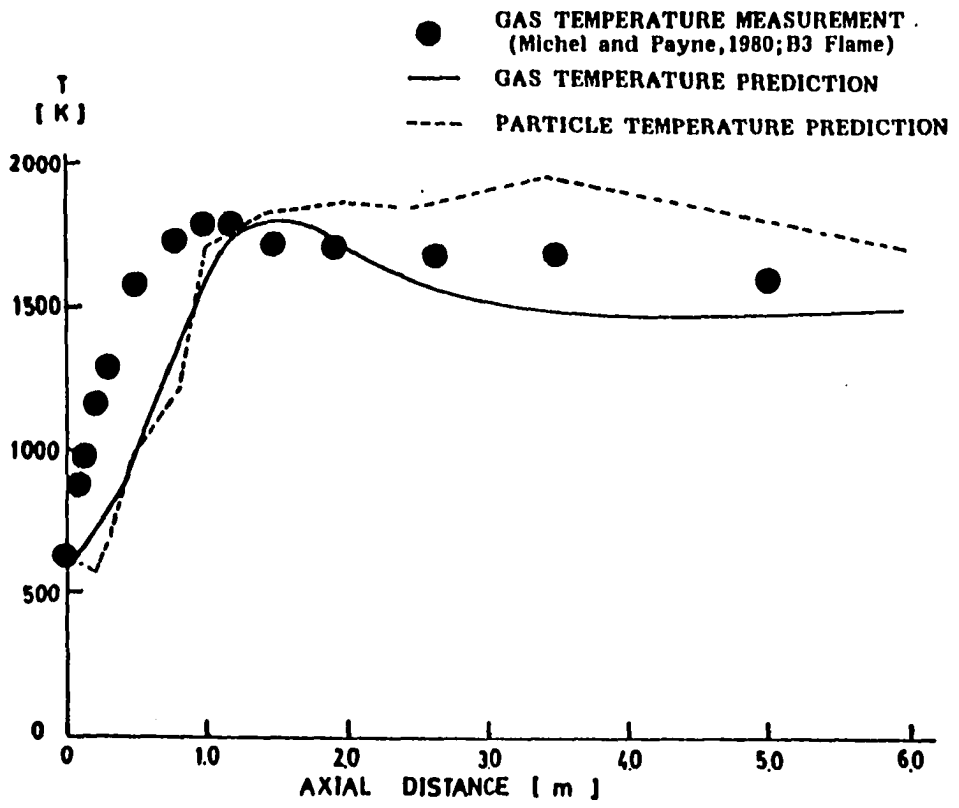

Fig. 6.14 Comparison of gas and particle temperature profiles along the centerline (B3 flame)

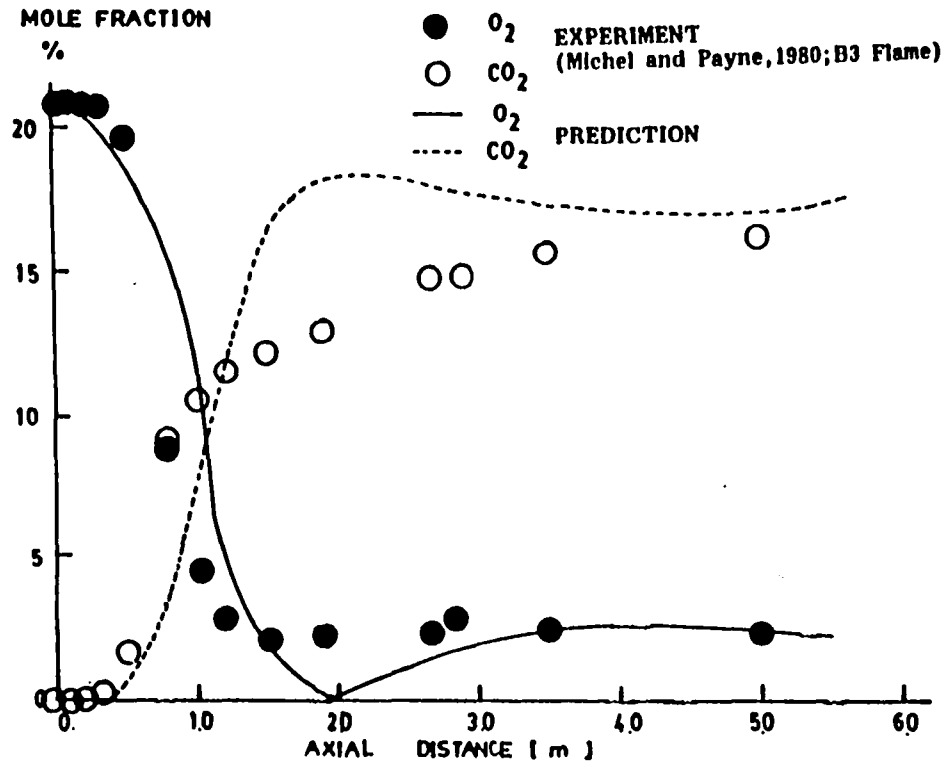

Fig. 6.15 Comparison of species concentration profiles along the centerline (B3 flame)

6.3 Concluding Remarks

A comprehensive computer code developed for the calculation of pulverized coal combustion is evaluated against a series of IFRF experimental data. The predicted and measured values show reasonably good agreement. Proper model developments for flame quenching due to high inlet stream velocity and minor species calculation like CO are of primary importance for better predictions.

CHAPTER 7

MOMENT CLOSURE METHOD FOR NITROGEN OXIDE FORMATION IN PULVERIZED COAL COMBUSTION

Pollutants arising from the reactions in a pulverized coal-fired furnace can be categorized into two groups (Mater and Ree, 1979). The first group includes pollutants which are common to all industrial combustion systems: CO, soot, unburned hydrocarbon and NO_x due to the fixation of atmospheric N_2. The second group includes pollutants from the impurities in coal. Dominant species among these are sulfurous and nitrogeous pollutants. Nitrogen pollutant consists of nitrogen oxide (NO), nitrogen dioxide (NO_2), and ammonia (NH_3). Of the major pollutants resulting from the combustion of coal, NO is the predominant species formed during the combustion process, and makes up 90-95% of the nitric oxides emitted (Chen et al., 1981).

Nitrogen oxide formation can be controlled efficiently by understanding the mechanism of NO formation in combustion systems instead of removing NO from the stack gases (Wendt, 1983). To this end Hill (1983) has made a systematic parametric study and has proposed a model for the NO formation in pulverized coal combustion systems.

The purpose of this chapter is to propose a simplified model for the formation of fuel bound NO of coal particle and evaluate the model by the comparison with the IFRF experimental A1 flame data (Michel and Payne, 1980).

7.1 NO FORMATION MECHANISM

Since this chapter deals with the modeling of fuel NO formation in pulverized coal combustion, thermal and prompt NO formations are exlcuded. Recent studies (Wendt, 1980; Heap et al., 1978) indicate that the fuel NO account for 60% to 80% of the NO formed. Chiger (1981) reports that thermal NO accounts for only 10% to 20% of the total NO. Hill (1983) has concluded that fuel NO is more than 95% of the total NO formed in the coal containing 1-2% nitrogen.

Coal Devolatilization

Coal contains approximately 1-2% nitrogen by weight depending on the coal type. This nitrogen is released from the coal into the gas phase during the devolatilization process. In the proposed model two basic assumptions are made regarding coal devolatilization, The first assumption is that nitrogen is devolatilized at a rate equal to the rate of coal weight loss. However, since the evolution of nitrogen has a greater temperature dependence than the evolution of volatiles occurs, 70-90% of coal nitrogen is evolved during devolatilization at high temperature (Blair et al., 1977). Thus the fraction of nitrogen evolved during devolatilization is taken to be about 80%. The second assumption is that most of the nitrogen devolatilized from the coal is evolved as HCN (Heap et al., 1978). Thus the amount of HCN formed from devolatilized nitrogen can be calculated from the following equation:

$$W_o = 0.8CF_N \frac{S_{p,v}}{F_v} \tag{7.1}$$

In this equation, F_N is the mass fraction of nitrogen in the coal, $S_{p,v}$ is the mass source term of coal-off gas due to devolatilization, F_v is the fraction of volatiles in coal, and C is a constant ($\cong$ 0.8-1.0) used to specify the percentage of coal nitrogen initially converted to HCN (Hill, 1983). The coefficient 0.8 denotes the fraction of nitrogen evolution due to devolatilization, as mentioned above.

Homogeneous NO reaction

The assumption that most (80-100%) of the devolatized nitrogen is initially converted to HCN in the gas phase is the starting point in the modeling of NO formation. The HCN can then react, in a parallel fashion, to NO or N_2 in the gas phase. The global reaction rates of these parallel reactions, $\dot{\omega}_1$ and $\dot{\omega}_2$, for NO and N_2 generation respectively, have been reported by De Soete (1975),

$$\dot{\omega}_1 = A_1 X_{HCN} X_{O_2}^b \exp(-E_1/RT) \tag{7.2}$$

$$\dot{\omega}_2 = A_2 X_{HCN} X_{NO} \exp(-E_2/RT) \tag{7.2}$$

where A, X, E and R stand for preexponential factor, mole fraction, activation energy and universal gas constant, respectively. The order of reaction, b in Eq. (7.2), varies according to mole fraction of oxygen. The order is zero for O_2 mole fractions greater than 18,000 ppm and 1 for mole fractions of O_2 less than 2,500 ppm.

In the range of 2500-18,000 ppm, b changes linearly as a function of mole fraction. Inspection of a series of IFRF experimental data (Michel and Payne, 1980) has shown that the mole fraction of O_2 greater than 1%. Therefore, it is reasonable to assume that the order of reaction is zero. Assuming this order of reaction, Eq. (7.2) can be written as

$$\dot{\omega}_1 = A_1 \, X_{HCN} \exp(-E_1/RT) \tag{7.3}$$

Heterogeneous Reaction

The nitrogen remaining in the coal after devolatilization can be heterogeneously oxidized to form NO. In this NO model, the heterogeneous NO formation is handled in a manner exactly analogous to homogeneous NO formation (Hill, 1983). In other words, as the char oxidizes, nitrogen is released into the gas phase to form HCN. The reduction of NO by interaction of char particle has been reported by Levy et al. (1981) with a reaction rate term given by

$$\dot{\omega}_3 = A_3 \exp(-E_3/RT) \, P_{NO} \tag{7.4}$$

where A_E is the external surface area of the char in m^2/gm and P_{NO} is the partial pressure of NO in atmospheres.

In summary, NO reaction sequence can be represented schematically as shown in Fig. 7.1. The kinetic parameters employed in this NO model are presented in Table 7.1. The volumetric reaction rates of $\dot{\omega}_1$, $\dot{\omega}_2$ and $\dot{\omega}_3$ can be expressed in terms of mass fraction (Y) as

$$\dot{\omega}_1 = \rho A_1 \frac{M_{mix}}{M_{HCN}} Y_{HCN} e^{-E_1/RT} \tag{7.5}$$

$$\dot{\omega}_2 = \rho A_2 \frac{M^2_{mix}}{M_{HCN} M_{NO}} Y_{HCN} Y_{NO} e^{-E_2/RT} \tag{7.6}$$

$$\dot{\omega}_3 = M_p n_p A_3 A_E M_{mix} Y_{NO} e^{-E_3/RT} \tag{7.7}$$

where m_p, n_p, M_{mix} and Y denote particle mass and number density, mixture molecular weight, species mass fraction, respectively.

7.2 MOMENT CLOSURE METHOD

To model the NO reaction process, the effect of turbulent fluctuation on chemical reaction should be appropriately accounted for. However, due to the complex nature of these processes, only two models (Hill, 1983; Fiveland et al., 1987) have been published, to the author's knowledge. These are similar to each other, in that the reaction rates are only a function of local stoichiometry or fuel mass fraction, and the effects of turbulent fluctuations are accounted for by an appropriate probability density function.

The basic idea of the model in this study is to neglect the effect of temperature fluctuation on the chemical reaction, and therefore the effect of turbulence on NO formation through species fluctuation. This argument is supported by the work of De Soete (1975), in which a rather small effect of temperature on the NO yield is observed over a wide range of temperature. Thus, neglecting the fluctuation of temperature and density, the mean reaction rate for $\dot{\omega}_1$, $\dot{\omega}_2$ and $\dot{\omega}_3$ in a turbulent flow can be written as

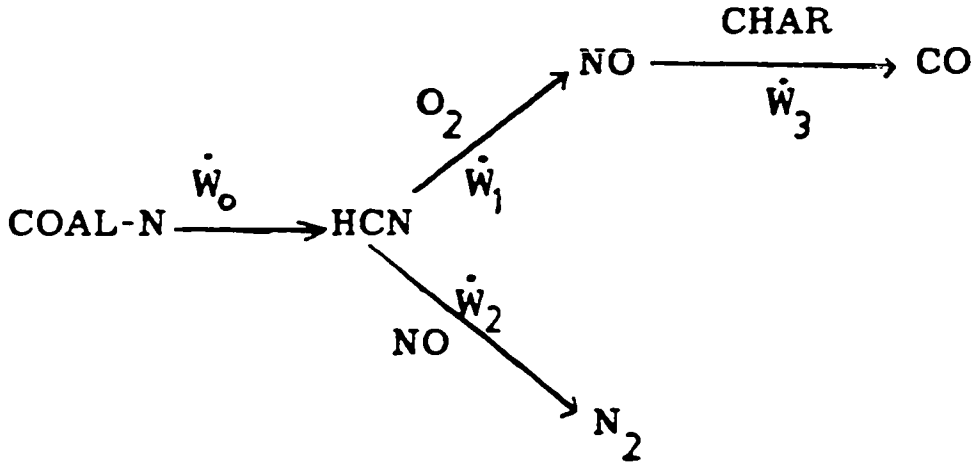

Fig. 7.1 Schematic NO reaction sequence

Table 7.1

Kinetic parameters used in the NO Model

Reaction	Pre-exponential Factor	Activation Energy (kcal/mole)
$\dot{\omega}_1$	1.0×10^{10}	67
$\dot{\omega}_2$	3.0×10^{12}	60
$\dot{\omega}_3$	4.1×10^{4}	34

$$\bar{\dot{\omega}}_1 = \bar{\rho}\, A_1 \frac{\bar{M}_{mix}}{M_{HCN}} \bar{Y}_{HCN}\, e^{-E_1/RT} \tag{7.8}$$

$$\bar{\dot{\omega}}_2 = \bar{\rho}\, A_2 \frac{\bar{M}^2_{mix}}{M_{HCN}\, M_{NO}} e^{-E_2/RT} (\bar{Y}_{HCN}\, \bar{Y}_{NO} + \overline{Y'_{HCN}\, Y'_{NO}}) \tag{7.9}$$

$$\bar{\dot{\omega}}_3 = M_p\, n_p\, A_3\, A_E\, \bar{M}_{mix}\, \bar{Y}_{NO}\, e^{-E_3/RT} \tag{7.10}$$

In the above equations, the only unknown term is turbulent correlation term $Y'_{HCN}\, Y'_{NO}$. In order to evaluate the correlation term, a balance equation can be derived (Bilger, 1980) as

$$\bar{\rho}\, \bar{u}_k \frac{\partial}{\partial x_k} (\overline{Y'_{HCN}\, Y'_{NO}}) = - \frac{\partial}{\partial x_k} (\overline{\rho\, u'_k\, Y'_{HCN}\, Y'_{NO}})$$

$$- \overline{\rho\, u'_k\, Y'_{HCN}} \frac{\partial \bar{Y}_{NO}}{\partial x_k} - \bar{\rho}\, \overline{u'_k\, Y'_{NO}} \frac{\partial \bar{Y}_{HCN}}{\partial x_k}$$

$$- \overline{2\, \rho\, D \frac{\partial Y'_{HCN}}{\partial x_k} \frac{Y'_{NO}}{\partial x_k}} + \overline{Y'_{HCN}\, \dot{\omega}_{NO}} + \overline{\dot{\omega}_{HCN}\, Y'_{NO}} \tag{7.11}$$

The first three terms on the right side of Eq. (7.11) can be handled via gradient transport method. The modeling of the fourth dissipation term is based on the suggestion of Bilger (1980)

$$\overline{2\rho D \frac{\partial Y'_{HCN}}{\partial x_k} \frac{\partial Y'_{NO}}{\partial x_k}} \simeq \text{const}\, \frac{\varepsilon}{k}\, \overline{Y'_{NO}\, Y'_{HCN}}\, (1 + \frac{a_3}{R_T}) \tag{7.12}$$

where a_3 is a constant and R_T the turbulence Reynolds number. In this study, the following expression is employed:

$$\overline{2\rho D \frac{\partial Y'_{HCN}}{\partial x_k} \frac{\partial Y'_{NO}}{\partial x_k}} = C_{g_2}\, \frac{\varepsilon}{k}\, \overline{Y'_{NO}\, Y'_{HCN}} \tag{7.13}$$

The empirical constant C_{g_2} is given as the same value used in fast chemistry turbulent combustion models (for example, Khalil et al., 1975). The remaining task is to model the last two terms on the right hand side of Eq. (7.11) into a more tractable form, that is,

$$\overline{Y'_{HCN}\,\dot{\omega}_{NO}} + \overline{Y'_{NO}\,\dot{\omega}_{HCN}}$$

$$= \overline{Y'_{HCH}\,(\dot{\omega}_1-\dot{\omega}_2-\dot{\omega}_3)} + \overline{Y'_{NO}\,(\dot{\omega}_o-\dot{\omega}_1-\dot{\omega}_2)}$$

$$\simeq \frac{\rho A_1 M_{mix}}{M_{HCN}} e^{-E_1/RT} (\overline{Y'_{HCN}\,Y'_{HCN}} - \overline{Y'_{NO}\,Y'_{HCN}})$$

$$- \frac{\rho A_2 M_{mix}}{M_{HCN}\,M_{NO}} e^{-E_2/RT} (\bar{Y}_{HCN}\,\overline{Y'_{HCN}\,Y'_{NO}} + \bar{Y}_{NO}\,\overline{Y'_{HCN}\,Y'_{HCN}}$$

$$+ \bar{Y}_{HCN}\,\overline{Y'_{NO}\,Y'_{NO}} + \bar{Y}_{NO}\,\overline{Y'_{NO}\,Y'_{HCN}}) \qquad (7.14)$$

In the derivation of Eq. (7.14), correlations of $\overline{Y'_{HCN}\dot{\omega}_3}$ and $\overline{Y'_{NO}\dot{\omega}_o}$ have been neglected, since the species Y_{HCN} and Y_{NO} are not directly involved with the reaction source terms $\dot{\omega}_o$ and $\dot{\omega}_3$, respectively. In addition, triple species fluctuations such as $\overline{Y'^2_{NCH}\,Y'_{NO}}$ are neglected. In Eq. (7.14), further modeling is necessary for the positive definite correlation terms $\overline{Y'_{HCN}\,Y'_{HCN}}$ and $\overline{Y'_{NO}\,Y'_{NO}}$. For $\overline{Y'_{HCN}\,Y'_{HCN}}$, a balance equation can be derived in a similar way of Eq. (7.11) as

$$\bar{\rho}\,\bar{u}_k \frac{\partial}{\partial x_k} (\overline{Y'_{HCN}\,Y'_{HCN}}) = - \frac{\partial}{\partial x_k} (\bar{\rho}\,\bar{u}_k\,\overline{Y'_{HCN}\,Y'_{HCN}})$$

$$- 2\bar{\rho}\,\overline{u'_k\,Y'_{HCN}} \frac{\partial \bar{Y}_{HCN}}{\partial x_k} - 2\rho D \overline{\frac{\partial Y_{HCN}}{\partial x_k} \frac{\partial Y_{HCN}}{\partial x_k}}$$

$$+ 2\,\overline{Y'_{HCN}\,\dot{\omega}_{HCN}} \qquad (7.15)$$

Except for the last term on the right side, the modeling of other terms has already been indicated. For the last term,

$$\overline{2\, Y'_{HCN}\, \dot{\omega}_{HCN}} = 2\, \overline{Y'_{HCN}\, (\dot{\omega}_o - \dot{\omega}_1 - \dot{\omega}_2)}$$

$$= \overline{2\, Y'_{HCN}\, (\dot{\omega}_o + \dot{\omega}'_o)} - \overline{2\, Y'_{HCN}\, \dot{\omega}_1} - \overline{2\, Y'_{HCN}\, \dot{\omega}_2'} \qquad (7.16)$$

The last two terms of Eq. (7.16) can be expressed in terms of calculable terms such as $\overline{Y'_{HCN}\, Y'_{HCN}}$ and $\overline{Y'_{HCN}\, Y'_{NO}}$ but the first term involve volumetric souce term of species Y_{HCN} due to coal-off process. In order to arrange the first term in a tractable form, the following simple relation is proposed:

$$\frac{\dot{\omega}_o'}{\bar{\dot{\omega}}_o} = -\alpha \frac{Y'_{HCN}}{\bar{Y}_{HCN}} + (1 - \alpha) \frac{Y'_{HCN}}{\bar{Y}_{HCN}} \qquad (7.17)$$

where α denotes the fraction of the coal-off gas which is in non-premixed state. The value of α is assumed to be 0.7 in this study. Thus, the first term of Eq. (7.16) can be written as

$$\overline{2\, Y'_{HCN}\, (\dot{\omega}_o + \dot{\omega}'_o)} = 2\, \frac{\bar{\dot{\omega}}_o}{\bar{Y}_{HCN}} (1-2\alpha)\, \overline{Y'_{HCN}\, Y'_{HCN}} \qquad (7.18)$$

Similarly, the balance equation for $\overline{Y'_{NO}\, Y'_{NO}}$ can be derived and modeled, except for the correlation term between species fluctuation of Y_{NO} and source term $\dot{\omega}_3$, that is, $\overline{\dot{\omega}_3 Y'_{NO}}$. The contribution of this term is neglected, since the reaction of $\dot{\omega}_3$ is associated with slow chemistry (Hill, 1983).

7.3 MODEL EVALUATION

Evaluation of the proposed moment closure method has been made against IFRF experimental data (Michel and Payne, 1980). Figures (7.2) - (7.5) show comparison of predicted and measured centerline and radial profiles for NO and HCN species. The first (Fig. 7.2) shows comparison of predicted and measured centerline HCN profiles together with the prediction of Hill (1983). The HCN levels are also illustrated in Fig. 7.3, which shows radial profiles of HCN at axial locations of 0.75, 1.0, and 2.0 m. The general trends of HCN profiles are in good agreement with experimental data, while the prediction of Hill (1983) overestimate the value of HCN along the centerline.

In Fig. 7.4, comparison is also made between the prediction using the moment closure method and that using the mean chemical reaction obtained by neglecting turbulent fluctuations altogether. The difference between these two calculations is negligible in the range of high HCN and NO concentrations (X = 1.0 ~ 2.0 m), but increases linearly along the centerline. The higher predictions of NO in the moment closure method can be explained by noting the correlation of $\overline{Y'_{HCN}\ Y'_{NO}}$ in Eq. (7.9) is negative, due to the non-premixedness of HCN and NO species. In other words, the negative correlation decreases the reaction rate of N_2 formation, i.e., increases NO production. The close agreement between the two predictions in this study in the region of high NO and HCN concentration can be attributed to the substantial premixing due to the high concentrations of these species and slow chemistry associated

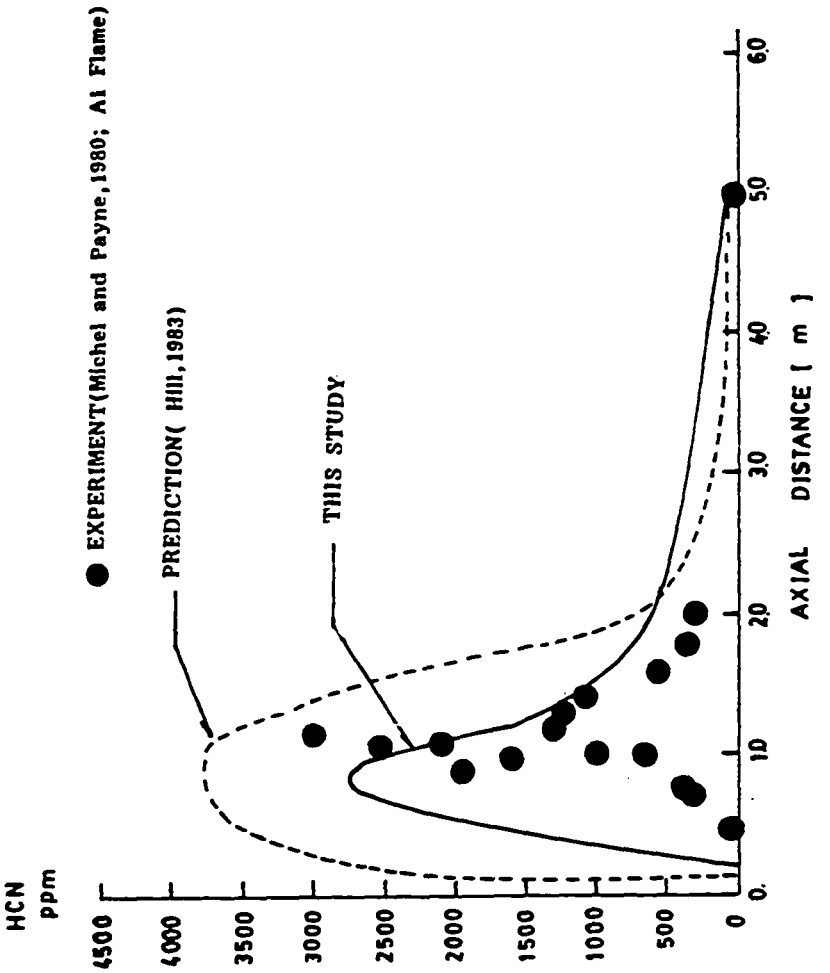

Fig. 7.2 Comparison of predicted and measured profiles of HCN along the centerline

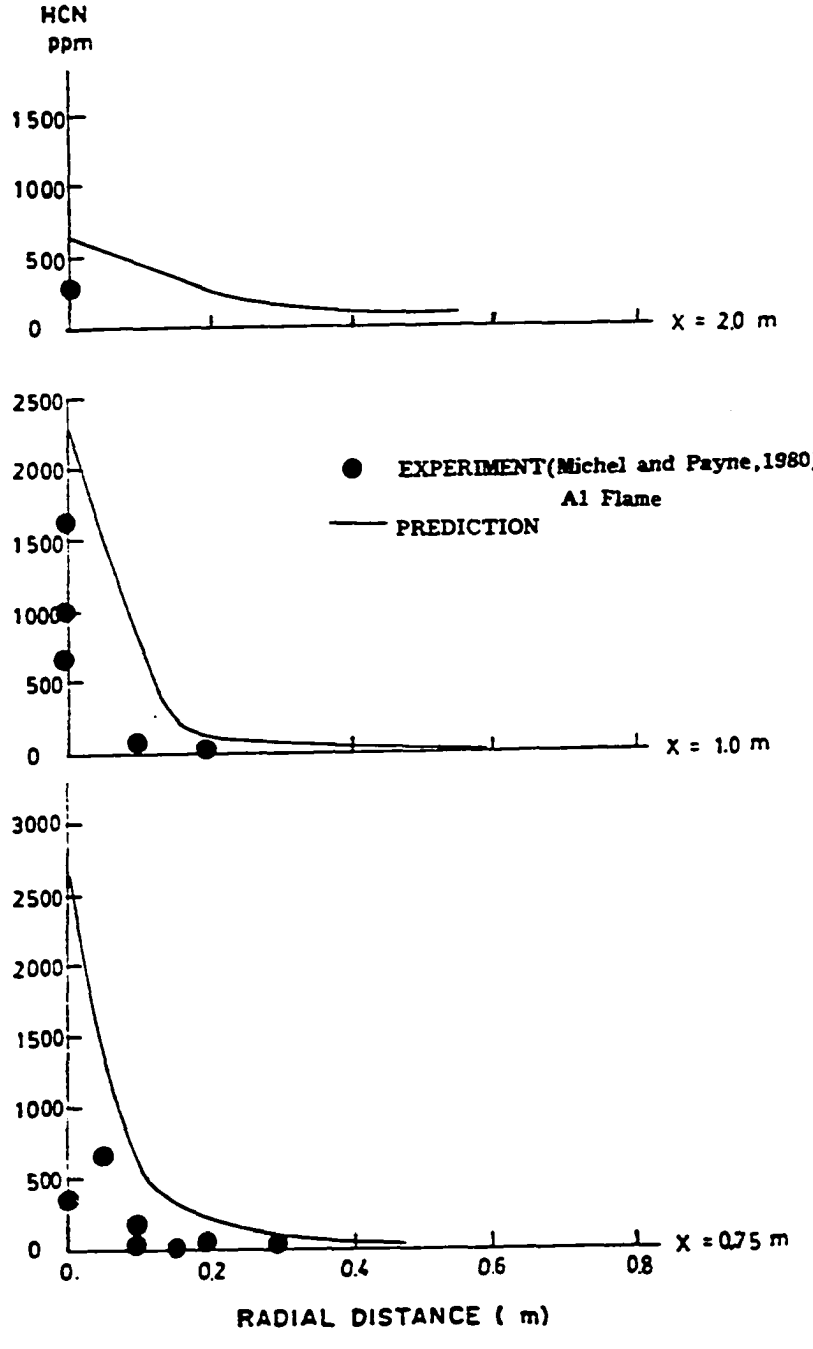

Fig. 7.3 Comparison of predicted and measured HCN radial profiles

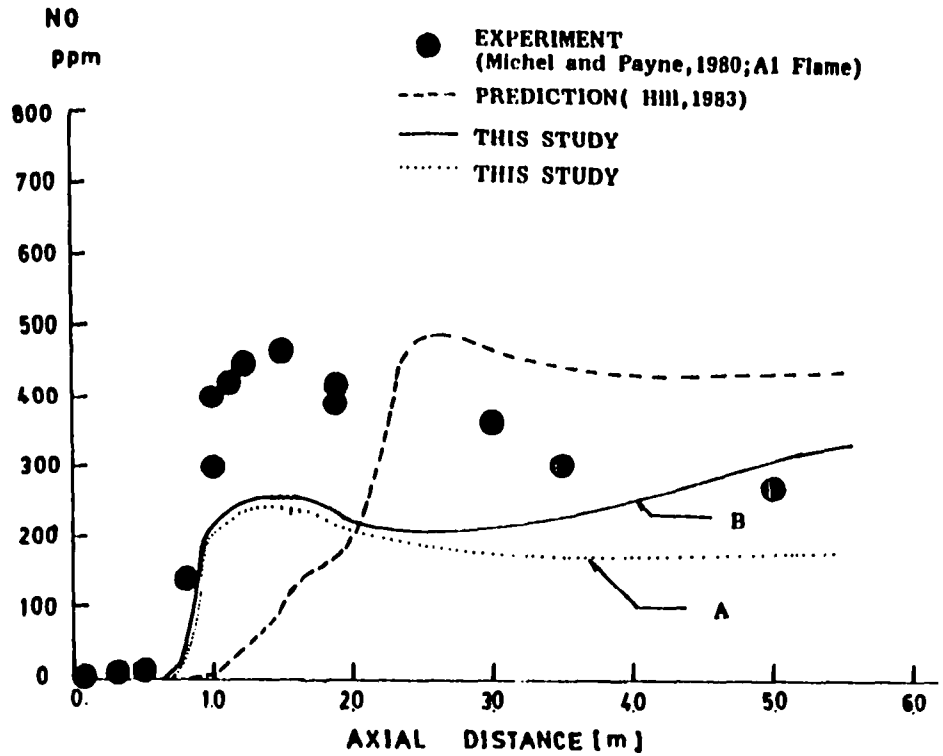

Fig. 7.4 Comparison of predicted and measured NO concentration profiles along the centerline

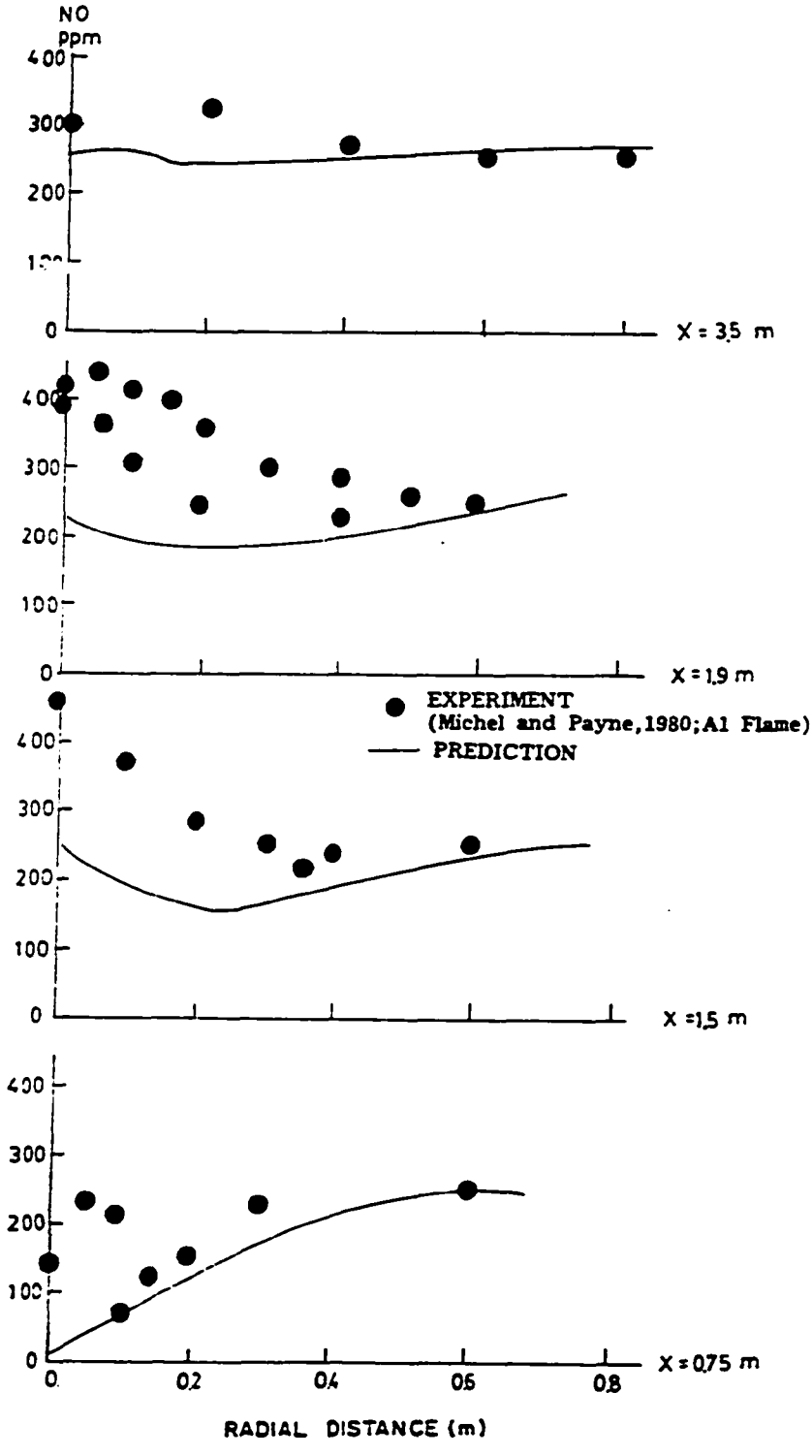

Fig. 7.5 Comparison of predicted and measured radial profiles of NO concentration

with the reaction. This implies that the correlation of $\overline{Y'_{HCN}Y'_{NO}}$ in Eq. (7.9) will be positive. The underestimation of predictions made by this study on the range of axial distances between 1-2 m, is believed to be due to the effect of thermal NO formation. This production may be significant in this high temperature range. The NO levels are further illustrated in Fig. 7.5, which shows radial profiles of NO at axial locations of 0.75, 1.5, 1.9 and 3.5 m. The general trend is good agreement, but values are underestimated, because of the neglect of thermal NO contribution in this study.

7.4 CONCLUDING REMARKS

A moment closure method is developed to predict nitrogen oxide formation in coal-fired processes and this model is evaluated by comparison of predictions with experimental data. The model is based on the assumption that temperature and density fluctuations do not strongly influence NO formation and that thermal NO formation can be neglected. In general, the overall predicted trends of NO agree with experimental data but values are underestimated due to the neglect of thermal NO formation.

CHAPTER 8

SUMMARY OF PRESENT WORK AND RECOMMENDATIONS FOR FUTURE WORK

Based on the work done in this dissertation, a number of useful concluding remarks can be made regarding the modeling of individual processes as well as on the overall comprehensive modeling of the pulverized coal combustion process. Since the major conclusions have been given at the end of appropriate chapters, only a brief summary of important results is provided below in section 8.1 and recommendations for future work are presented in section 8.2.

8.1 SUMMARY

The objective of this dissertation study is to evaluate and improve the modeling of individual processes associated with single- and two-phase turbulent reaction processes, and in particular the pulverized coal combustion process. Improved modeling of individual processes can then be combined to obtain a reliable comprehensive computer code. Primary emphasis in this work has been placed on the modeling of non-equilibrium turbulent reactions, turbulent particle dispersion, and pollutant species formation. In addition, contributions have been made towards improving the numerical algorithm used in the solution of the differential equations. Furthermore, a systematic study has been made of the two equation

(k-ε) turbulence model using the wall function approach, fast chemistry turbulent reaction models such as eddy breakup model and the conserved scalar model, models for coal particle reactions and the four flux radiation model. Specific contributions made in this study are summarized below.

Turbulent Reaction: Two turbulent reaction models are developed for resolving nonequilibrium effects. The first model is a modified perturbation model for the calculation of nonequilibrium quenching effect in intensive turbulent combustion. This method is validated by comparison with experimental data for natural gas-air flame and appears to be suited for single- and two-phase flame stability studies.

In addition to the above model for fast turbulent combustion, a moment closure method is developed for the simulation of moderately fast or slow reactions and this model is applied to the modeling of fuel bound nitrogen oxide formation. Further discussion in this is given later.

Turbulent Particle Dispersion: A systematic performance evaluation of existing turbulent particle dispersion models such as the empirical gradient models and the stochastic method has been made. An improvement is made to the stochastic method by incorporating the effects of particle fluctuation velocities at the inlet stream. With this modification significant improvement in particle dispersion predictions are obtained compared to the predictions of the gradient models and the stochastic method without this modifica-

tion. Twenty stochastic calculations per particle size group and starting location are necessary for statistical accuracy of this method. Further a reasonable number of representative particle trajectories defined by the number of particle size groups and initial starting locations at the inlet stream are necessary to maintain accuracy.

Comprehensive Computer Code: The comprehensive computer code implemented using an eddy breakup model and the improved stochastic method shows good agreement with a series of experimental data in an IFRF furnace. Some deficiencies noted are in the prediction of minor species like carbon monoxide and flame lift-off phenomena.

Nitrogen Oxide Formation: Fuel bound nitrogen oxide is modeled using the basic idea of the moment closure method mentioned earlier. The justification of this method, which assumes that the effect of turbulence is transmitted only through species fluctuation is supported by the experimental evidence that the formation of nitrogen oxide is insensitive to the variations or fluctuations of flame temperature. The formation of nitrogen oxide is associated with the decay of hydrogen cyanide by two competing reaction schemes, and is followed by the destruction of nitrogen oxide due to reaction with char particle. This model is tested against experimental data and shows reasonable agreement.

Numerical Solution Methods: Since the performance of computational algorithm is strongly dependent on the proper resolution of pres-

sure-velocity coupling, a systematic performance evaluation of existing algorithms such as SIMPLER, SIMPLEC and PISO for various flow situations has been made. Based on this study, a new algorithm that uses a novel source term decomposition method is developed for high swirling flow situations. A significant improvement in convergence characteristics is noted compared to that of other conventional algorithms.

8.2 RECOMMENDATIONS FOR FUTURE WORK

Due to the diversity and complexity of subject material associated with pulverized coal combustion processes, further research is necessary to improve the phenomenological modeling of the various interesting processes.

In addition, two major tasks are necessary. These are to extend the comprehensive code to 3-dimensional geometry and to adapt the computer code to handle more complicated geometries like a quarl. These are tasks of primary importance since experimental data is generally available for such geometries. Other recommendations on phenomenological modeling are:

Turbulent Reaction: The phenomenological eddy breakup model employed for coal-off gas reactions does not provide a sound basis for the calculation of the partially premixed combustion of coal-off gas. In addition, the universality of the eddy breakup constants have not been validated for a wide range experimental data. Therefore, model improvement together with the validation tests are

desirable. As mentioned earlier, the modeling of flame lift-off and blow-out is of major importance in the study of flame stability and the application of the modified perturbation model appears promising in this regard and should be pursued.

Turbulent Particle Dispersion: A number of important physical concepts have been overlooked in the modeling of turbulent particle dispersion. For example, coherent structures, Basset force effects and impulsive or explosion-like particle motion due to eruption of coal-off gas. These effects on the particle trajectory calculation should be considered together with the influence of pore structure on the particle dynamic behavior. The validity of particle dispersion models for swirling flows remains to be explored.

Pollutant Species Formation: The model of pollutant species formation is limited to the case of fuel bound nitrogen oxide. Therefore, extensions to include thermal and prompt nitrogen oxide formation and also other pollutant species like SO_x is desirable.

REFERENCES

Anson, D., F. D. Moles and P. J. Street, "Structure and surface area of pulverized coal during combustion, Combustion and Flame 17, 321 (1971)

Anthony, D. B., J. B. Howard, H. C. Hottell and H. P. Meissner, Fifteenth Symposium (International) on Combustion, The Combustion Institute, p. 1303 (1975)

Baker, R. J., P. Hutchison, E. E. Khalil and J. H. Whitelaw, "Measurement of three velocity components in a model furnace with and without combustion," Fifteenth Symposium (International) on Combustion, The Combustion Institute, p. 553 (1975)

Batchelor, G. K., "The Theory of Homogeneous Turbulence," Cambridge University Press, New York, (1953)

Baum, M. M. and P. J. Street, "Predicting the combustion behavior of coal particles," Combustion Science and Technology, 3, pp. 231-243 (1971)

Bilger, R. W., Prog. Energy Combustion Sci., 1 87 (1976)

Bilger, R. W., Combustion and Flame 30, 277 (1977)

Bilger, R. W., Combustion Science and Telchnology 19, 89 (1979)

Bilger, R. W., Combustion Science and Technology 22, 251 (1980a)

Bilger, R. W., "Turbulent flows in nonpremixed reactants," in Turbulent Reacting Flow, Ed. P. A. Libby and F. A. Williams, Springer-Verlag, p. 65 (1980b)

Blair, D. W., J. O. L. Wendt and W. Bartok, "Evolution of niteogen and other species during controlled pyrolysis," Sixteenth

Symposium (International) on Combustion, pp. 475-489, The Combustion Institute, Pittsburgh, PA (1977)

Borghi, R. and Dutoya, D., Seventeenth Symposium (International) on Combustion, The Combustion Institute, Pittsburgh, 223 (1979)

Boysan, F., R. Weber, J. Swithenbank and C. J. Lawn, "Modeling coal-fired cyclone combustors," Combustion and Flame 63, 73 (1986)

Boyd, R. K. and J. H. Kent, "Three-dimensional furnace computer modeling," 21st Symposium (International) on Combustion, Munich, Germany (Aug. 1986)

Brzustowski, T. A., "Mixing and chemical reactions in industrial flames and their models, Physic. Chemical Hydrodynamics 1, p. 27 (1980)

Chakravarty, A., F. C. Lockwood and G. Sinicropi, Combustion Science and Technology 42, 67 (1984)

Chen, S. L., M. P. Heap, D. W. Pershing, R. K. Nihart and D. P. Rees, "The influence of coal composition on the formation and control of NO_x in pulverized coal flames," WSS/CI, University of California, Irvine, CA (1980)

Chu, C. M. and S. W. Churchill, "Numerical solution of problems in multiple scattering of electromagnetic radiation," J. phys. chem. 59, 00. 955 (1955)

Crowe, C. T., M. P. Sharma, and D. E. Stock, "The particle-source in-cell (PSI-Cell) model for gas-croplet flows," Journal of Fluids Engineering, Transactions of the ASME, p. 325 (1977)

Davies, J. T., Turbulence Phenomena, Academic Press, 19 (1972)

De Sote, G. G., "Overall reaction rates of NO and N_2 formation from fuel nitrogen," 15th Symposium (International) on Combustion, The Combustion Institute, Pittsburgh, PA p. 1093 (1975)

Driscoll, R. J., "The Influence of Spectral Transfer and Molecular Diffusion on Turbulent Mixing and Combustion," Ph.D. Dissertation, State University of New York, Buffalo (1982)

Dukowicz, J. K., "A Particle-Fluid Numerical Model for Liquid Sprays," Journal Comp. Phys. 35, 229 (1980)

Elgobashi, S. E. and W. M. Pun, "A theoretical and experimental study of turbulent diffusion flames in cylinderical furnaces," 15th Symposium (International) on Combustion, The Combustion Institute, Pittsburgh, PA (1974)

Faeth, G. M., "Turbulence/Drop Interactions in Sprays," AIAA Paper No. 86-0136 (1986)

Favre, A., "Problems of Hyrodynamics and Coninum Mechanics", p. 231 Society for Industrial and Applied Mechanics. (1969)

Fennimore, C. P. and J. H. Fraenkel, Eighteenth Symposium (International) on Combustion, The Combustion Institute, 143 (1981)

Field, M. A., "Rate of combustion of sized-graded fractions if char from a low-rank coal between 1200K and 2000K", Combustion and Flame, 13, pp. 237-252 (1969)

Fiveland, W. A., R. A. Wessel and D. Eskinazi, "Pollutant model for predicting formation and reduction of nitric oxides in three-dimensional, pulverized-fuel-fired furnaces," presented ASME National Heat Transfer Conference, Pittsburgh, PA Aug. 9-12, (1987)

Fletcher, T. H., "Theoretical Modeling of Reacting Coal Particles in Pulverized Coal Combustion and Gasification," M.S. thesis, Department of Chemical Engineering, Brigham Young University, Provo, Utah (1980)

Fletcher, T. H., "A Two-Dimensional Model for Coal Gasification and Combustion," Ph.D. dissertation, Department of Chemical Engineering, Brigham Young University, Provo, Utah (1983)

Glassman, I., "Combustion," Academic Press, New York (1977)

Hassan, M. A., Lockwood, F. C. and Moneib, H. A., Paper presented at Italian Flame Day, 1980

Gosman, A. D. and F. C. Lockwood, "Incorporation of a flux model for radiation into a finite difference procedure for furnace calculations". 14th Sumposium (International) on Combustion, The Combustion Institute (1978)

Gosman, A. D. and E. Ioannides, "Aspect of simulation of liquid fuelled combustors", AIAA paper No. 81-0323 (1981)

Heap, M. P., T. J. Tyson, G. R. Chichanowicz and C. J. Kau, "Environmental aspects of low BTU gas combustion," 16th Symposium (International) on Combustion, The Combustion Institute, Pittsburgh, PA p. 535 (1977)

Hill, S. C., "Modeling of nitrogen pollutants in turbulent pulverized coal flames," Ph.D. Dissertation, Chemical Engineering Department, Brigham Young University, Provo, Utah (1983)

Hottel, H. C., "Heat Transmission," 3rd ed., New York, McGraw-Hill (1954)

Hutchinson, P., E. E. Khalil, J. H. Whitelay and G. Wigley, "The calculation of furnace-flow properties and their experimental verification," J. of Heat Transfer, p. 276 (1976)

Issa, R. I., "Solution of the Implicit Discretized Fluid Flow Equations by Operator Splitting," Mechanical Engg. Report, FS/82/15, Imperical College, London, (1982).

Issa, R. I., A. D. Gosman and A. P. Watkins, The Computation of Compressible and Incompressible Recirculating Flows by a Non-Iterative Implicit Scheme, J. Comp. Phys. (1986)

Janica, J. D. and Peters, N., Nineteenth Symposium (International) on Combustion, The Combustion Institute, 367 (1982)

Jones, W. P. and J. H. Whitelaw, "Calculation methods for reacting turbulent flows," Combustion and Flame 48, 1 (1982)

Jones, W. P. and J. H. Whitelaw, "Modeling and Measurements in turbulent combustion," 20th Symposium (International) on Combustion, The Combustion Institute, pp. 239-249 (1984)

Khalil, E. E., D. B. Spalding and J. H. Whitelaw, "The Calculation of Local Flow Properties of Two-Dimensional Furnaces," Int. J. Heat Mass Transfer 18, 775 (1975)

Kent, J. H. and R. W. Bilger, Fourteenth Symposium on Combustion, p. 615, The Combustion Institute (1973)

Knight, D. D. and B. T. Murray, "Theoretical investigation of interaction and coalescence of large scale structures in turbulent mixing layers," in The Role of Coherent Structures in Modeling Turbulence and Mixing, edited by J. Jimenez (Springer, Berlin), p. 62 (1981)

Kobayashi, H., J. B. Howard and A. F. Sarofim, Sixteenth Symposium (International) on Combustion, The Combustion Institute, p. 719 (1977)

Laufer, J., "New trends in experimental turbulence research," in Annual Review of Fluid Mechanics, vol. 7, Annual Review, Inc. Palo alto, Calif.

Latimer, B. R. and A. Pollard, "Comparison of pressure-velocity coupling solution algorithms," Numerical Heat Transfer, 8, pp. 635-652 (1985)

Launder, B. E. and D. B. Spalding, "Mathematical Models of Turbulence," Academic Press, New York, (1972)

Launder, B. E. and S. Elghobashi, Third Symposium on Turbulent Shear Flows, University of California, Davis, 1513 (1981)

Launder, B. E., G. J. Reece and W. Rodi, "Progress in the development of Reynolds stress closure," Journal of Fluid Mechanics, vol. 68, part 3 pp. 537-566 (1975)

Leavitt, D. R., "Coal Dust and Swirl Effects on Gas and Particle Mixing Rates in Confined Jets," M.S. thesis, Department of Chemical Engineering, Brigham Young University, Provo, Utah (1980)

Lester, T. W., W. R. Seeker and J. F. Merklin, Eighteenth Symposium (International) on Combustion, The Combustion Institute, p. 1257, (1981)

Lewis, M. H. and L. D. Smoot, Combustion and Flame 42, 183 (1981)

Liew, S. K., N. C. Bray and C. B. Moss, Combustion and Flame 56, 199 (1984)

Libby, P. A. and F. A. Williams, "Turbulent Reacting Flows," Springer-Verlag, New York (1980)

Lilley, D. G., "Modeling of combustor swirl flows," Acta Astronautica, 1 pp. 1129-1147 (1974)

Lilley, D. G. and D. L. Rhode, NASA contract report 3442, (1982)

Lockwood, F. C., A. P. Salooja and S. A. Syed, "A prediction method for coal-fired furnaces," Combustion and Flame 38, 1 (1980)

Magnussen, B. F. and H. Hjertager, "On mathematical modeling of turbulent combustion with special emphasis on soot formation and combustion," 16th Symposium (International) on Combustion, The Combustion Institute, p. 719 (1976)

Malte, P. C. and D. P. Rees, "Mechanisms and kinetics of pollutant formation during reaction of pulverized coal," in Pulverized-coal Combustion and Gasification (Ed. L. D. Smoot and D. T. Pratt), Plenum Press, New York (1979)

Memmott, V. J., "Rates of mixing of particles and gases in confined jet," M.S. thesis, Department of Chemical Engineering, B.Y.U., Provo, Utah (1977)

Melville, E. K. and N. C. Bray, "A model of the two-phase turbulent jet," Int'l J. Heat Mass Transfer 22, p. 647 (1979)

Michel, J. B. and R. Payne, "Detailed measurement of long pulverized coal flames for the characterization of pollutant formation," IFRF Document No. F09/a/23, Ijmuiden, The Netherlands (1980)

Mitchell, R. E., Sarofim, A. F. and Clomburg, L. A., Combustion and Flame 30, 227 (1980)

Owen, F. K., "Measurements and observations of turbulent recirculating jet flows," AIAA Journal 14, 11, O. 1556 (1976)

Patankar, S. V. and D. B. Spalding, "A calculation procedure for heat, mass and momentum transfer in three dimensional parabolic flows," Int. J. Heat Mass Transfer 15, pp. 1767-1806 (1972)

Patankar, S. V., "Numerical Heat Transfer and Fluid Flows," Hemisphere, Washington, D.C., (1980)

Pershing, D. W. and J. O. L. Wendt, "Relative contributions of volatile nitrogen and char nitrogen to NO_x emissions from pulverized coal flames," paper presented at 83rd National meeting of AIChE, Houston, Texas (1977)

Peters, M. and F. A. Williams, "Liftoff characteristics of turbulent jet diffusion flames," AIAA Journal 21, 3, p. 423 (1983)

Pohl, J. H. and A. F. Sarofim, "Devolatilization and oxidation of coal nitrogen," 16th Symposium (International) on Combustion, The Combustion Institute, Pittsburgh, PA (1977)

Raithby, G. D. and G. E. Schneider, "Numerical Solution of Problems in Incompressible Fluid Flow; Treatment of the Velocity-Pressure Coupling," Numerical Heat Transfer, Vol. 2, No. 2, pp. 417-440 (1984)

Ramos, J. I., "Turbulent nonreacting swirling flows," AIAA Journal 22, 6, p. 846 (1984)

Reynolds, W. C., "Computation of turbulent flows," in Annual Review of Fluid Mechanics, Vol. 8, Annual REviews, Inc., Palo Alto, Calif.

Richardson, J. M., H. C. Howard and R. W. Smith, Fourth Symposium (International) on Combustion, Williams and Wilkins (1953)

Roshko, A., "Structure of turbulent shear flows: A new look," AIAA Journal 14, pp. 1349-1357 (1976)

Rubesin, M. W., "Numerical turbulence Modeling," AGARD Lecture Series No. 86 on Computational Fluid Dynamics, (1977)

Sarofim, A. F. and Hottel, H. C., "Radiative heat transfer in combustion chambers: Influence of alternative fuels," Sixth International Heat Transfer Conference, Toronto, Canada (1978)

Shih, Tsan-Hsing and J. L. Lumley, "Second-order modeling of particle dispersion in a turbulent flow," J. Fluid Mech. 163, pp. 349-363 (1986)

Shuen, J. S., L. D. Chen and G. M. Faeth, "Evaluation of a Stochastic Model of Particle Dispersion in a Turbulent Round Jet," AIChE J. 29, 167 (1983 a)

Shuen, J. S., A. S. P. Solomon, Q. F. Zhang and G. M. Faeth, "A Theoretical and Experimental Study of Turbulent Particle Laden Jets," NASA Contract Report No. 168293 (1983 b)

Shuen, J. S., L. D. Chen and G. M. Faeth, "Predictions of the Structure of Turbulent Particle-Laden Round Jets," AIAA J. 21, 1483 (1983 c)

Smith, P. J., "Theoretical modeling of coal and gas fired turbulent combustion and gasification process," Ph.D. Dissertation, Department of Chemical Engineering, Brigham Young University, Provo, Utah (1979)

Smith, P. J., T. J. Fletcher and L. D. Smoot, "Model for Pulverized Coal-Fired Reactors," 18th Symposium (International) on Combustion, The Combustion Institute, Pittsburgh, PA, 1285 (1981)

Smoot, L. D., "Pulverized Coal Diffusion Flames - A Perspective Through Modeling," 18th Symposium (International) on Combustion, The Combustion Institute, Pittsburgh, PA 1185 (1981)

Smoot, L. D., and D. T. Pratt, Pulverized Coal Combustion and Gasification, Plenum Press, New York and London (1979)

Smoot, L. D., and P. J. Smith, Coal Combustion and Gasification, Plenum Press, New York and London (1985)

Solomon, A. S. P., J. S. Shuen, Q. F. Zhang and G. M. Faeth, "Structure of Nonevaporating Sprays: I. Near-Injector Conditions and Mean Properties," AIAA J. 23, 1548 (1985 a)

Solomon, A. S. P., J. S. Shuen, Q. F. Zhang and G. M. Faeth, "Structure of Nonevaporating Sprays: II. Drop and Turbulent Properties," AIAA J. 23, 1724 (1985 b)

Solomon, A. S. P., J. S. Shuen, Q. F. Zhang and G. M. Faeth, "Measurements and Predictions of the Structure of Evaporating Sprays," J. Heat Trans. 107, 679 (1985 c)

Spalding, D. B., "Mixing and Chemical Reaction in Steady Confined Turbulent Flame," 13th Symposium (International) on Combustion, The Combustion Institute, 649 (1971)

Svehla, R. A., "Estimated Viscosities and Thermal Conductivities of Gases at High Temperatures," NASA Technical Report R-132 (1963)

Syed, S. A. and G. J. Sturgess, "Validation Studies of Turbulence and Combustion Models for Aircraft Gas Turbine Combustors," Momentum and Heat Transfer Processes in Recirculating Flows, edited by B. E. Launder and J. A. C. Humphrey, presented at the Winter Annual Meeting of the ASME, Chicago (Nov. 1980)

Tennekes, H. and J. L. Lumley, "A First Course in Turbulence," The MIT Press, (1972)

Truelove, J. S., "Prediction of the Near-burner Flow and Combustion in Swirling Pulverized Coal Flames," appeared in 21st Symposium (International) on Combustion, Munich, Germany (Aug. 1986)

Ubhayaker, S. K., D. B. Stickler, C. W. von Rosenberg and R. E. Gannon, "Rapid devolatization of pulverized coal in hot combustion gas," 16th Symposium (International) on Combustion, The Combustion Institute, Pittsburgh, PA (1976)

Van Doormaal, J. P. and G. D. Raithby, "Enhancements of the SIMPLE Method for predicting incompressible fluid flows," Numerical Heat Transfer, Vol. 7, pp. 147-163 (1984)

Van Wylen, G. J. and R. E. Sonntag, "Fundamentals of classical thermodynamics," John Wiley and Sons, New York (1978)

Varma, S. A., "Radiative heat transfer in a pulverized coal flame," in Pulverized Coal Combustion and Gasification (Eds. L. D. Smoot and D. T. Pratt), Plenum Press, p. 83 (1979)

Wendt, J. O. L., "Fundamental coal combustion mechanism and pollutant formation in furnaces," Prog. Energy Combustion Sci., 6, p. 201 (1980)

Wallis, G. B., One-Domensional and Two-Phase Flow, McGraw-Hill, New York (1969)

Williams, F. A., Combustion Theory, 2nd ed., The Benjamin/Cummings Publishing Company, Inc. Menlo Park, CA (1985)

Yuu, S., N. Yasukouchi, U. Hirosawa and I. Jotaki, "Particle Turbulent Diffusion in a Dust Laden Round Flame," AIChE J. 24, 509 (1978)

Zhang, Q. F., J. S. Shuen, A. S. P. Solomon and G. M. Faeth, "Structure of Ducted Particle-Laden Jets," AIAA J. 23, 1123 (1985)

VITA

Dong Soon Jang was born in Yeo Ju, Korea on March 20, 1953. He grew up at his hometown, watching the flow of the Han River, which went through the town. He left the river for his high school study. He graduated from Kyung Dong high school and entered Seoul National University in March, 1971. His major was Nuclear Engineering. After his college graduation (February, 1975), he joined Korean Agency for Defence Development as a researcher. He worked at this research institute for six years and ten months in the fields of liquid dissemination and two-phase explosion. In January, 1982, he started his graduate study in the field of hazardous waste incineration for a master degree. After master degree, on May, 1984, he worked on the field of numerical computation of heat transfer and fluid flow, specializing in modeling and predictions of turbulent combustion. He is now a candidate for the Ph.D. degree to be awarded at the commencement on December, 1987, dreaming to model the flow of his life as well as the turbulent spectra of the hometown river.

DOCTORAL EXAMINATION AND DISSERTATION REPORT

Candidate: Dong Soon Jang

Major Field: Mechanical Engineering

Title of Dissertation: Single - and two-phase reacting flow predictions-modeling of nonequilibrium effects, turbulent particle dispersion and nitrogen oxide formation in pulverized coal combustion.

Approved:

Major Professor and Chairman

Dean of the Graduate School

EXAMINING COMMITTEE:

Date of Examination:

November 9, 1987